Electrochemical Society

UNIV. OF MICHIGAN
MAR - 5 1954
ENGINEERING LIBRARY

ELECTROCHEMICAL INDUSTRY

Canada

Chlorine ...

for Refrigerants

Ice making, air conditioning and countless other cooling operations depend upon the economy and efficiency of chlorine-made refrigerants.

Uniformly high quality GLC GRAPHITE ANODES play an equally important part in helping the electrolytic industry meet the growing civilian and defense needs for chlorine and caustic soda.

ELECTRODE DIVISION

Great Lakes Carbon Corporation

Niagara Falls, N.Y. GLC® Morganton, N. C.

Graphite Electrodes, Anodes, Molds and Specialties

Sales office: Niagara Falls, N.Y. **Other offices:** New York, N.Y., Oak Park, Ill., Pittsburgh, Pa

Sales Agents: J. B. Hayes, Birmingham, Ala.; George O'Hara, Long Beach, Cal.; Great Northern Carbon & Chemical Co., Ltd., Montreal, Canada

Overseas Carbon & Coke Company, Inc., Geneva, Switzerland; Great Eastern Carbon & Chemical Co., Inc., Chiyoda-Ku, Tokyo

Low-Temperature Electrolytes

Study of Some Physical Properties of the Calcium Halide-Water Systems over the Temperature Range of 25° to −60° C[1]

FRED RAKOWSKY AND A. B. GARRETT

McPherson Chemical Laboratory, The Ohio State University, Columbus, Ohio

ABSTRACT

Data are given for electrical conductivity, freezing points, density, and viscosity of several solutions of calcium chloride, bromide, and iodide over the temperature range of 25° to −60°C. Halide solutions have the following eutectics: calcium chloride, −55°; calcium bromide, −83°; and calcium iodide, −77°C. The calcium iodide-water system has an incongruent melting point at −23.5°C. The electrical conductance-viscosity product shows considerable deviation from Walden's rule.

PURPOSE OF THE INVESTIGATION

The purpose of the investigation was to determine some of the physical properties of calcium halide-water systems over the temperature range 25° to −60°C. These systems show some promise as low-temperature electrolytes.

The phase diagram for the calcium chloride-water system has been determined by Rooseboom (1). Jones and Getman (2) have recorded some data on freezing points, electrical conductivities, refractive indices, and specific gravities of some dilute calcium halide solutions. No other data are available for these systems.

APPARATUS AND PROCEDURE

The constant-temperature cryostat used for density and viscosity measurements was similar to that of earlier work (3), except that the thermostat-bath medium was alcohol instead of air. Temperature was controlled within ±0.2°C over the entire temperature range.

Density, viscosity, and electrical conductivity measurements were made in the manner already described (3). Uncertainty of density values is less than ±0.0002 g/ml. Uncertainty in relative viscosity values above −20°C is less than 0.5%; for lower temperatures (−20° to −60°C) uncertainty increases to about 3%.

Temperature readings were taken with a thermometer calibrated by a platinum resistance thermometer which was calibrated at the National Bureau of Standards.

The cryostat used for special conductivity measurements was similar to one previously used (3) except that the inner Pyrex tube was replaced by a 12-in. Pyrex test tube suspended in the Dewar after the desired temperature had been reached by adding dry ice to the bath liquid. A temperature control of ±0.2°C was easily maintained. Uncertainties in the measurements of conductivities are less than 0.1% above −20°C and less than 2% at −60°C.

Thermal analyses were made in the following

[1] Manuscript received August 13, 1953.

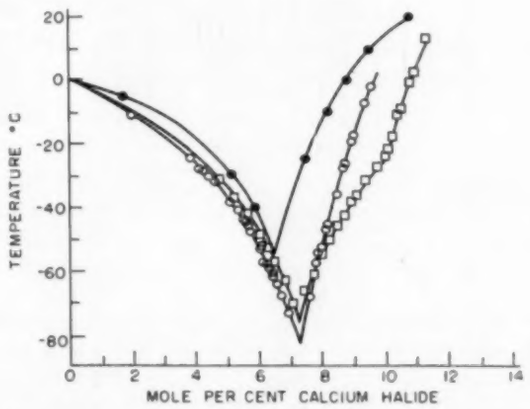

FIG. 1. Freezing points of calcium halide solutions. ●—$CaCl_2$-H_2O system (Rooseboom); ○—$CaBr_2$-H_2O system; □—CaI_2-H_2O system.

TABLE I. *Melting points*

Temp, °C	Mole %	Temp, °C	Mole %
Getman and Jones data		Data this investigation*	
Calcium bromide-water system			
−13.1	2.8	−14.5	2.8
−17.5	3.38	−17.7	3.38
−30.5	4.59	−31.0	4.59
−47	5.88	−49.0	5.88
Calcium iodide-water system			
−10	2.4	−11	2.4
−27	4.45	−28.0	4.45
−60	6.47	−56.5	6.47

* Data interpolated from Fig. 1.

TABLE II. *Density of calcium halide solutions*

Temperature, °C	Density (g/ml)		
	Solutions of $CaCl_2$		
	30.8 wt % 6.80 mole %	29.6 wt % 6.45 mole % (eutectic)	28.4 wt % 6.14 mole %
25	1.2909	1.2784	1.2649
20	1.2937	1.2808	1.2676
0	1.3041	1.2909	1.2775
−20	—	1.3011	1.2873
−40	1.3261	1.3121	1.2971
−60	Frozen	Frozen	Frozen

Temperature, °C	Solutions of $CaBr_2$			
	51.27 wt % 8.66 mole %	47.6 wt % 7.90 mole %	46.6 wt % 7.26 mole % (eutectic)	37.9 wt % 6.22 mole %
25	1.6671	1.6191	1.5757	1.5019
20	1.6715	1.6233	1.5787	1.5051
0	1.6870	1.6383	1.5937	1.5185
−20	1.7037	1.6542	1.6089	1.5325
−40	1.7213	1.6711	1.6255	1.5473
−60	1.7416	1.6900	1.6426	Frozen

Temperature, °C	Solutions of CaI_2	
	57.4 wt % 8.31 mole %	56.6 wt % 8.21 mole %
25	1.9214	1.9114
20	1.9259	1.9156
0	1.9453	1.9350
−20	1.9653	1.9546
−40	1.9860	1.9752
−60	—	1.9964

TABLE III. *Relative viscosity (relative to water at 25°C) of calcium halide solutions*

Temperature, °C	Viscosity — $\eta = \frac{t_1 d_1}{t_2 d_2}$		
	Solutions of $CaCl_2$		
	30.8 wt % 6.80 mole %	29.6 wt % 6.45 mole % (eutectic)	28.4 wt % 6.14 mole %
25	3.150	2.928	2.765
20	3.583	3.279	3.017
0	6.072	5.527	5.087
−20	12.42	11.47	10.25
−40	35.04	31.09	27.91
−60	Frozen	Frozen	Frozen

Temperature, °C	Solutions of $CaBr_2$			
	51.37 wt % 8.66 mole %	47.3 wt % 7.90 mole %	46.6 wt % 7.26 mole % (eutectic)	37.9 wt % 6.22 mole %
25	4.667	3.490	2.950	2.293
20	5.180	3.888	3.309	2.478
0	8.738	6.425	5.341	4.001
−20	17.83	12.85	10.35	7.594
−40	50.94	34.62	27.11	19.18
−60	294.4	178.1	139.8	Frozen

Temperature, °C	Solutions of CaI_2	
	57.4 wt % 8.31 mole %	56.6 wt % 8.21 mole %
25	4.142	4.092
20	4.844	4.502
0	7.428	7.300
−20	14.65	13.84
−40	37.72	34.83
−60	163.2	151.1

apparatus contained in a clear glass Dewar filled with a dry ice-alcohol mixture: a 15-ml sample contained in a Pyrex test tube was partially insulated from the cooling bath by placing this test tube inside a larger test tube which gave a 0.3-cm air space between the two concentric test tubes. The outer tube was filled with enough ethanol so as just to touch the bottom of the inner tube. A spiral glass stirrer, driven by a variable speed motor, was provided. Freezing or melting points of solutions were determined by means of a calibrated toluene thermometer with one-degree centigrade divisions. Readings were accurate to within ±0.5°C.

Materials

All salts were Baker and Adamson reagent quality. Solutions of calcium halides were standardized by calcium and halogen analysis according to procedures described by Pierce and Haenisch (4).

Standard solutions of sodium oxalate were made from National Bureau of Standards sodium oxalate. Solutions of potassium permanganate were standardized against National Bureau of Standards sodium oxalate.

Discussion

Data are shown in Tables I, II, III, and IV, and in Fig. 1.

Density-temperature relationships are linear for all three halides studied over the temperature range of −60° to 25°C. The density-concentration relationship for the calcium bromide-water system is linear over the range of 37.9–51.3 weight % calcium bromide.

Viscosity-temperature data of all three halide systems give the high increase at low temperature observed for many other salt solutions over this temperature range (3).

Electrical conductivity of all three halide systems at low temperature decreases to about 5 to 10 % of the values at room temperature.

Presumably because of their high concentration, these solutions show the expected deviations from Walden's rule (5) of the constancy of the conductance-viscosity product (over the temperature range studied).

Rooseboom (1) reports a eutectic temperature of

TABLE IV. *Specific conductivity of calcium halide solutions*

Temperature, °C	Specific conductivity (ohms^{-1} cm^{-1})	
	Solutions of $CaCl_2$	
	30.8 wt % 6.80 mole %	28.4 wt % 6.14 mole %
25	0.1089	—
20	0.1027	0.1110
0	0.0750	0.0814
−20	0.0475	0.0524
−40	0.0214	0.0239
−60	0.0056	Frozen

Temperature, °C	Solutions of $CaBr_2$			
	51.27 wt % 8.66 mole %	47.6 wt % 7.90 mole %	46.6 wt % 7.26 mole % (eutectic)	37.9 wt % 6.22 mole %
25	—	—	—	0.1365
20	0.1012	0.1129	0.1188	0.1275
0	0.0714	0.0819	0.0863	0.1275
−20	0.0413	0.0483	0.0536	0.0608
−40	0.0169	0.0223	0.0238	0.0303
−60	0.0035	0.0054	0.0065	0.0086

Temperature, °C	Solutions of CaI_2	
	57.4 wt % 8.31 mole %	56.6 wt % 8.21 mole %
20	0.0986	0.1009
0	0.0710	0.0718
−20	0.0431	0.0438
−40	0.0193	0.0198
−60	0.0053	0.0056

−55°C for calcium chloride-water (6.45 mole % salt). The calcium bromide-water system has a eutectic at −83°C (7.26 mole % $CaBr_2$). This is the lowest of these three calcium halides (Fig. 1). The calcium iodide-water system has a eutectic at −77°C (7.25 mole % CaI_2) and an incongruent melting point at 23.5°C (9.95 mole % CaI_2) (Fig. 1). The solid phase, presumably a hydrate, was not identified. Iodide solutions decompose readily from air oxidation and must be protected with an inert atmosphere. Freezing point data of Getman (covering the range of 0 to approximately 6 mole %) are in good agreement with Rooseboom's data for calcium chloride and with the present data for calcium bromide and calcium iodide (see Table I).

A comparison of characteristics of these three halides indicated that calcium bromide has many desirable characteristics for a low-temperature electrolyte (6).

Any discussion of this paper will appear in a Discussion Section to be published in the December 1954 issue of the JOURNAL.

REFERENCES

1. H. W. B. ROOSEBOOM, *Z. physik. Chem.*, **4,** 31 (1889).
2. H. C. JONES AND F. H. GETMAN, *Z. physik. Chem.*, **49,** 385 (1904).
3. A. B. GARRETT AND S. WOODRUFF, *J. Phys. Chem.*, **55,** 477 (1951).
4. W. C. PIERCE AND E. L. HAENISCH, "Quantitative Analysis," pp. 300, 430, John Wiley and Sons, Inc., New York (1948).
5. O. WALDEN AND H. ULICH, *Z. physik. Chem.*, **107,** 219 (1923); H. ULICH, *Fortschr. Chem.*, **18,** 33 (1926).
6. A. B. GARRETT, J. WELSH, S. WOODRUFF, R. COPPER, AND J. HEIKS, *J. Phys. Chem.*, **53,** 505 (1949).

Radioactive Tracers in the Study of Pitting Corrosion on Aluminum[1]

P. M. Aziz[2]

Institute for the Study of Metals, University of Chicago, Chicago, Illinois

ABSTRACT

Radioactive cobalt and lead ions in solution have been used to study the distribution of local cathodes on aluminum alloy specimens which were actively pitting, and to study the processes of film breakdown and repair on aluminum alloy specimens after introducing them into a corrosive environment. In the study of pitting, radioactive ions were introduced into the solution after pitting of the sample had proceeded for a predetermined length of time. The tracer was then permitted to plate out onto local cathodes, and, after washing and drying, autoradiographs of the surface were prepared. Results indicate that after a pit is a few hours old it is surrounded by a ring of cathodic surface and outside this is an annular ring of passive surface which prevents lateral expansion of the corrosive attack, the remainder of the surface being cathodic. In the study of the mechanism of film breakdown and repair, samples with different surface treatments were placed in the solution and radioactive ions were introduced after various predetermined times, exchange permitted to take place, samples washed and dried, and autoradiographs prepared of the surface. Results indicate that, on contact with the solution, the surface oxide film breaks down and is then repaired by reaction with the solution.

Introduction

Passive metals, such as aluminum and its alloys, and the stainless steels are very slowly attacked even in the presence of oxygen by such media as natural waters and dilute solutions of fruit acids. The attack may be localized in the form of pits which can perforate thin sheet with potentially serious consequences.

Several investigations have been carried out on the nature of pitting corrosion, but these studies have dealt with either the electrochemical nature of the attack (1, 2), or phenomena such as the probability of pitting (3, 4), and have not been directly concerned with the reason for the localization of the attack. However, qualitative views concerning the cause of this localization are held, and it is generally thought to be due to an isolated breakdown in the protective oxide film leading to localized attack of the metal. If this is the case, local cathodes must be confined to an area near the pit mouth since most of the surface remains covered with an inert oxide film. Hence, if distribution of the cathodic elements on the surface of a pitting metal is determined, a clue to the mechanism of the localization may be obtained.

If the ion of a metal, more electropositive than the corroding metal, is introduced into the solution, it will plate out electrochemically on the local cathodes, and a determination of distribution of the plated material will give the location of cathode elements. Radioactive tracers of heavy metals such as lead and cobalt are ideally suited for this application since they can be detected in trace amounts by means of the radiation which they emit and, hence, they may be introduced into the corrosive environment in only slight concentration, thereby reducing danger of altering the cathode distribution by the process of measurement. Radioactive isotopes have been used previously in the study of corrosion mechanisms (5, 6), and references can be made to the excellent review by Simnad (7) of literature dealing with the use of radioisotopes in the study of metal surface reactions in solution. None of these studies has dealt with the distribution of cathode elements on a pitting surface; the present work is concerned with the study of this distribution on pitting aluminum surfaces, using radioactive isotopes of the heavy metals, lead and cobalt, and its effect on the distribution of corrosion. Distribution was determined by preparing autoradiographs of metal specimens after exchange of the corroding surface with the radioisotope.

Experimental

Materials

The metal used in this investigation was "Super Purity" aluminum, (99.99% Al) alloyed with

[1] Manuscript received April 27, 1953. This paper was prepared for delivery before the Wrightsville Beach Meeting, September 13 to 16, 1953.

[2] Present address: % Aluminium Laboratories Limited, Box 84, Kingston, Ontario, Canada.

0.5% iron and 0.3% silicon. The finished metal was supplied in the form of cold rolled sheet 0.064 in. thick.

The radioactive isotopes used were Co^{60} and Pb^{210} in the form of chloride solutions in distilled water. The activity of the solutions was 1 microcurie per 0.1 ml of solution and the total cation concentration was 1 ppm.

Autoradiographs were prepared on Kodak no-screen x-ray film. Precautions recommended by Yagoda (8) for the prevention of spurious results were observed.

Chicago tap water was the corrosive medium used in all the work described herein. This is a moderately hard water with hardness reported as $CaCO_3$ of 140 ppm. It is filtered and chlorinated to a free chlorine content of 0.14 lb per million gallons of water.

Procedure

Metal samples, in the form of one-inch squares of sheet, were annealed one-half hour at 350°C and furnace cooled. They were then etched in 85% orthophosphoric acid at 70°C for two minutes and washed in six changes of tap water. Washing in tap water was necessary since it was found that using distilled water passivated the surface and no exchange with the tracer took place. Following this treatment, three types of experiment were carried out.

1. Samples were immediately transferred to a 200-ml crystallizing dish containing 150 ml of water, and pitting was permitted to proceed for the desired length of time. On these small samples it was found that pitting did not initiate spontaneously on all samples, and it was necessary to initiate pits artificially so by touching the point of a dissecting needle to the surface of the metal. Comparison of natural with artificially initiated pits showed no difference in their cathode structures, and artificial initiation was used throughout. After pitting had proceeded for the desired length of time, the sample was removed from the water in a horizontal position and 0.1 ml of the solution of radioactive tracer introduced into the film of water retained on the surface of the specimen. Exchange took place for ten minutes, the sample was washed with distilled water, dried with alcohol; and an autoradiograph prepared of the surface. The autoradiographic exposure employed was 1½ hours, with one exception, which will be noted in the proper context. Distribution of local cathodes on the surfaces of samples, which had pitted for time periods of from 6 hours to 14 days, was examined in this manner using both Co^{60} and Pb^{210}.

2. Coarse-grained samples were etched, washed, and exposed to water for 24 hours, exchanged with Co^{60}, and autoradiographs prepared of the surface to determine whether crystal structure had any effect on the distribution of local cathodes.

3. Two series of nine samples each were etched and washed as previously described, and one set was immediately placed in tap water, while the other set was permitted to oxidize in air for 24 hours and was then placed in the water. Samples were then removed from the water after the following periods of immersion: 30 sec, 5 min, 10 min, 20 min, 40 min, 90 min, 120 min, 3 hr, 24 hr. They were permitted to exchange with Co^{60} and autoradiographs prepared as described in section 1.

This series of experiments was designed to determine how the oxide film forms on a stripped active surface on immersion in a corrosive medium, and what happens to a protective oxide film on immersion in a corrosive medium.

Results and Discussion

1. Fig. 1 shows autoradiographs of pits exchanged with Pb^{210} after pitting for six hours to fourteen days, while Fig. 2 shows autoradiographs of pits in

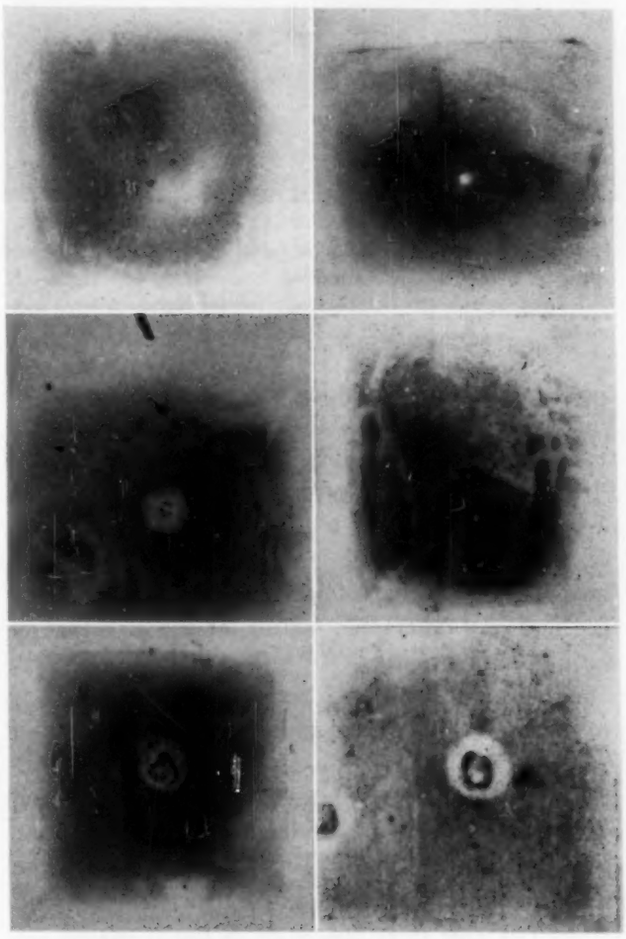

Fig. 1. Autoradiographs of pits of indicated age exchanged with Pb^{210}. Top left—6 hours old; top right—24 hours old; center left—3 days old; center right—5 days old; bottom left—7 days old; bottom right—14 days old.

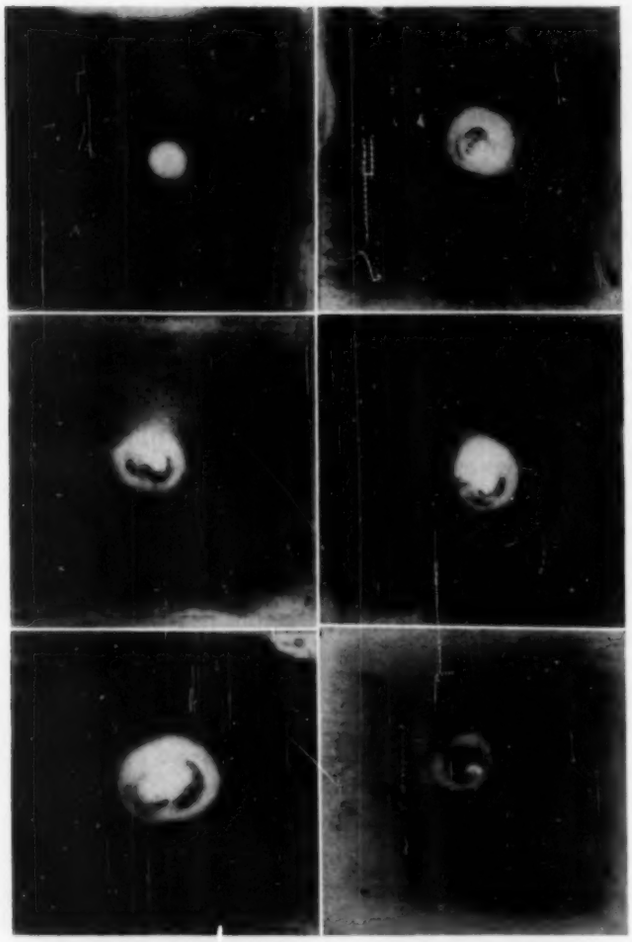

FIG. 2. Autoradiographs of pits of indicated age exchanged with Co^{60}. Top left—6 hours old; top right—24 hours old; center left—3 days old; center right—5 days old; bottom left—7 days old; bottom right—14 days old.

the same alloy and under the same conditions as Fig. 1 but exchanged with Co^{60}. Local cathode distribution is shown up in greater detail with the Pb^{210} than with the Co^{60}, but the general pattern obtained is the same with both radioisotopes. It was not found possible to detect any correlation between distribution of local cathodes on the surface and any detectable feature of the structure of the underlying metal.

The mouth of the pit is surrounded by an annular ring of cathodic surface, and about this is a ring of inert surface, neither anode nor cathode. The remainder of the surface is cathodic, since deposition of radioactive tracer had taken place over it. As shown by the Pb^{210} this distribution becomes more sharply defined as the pit grows older. Use of Co^{60} brings out this distribution at a much earlier pit age.

Microscopic examination of the inert area about the mouth of the pit showed that it was covered with a thick film, presumably of hydrated aluminum oxide. Fig. 3 is a photomicrograph taken in this

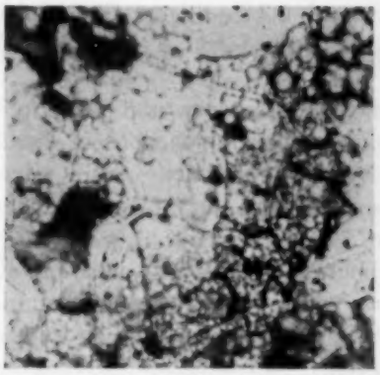

FIG. 3. Photomicrograph of inert area of 7-day old pit in Fig. 1.

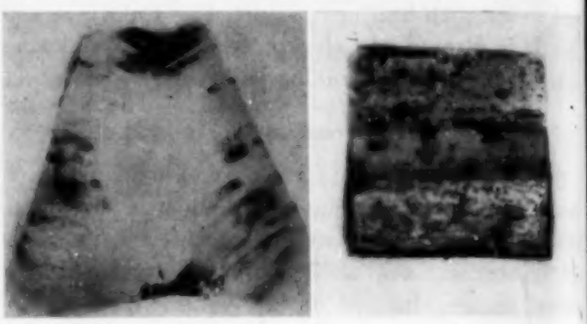

FIG. 4. Autoradiograph of coarse-grained aluminum, corroded, exchanged with Co^{60}. Left—ingot; right—sheet.

inert area of the sample from which the seven day old pit in Fig. 1 was prepared.

2. Specimens from which the autoradiographs of Fig. 4 were prepared were cut from a large-grained ingot and a sheet of high purity aluminum, respectively. The latter possessed a banded texture and the autoradiographs followed the general pattern of the crystal structure.

3. Fig. 5 shows autoradiographs prepared from phosphoric acid etched samples exposed to water for periods of 30 sec to 24 hr, while Fig. 6 shows autoradiographs prepared from samples which were oxidized in air previous to exposure in the water. The normal autoradiographic exposure of 1½ hr gave negative results with the etched sample which had been immersed in water 24 hr (Fig. 5) and this autoradiograph was given a 24-hr exposure.

With both methods of preparation, etching and etching with subsequent air oxidation, the surface is highly reactive on initial immersion in the water and exchanges extensively with the radioactive ion but, as the period of exposure increases, activity decreases and after 24 hr the surface is passive. Because of a lack of reproducibility of behavior from sample to sample, the sequence of changes is not clear cut, but this general trend has been verified with experiments on a large number of specimens. It is interesting that the thin air-formed oxide film is not protective when the sample is immersed in

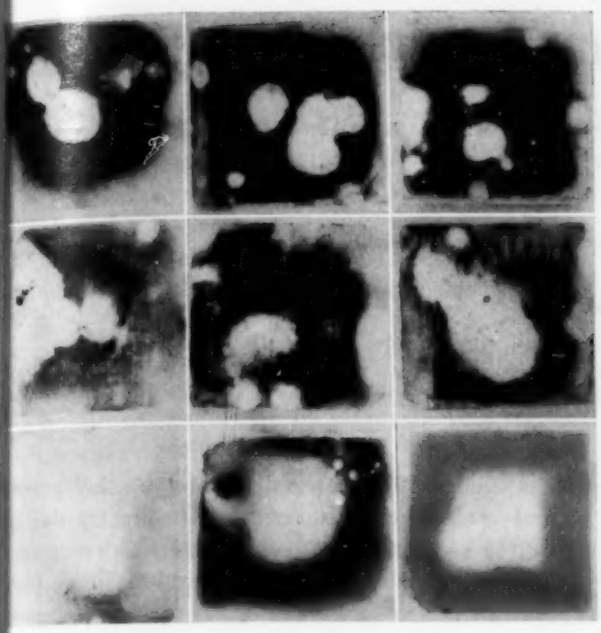

FIG. 5. Cobalt^{60} autoradiographs of samples etched and exposed to water for the times shown. Top left—30 sec; top center—5 min; top right—10 min; center left—20 min; center center—40 min; center right—90 min; bottom left—120 min; bottom center—3 hours; bottom right—24 hours.

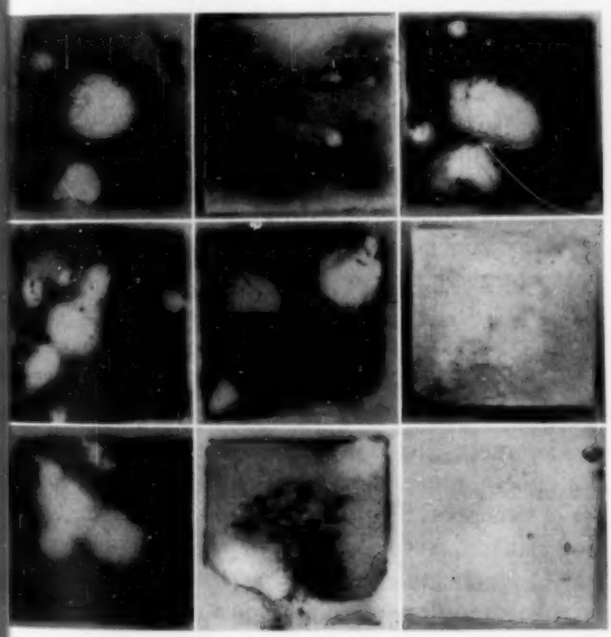

FIG. 6. Cobalt^{60} autoradiographs of samples, etched, air-oxidized, and exposed to water for times shown. Top left—30 sec; top center—5 min; top right—10 min; center left—20 min; center center—40 min; center right—90 min; bottom left—120 min; bottom center—3 hr; bottom right—24 hr.

the water, but either breaks down and then repairs itself by reaction with the corrosive medium, or else is so thin that it permits the passage of electrical current and allows some corrosion to take place. A previous publication (9) has dealt with a probable mechanism of pitting corrosion in aluminum and this may be amplified here in view of the present findings. In addition, Edeleanu and Evans (10) discuss a view of pitting corrosion which is in essential agreement with the present work.

When the specimen is immersed in the water any air-formed film present on its surface breaks down and general corrosion ensues, with anodic and cathodic reactions taking place at neighboring sites over the surface. These reactions result in the formation of alkali at the cathodes and in the passage of aluminum into solution at the anodes as aluminum ions. These aluminum ions hydrolyze, forming alumina with a resultant decrease in the *p*H of the solution. In time, the alkaline cathodic products of reaction and the acid products of reaction intermingle as a result of diffusion and convection; the *p*H of the anodic solution rises and when the solubility product of the alumina is exceeded it precipitates from solution. If the alumina is precipitated as an adherent protective film on the surface of the metal, corrosion reaction is stifled and the metal becomes passive as shown by the 24-hr autoradiographs of Fig. 5 and 6. However, if the surface is incompletely covered, the anodic and cathodic reactions are separated, precipitation of a film then takes place in the area between them, the anodic attack is localized, and a pit forms. As Fig. 1 shows, the configuration of local cathodes and of the passive localizing film about the anode take up circular symmetry, and in a sense the localization of the attack becomes autocatalytic.

ACKNOWLEDGMENTS

The author wishes to thank Professors C. S. Smith, N. H. Nachtrieb, G. V. Raynor, and C. S. Barrett for valuable discussion during the course of this work, and Aluminium Laboratories Limited for arrangements that made it possible to carry out this work at the Institute for the Study of Metals, University of Chicago.

Any discussion of this paper will appear in a Discussion Section to be published in the December 1954 issue of the JOURNAL.

REFERENCES

1. R. B. MEARS AND R. H. BROWN, *Trans. Electrochem. Soc.*, **74**, 519 (1938).
2. R. B. MEARS AND R. H. BROWN, *ibid.*, **81**, 455 (1942).
3. R. B. MEARS AND R. H. BROWN, *Ind. Eng. Chem.*, **29**, 1087 (1937).
4. P. M. AZIZ AND H. P. GODARD, *ibid.*, **44**, 1791 (1952).
5. M. T. SIMNAD. *This Journal*, **98**, 301 (1951).
6. M. T. SIMNAD, *Rev. met.*, **48**, 1 (1951).
7. M. T. SIMNAD, Institute of Metals Monograph, No. 13 (in course of publication).
8. H. YAGODA, "Radioactive Measurements with Nuclear Emulsions," John Wiley and Sons, Inc., New York (1949).
9. P. M. AZIZ, *Corrosion*, **9**, 3 (1953).
10. C. EDELEANU AND U. R. EVANS, *Trans. Faraday Soc.*, **47**, 1121 (1951).

The Mechanism of Metallographic Etching

I. The Reaction Potentials of a Two-Phase Brass in Various Etching Reagents[1]

GEORGE L. KEHL AND MAX METLAY[2]

School of Mines, Columbia University, New York, New York

ABSTRACT

Potentials generated by reaction of portions of small, single grains of each of the two phases of alpha-beta brass with various etching solutions have been measured. The potential of beta phase is consistently 0.01 to 0.03 volt more anodic than that of the alpha phase in the same reagent.

INTRODUCTION

Preparation of metallic specimens for metallographic examination involves use of well-established polishing and etching techniques (1). Innumerable etching reagents described in the literature have all been evolved through methods of trial and error, since the existing understanding of mechanisms of etching processes is not sufficiently precise to permit prediction of appropriate compositions. Inasmuch as metallographic etching in the usual sense consists of reaction between a polished metal surface and a liquid reagent resulting in alteration of the polished surface, the process is essentially one of controlled corrosion, and knowledge provided by the extensive literature of corrosion research (2, 3) gives a rational clue to mechanisms of etching. However, details must still be determined, and this communication is the first of a series dealing with these details.

Corrosion (and hence etching) proceeds by electrolytic action attending structural differences that exist on the specimen surface. Some discrete surface portions are anodic to others and, in consequence, suffer dissolution electrolytically under appropriate circumstances. In pure metals and in single phase alloys an electrolytic potential (polarized) is established between grains of different orientation, between the matrix and tramp secondary phases, between grain boundaries and grains proper, and along concentration gradients in heterogeneous single phase alloys. In multiple phase alloys there exists in addition a sharp difference in composition between structural phases.

To determine the influence of surface structure variations on electrolytic reactivity during etching, potential generated during the process is measured at the various types of sites described. In this research an alpha-beta brass of appropriate composition is used as the material of interest, and potentials of each phase measured independently during etching in a variety of conventional etching reagents. In principle this is accomplished by isolating a portion of one phase on the surface of a metallographic specimen, and protecting the remaining surface from the etching reagent by a covering of insulating resin. The exposed surface portion is allowed to react with the etching reagent, and the potential generated is measured with respect to a saturated calomel cell.[3] By making a large number of independent measurements on each phase during etching, average relative potentials of the two phases during reaction can be determined. Potential so measured is essentially the polarized potential attending local anodes and cathodes existing on the isolated surface area. Since metallographic etching generally takes place within a period of a few seconds to a few minutes, potentials at short times are of greatest interest. These are best obtained by use of a rapid recording potentiometer.

EXPERIMENTAL

Specimens

The metal used in this study is a commercial alpha-beta brass, or Muntz metal, of composition 60.75% copper, 38.55% zinc, remainder manganese, iron, silicon, and lead. Specimens were heated to 855°C for 15 min in argon and furnace cooled to enlarge grain size and to provide a nearly equilibrium structure.

Specimens are mounted in Bakelite by standard metallographic mounting methods. Both ends of a cylindrical mount are ground flat until the specimen is exposed. One side of the specimen is drilled and tapped; the other is ground and polished for metallographic examination. The specimen is very slightly relief-polished to reveal the structure, then coated with resin as described below. Mechanical support for the specimen, which also serves as the electrical contact, consists of a ⅜ in. diameter brass rod ap-

[1] Manuscript received August 3, 1953.

[2] Present Address: Department of Chemistry, Harpur College, State University of New York, Endicott, New York.

propriately threaded to fit into the tapped hole in the specimen.

Coating Technique

In order to make emf measurements on each phase, it is necessary to coat the entire specimen surface with a protective coating, except a portion of that phase whose potential is to be measured.

A previous method (4) for achieving this consisted of creating a hole with a specially shaped needle in a covering film of ethylcellulose applied to the specimen surface. This method has the disadvantage that the metal surface thus exposed may be cold worked to a degree significant with respect to subsequent potential measurements.

Two resin formulations have been used in these experiments, formulation No. I based on Epon resin 1001, and formulation No. II based on Vinylite resin VMCH. Formulation No. I has the advantage that it is extremely resistant chemically, and the disadvantage that it must be allowed to set overnight and that the minimum area left exposed is slightly larger than with formulation No. II. The latter formulation has the advantage of setting within an hour of coating, but is not quite as resistant chemically as No. I, and thus is not always successful in protecting the specimen, especially in longer runs. Results given in this communication were obtained with No. I, while No. II was used in subsequent experiments to be reported.

Formulation No. I.—Stock solution: Epon 1001[3] or Devran 654—6 parts by weight; acetone—1 part; toluene—1 part. Catalyst solution: diethylene triamine—10%; acetone—45%; toluene—45%.

Just before use, one part of catalyst solution is thoroughly mixed with two parts resin solution. This coating must be allowed to set overnight. It can be removed by soaking in acetone, then scraping with a dull instrument.

Formulation No. II.—Vinylite resin VMCH[5] is mixed with a small amount of cyclohexanone. A little acetone is added until viscosity and flow properties of the mixture are adjudged satisfactory. This coating will set in about one hour, and can be removed by swabbing with acetone.

Either resin formulation is applied by placing a few drops on the Bakelite mount around the specimen edges and it is subsequently distributed over the surface by means of a spade-like tool actuated by a micromanipulator. A piece of Saran tubing cut to an appropriate shape and attached to an applicator stick has been found convenient to serve as the distributing tool. During coating the specimen is observed by means of a low power microscope, so that the area to be left exposed can be kept free of resin, and the remainder of the sample can be thoroughly covered. A typical example of a coated specimen is shown in Fig. 1. The same specimen, after etching and removal of the resin coating, is shown in Fig. 2.

[3] Product of the Shell Chemical Company.
[4] Product of the Devoe Reynolds Company.
[5] Product of the Bakelite Division, Union Carbide and Carbon Corporation.

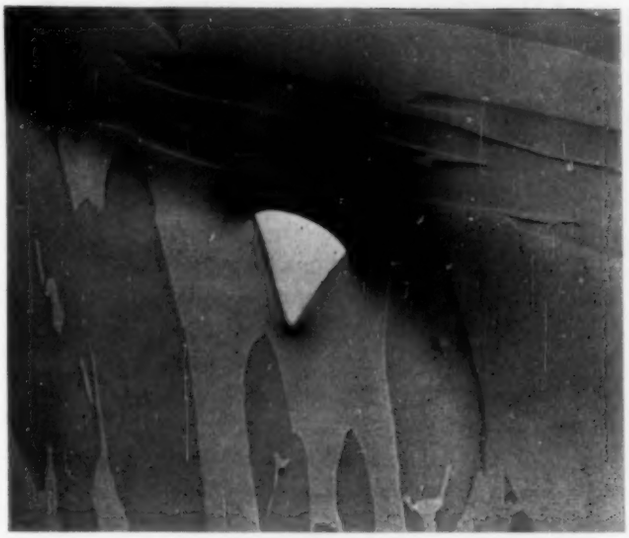

FIG. 1. Surface of alpha-beta brass as coated with resin except for an isolated portion of the beta phase (triangular area). Exposed area unetched. 150×.

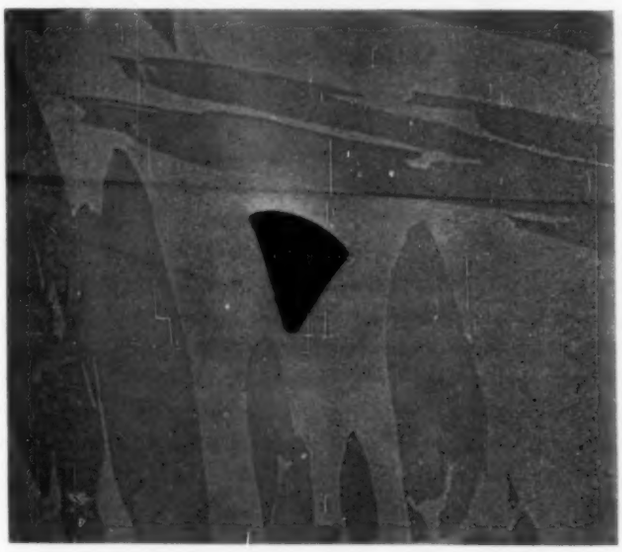

FIG. 2. Same as Fig. 1, except exposed area of beta phase is etched and the resin coating removed. 150×.

Apparatus

The electrical system used to measure electrode potentials consists of a Leeds and Northrup Type K-2 potentiometer with a Speedomax recording potentiometer connected across its galvanometer

leads. This system allows potential to be read as the sum of potentials indicated by the Type K-2 potentiometer and by the recorder. Therefore, the potentiometer is kept adjusted to supply a voltage within 50 millivolts of the reaction cell, so that the resultant emf remains within the recorder range. The recorder has a full scale travel time of two seconds, and is actuated at about 50 microvolts unbalance, with current drain of about 7×10^{-9} amp. This small order of current drain does not appreciably polarize the electrodes of the system, but if the emf is changing rapidly as it does at onset of the reaction, some external polarization undoubtedly takes place.

A saturated calomel cell is employed as the standard reference electrode. The design is conventional, except that a fritted glass disk of fine porosity separates the saturated KCl from the etching reagent.

Reagents

The reagents used in this study were in general the common etching reagents for brass (1):

[1] Ferric chloride reagent No. 1: 1 part $FeCl_3$, 10 parts conc. HCl, 113 parts H_2O; [2] ferric chloride reagent No. 2: 1 part $FeCl_3$, 10 parts conc. HCl, 20 parts H_2O; [3] ferric chloride reagent No. 3: 1 part $FeCl_3$, 1 part conc. HCl, 4 parts H_2O; [4] ammonium hydroxide—hydrogen peroxide reagent: 1 part conc. NH_4OH, 1 part 3% H_2O_2, 1 part H_2O; [5] copper ammonium chloride reagent: 10% copper ammonium chloride in water, plus NH_4OH to basicity; [6] ammonium persulfate reagent: 10% $(NH_4)_2S_2O_8$ in water; [7] ammonium persulfate—ammonium hydroxide reagent: 1.25 g $(NH_4)_2S_2O_8$, 25 cc conc. NH_4OH, 75 cc H_2O; [8] ammonium hydroxide reagent: 1 part conc. NH_4OH, 2 parts H_2O; [9] chromic acid reagent—10% CrO_3 in water, plus one drop conc. HCl for each 25 cc reagent, added immediately before use.

Measurements

The reaction cell containing the etching reagent and the calomel cell are immersed in a thermostatically controlled water bath at 25°C. The fritted disk is immersed in the reagent one or two minutes

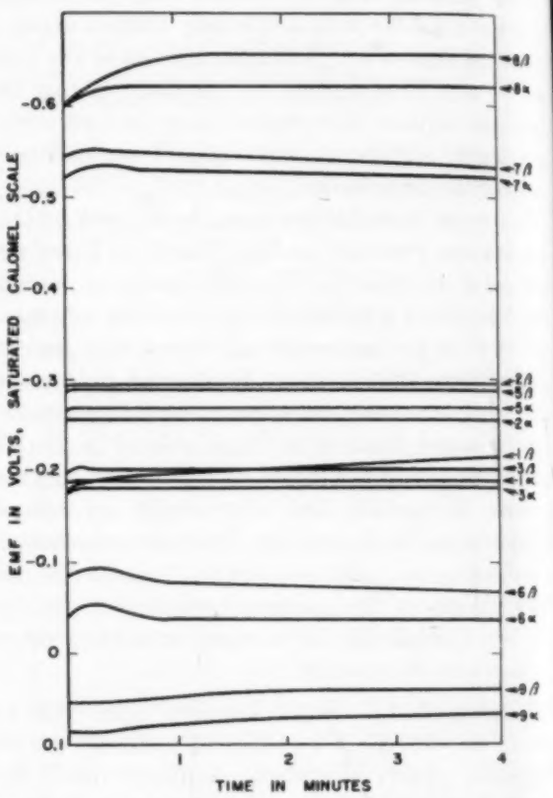

FIG. 3. Emf of isolated areas of alpha or beta brass on saturated calomel scale vs. time. Each curve is identified by number of the reagent, as listed in text, and by the phase exposed to reagent.

TABLE I. *Potentials of isolated alpha and beta phases in 60-40 brass in various etching reagents, in reference to a saturated calomel electrode of 25°C*

Reagent[a]	Range in potential, v		Usual potential spread in a single run, v		Average potential, v	
	Alpha	Beta	Alpha	Beta	Alpha	Beta
1. $FeCl_3$ No. 1[b]	−0.17 to −0.20	−0.17 to −0.20	0.005	0.05 to 0.1	−0.185	−0.19 to −0.21
2. $FeCl_3$ No. 2	−0.245 to −0.265	−0.282 to −0.295	0.002 to 0.01	0.005	−0.256	−0.293
3. $FeCl_3$ No. 3	−0.175 to −0.193	−0.20 to −0.29	0.005	0.005	−0.180	−0.20
4. NH_4OH-H_2O_2[c]	−0.41 to −0.45	−0.45 to −0.48				
5. $Cu(NH_4)_2Cl_4$	−0.26 to −0.27	−0.28 to −0.29	0.002	0.002	−0.267	−0.288
6. $(NH_4)_2S_2O_8$	−0.04 to −0.08	−0.07 to −0.11	0.01 to 0.03	0.03	−0.06	−0.08
7. $(NH_4)_2S_2O_8$-NH_4OH	−0.50 to −0.53	−0.54 to −0.55	0.01 to 0.03	0.01 to 0.03	−0.53	−0.545
8. NH_4OH	−0.62	−0.64 to −0.68			−0.62	−0.65
9. CrO_3	0.080 to 0.098	0.033 to 0.068	0.005 to 0.015	0.005 to 0.015	0.094	0.048

[a] Reagents are described more fully in the text.

[b] The potential for beta brass in this reagent rose gradually with time. Average potentials given indicate the range of the start of the runs. After about 10 min., the potential is about −0.25 to −0.27 volt.

[c] NH_4OH-H_2O_2 reagent gave very erratic results due to rapid formation of gas bubbles on the metal surface. Potentials varied rapidly and erratically over 50 to 100 mv, and more. Values given may be considered an informed guess.

before the specimen is to be immersed. The potentiometer is set at some emf value, determined approximately by an initial trial, electrical connections are made, and the mounted specimen is immersed in etching reagent. Care is taken that the top of the mount and the supporting rod remain out of contact with the reagent. The potential difference between specimen and calomel cell is then recorded by the Speedomax recorder. When it appears that the potential is changing so that it will no longer be within the recorder range, the potentiometer slide wire is reset to keep recorded potential within the instrument's range. True measured potential is then the sum of the potentiometer setting and the potential indicated by the recorder.

Results

A summary of results of potential measurements is given in Table I. For each reagent, the following information is given for each phase: (*a*) range of potential (with respect to saturated calomel) in volts, over all runs; (*b*) usual variation of potential in a single run; and (*c*) probable value of the potential in volts.

Fig. 3 shows variation of potential with time for several representative experiments with various etching reagents. Each curve is identified by the reagent number, as in the description above, and by the phase exposed.

Discussion

It can be seen from inspection of Table I that an appreciable difference exists between reaction potentials of alpha and beta phases, generally in the range of 0.01 to 0.03 volt, with beta always anodic to alpha. Since the beta phase is rich in zinc compared to the alpha, this behavior can reasonably be expected. The consistent small difference in emf seems to indicate, at least for the system under consideration, that if the phases were to be coupled, etching would proceed in part by galvanic action with the beta phase anodic to the alpha phase. Data supporting this statement will be included in a forthcoming communication relative to closed circuit potential measurements between the two phases.

An attempt to obtain data of the same kind for other systems showed that the magnitude of potential difference between anode and cathode depends, among other factors, on the dissimilarity of electrodes, as expected. At one extreme, that is, using similar electrodes, some attempts were made to determine reaction potentials of grain centers and grain boundaries of a small-grained single phase 90-10 alpha brass in ferric chloride reagent No. 1. Here etching is characterized by preferential dissolution at grain boundary regions.

Experiments indicate that grain boundaries are anodic to the grains proper, although techniques were not sufficiently sensitive to determine the difference with any accuracy. However, for other metals, it has been shown in several cases that grain boundaries are anodic to grain centers; for example, high purity (99.986%) aluminum in 20% HCl (5), 70-30 brass in 1% NH_4OH (6).

At the other extreme, potential measurements were made on an alloy possessing phases greatly dissimilar. Cadmium and bismuth are practically insoluble in each other in the solid state, and, as a consequence, alloys of this system consist essentially of two pure-metal phases. These alloys can be etched by means of a reagent consisting of one part I_2, three parts KI, and ten parts H_2O. This reagent preferentially attacks and darkens the cadmium phase. Measurements on selected compositions indicated the bismuth phase to have a potential of -0.09 ± 0.02 volt with respect to a saturated calomel electrode, while the corresponding potential for cadmium was -0.825 ± 0.001 volt, cadmium therefore being 0.735 volt anodic to bismuth.

All etching reagents employed in etching of alpha-beta brass, with the exception of ammonium hydroxide-hydrogen peroxide (reagent No. 4), have the characteristic of attacking the beta phase preferentially and darkening it metallographically relative to the alpha phase. As noted in Table I, emf values given for the ammonium hydroxide-hydrogen peroxide reagent can be considered only an informed guess, since there was a wide, rapid, and erratic variation of recorded potential, undoubtedly due to formation of oxygen bubbles on the metal surface. It is unfortunate that this situation exists, since it would be interesting to compare emf values in reagents which have opposite etching effects on the same alloy.

Acknowledgments

This research was made possible through support of the Atomic Energy Commission under Contract AT-(30-1)-1006.

The assistance of Dr. Erica Wasilewski and of Mr. Arthur Bauer with the experimental work is gratefully acknowledged.

Any discussion of this paper will appear in a Discussion Section, to be published in the December 1954 issue of the Journal.

References

1. G. L. Kehl, "Principles of Metallographic Laboratory Practice," McGraw-Hill Book Co., Inc., New York (1949).
2. H. H. Uhlig, Editor, "Corrosion Handbook," John Wiley & Sons, Inc., New York (1948).
3. R. B. Mears, *This Journal*, **97**, 316 (1950).
4. L. W. Smith and V. J. Pingel, *ibid.*, **98**, 48 (1951).
5. E. H. Dix, Jr., *Trans. Am. Inst. Mining Met. Engrs.*, **137**, 21 (1940).
6. R. B. Mears and R. H. Brown, *Ind. Eng. Chem.*, **33**, 1001 (1941).

The Kinetics of Oxidation of High Purity Nickel[1]

E. A. Gulbransen and K. F. Andrew

Westinghouse Research Laboratories, East Pittsburgh, Pennsylvania

ABSTRACT

The effect of time, temperature, and surface pretreatment on rate of oxidation of high purity nickel is studied for the temperature range of 400°–750°C using a vacuum microbalance technique. The data are compared to previous studies in the literature and with other metals. Oxidation data are interpreted in terms of the parabolic rate law and classical theory of diffusion.

Large deviations from the parabolic rate law are found to occur during the initial stages of reaction and smaller deviations over long periods of time, especially at low temperatures. However, reasonable values of heat and entropy of activation for the over-all reaction can be calculated; these are 41,200 cal/mole and −6.0 entropy units (eu), respectively. Parabolic rate law constants over the temperature range of 550°–700°C are given by

$$A = 3.8 \times 10^{-4} e^{-41,200/RT} \text{cm}^2/\text{sec}.$$

The negative value for entropy of activation for the over-all reaction when corrected for entropy of formation of the vacancies leads to a value of 1.5 for entropy of activation for diffusion. Theoretical considerations suggest that the latter term should have a value of 1.7–3.3 eu. The good agreement between theoretical and experimental entropies of activation suggests that diffusion is occurring largely through the lattice of nickel oxide and not at grain boundaries, at least for the temperature and time region over which analyses were made.

A comparison of present data with older studies in the literature shows a large variation in parabolic rate law constants. These variations are interpreted in terms of impurities increasing the concentration of nickel ion vacancies.

Introduction

The work reported in this paper is part of a larger study on the mechanism of oxidation of nickel-chromium and nickel-chromium-iron alloys at high temperatures. To interpret oxidation of practical metals containing impurities and alloys, it is necessary to have detailed knowledge of rates of oxidation of high purity metals. Several studies have already been reported (1–5).

A number of studies have been made on oxidation of nickel of widely varying purity at temperatures above 600°C (6–8). These results were summarized in a paper by Kubaschewsky and Goldbeck (9) and correlated with their own measurements. This study shows variations of 100 in values found for the parabolic rate law constant at a given temperature.

Using a volumetric method, Moore (10) studied oxidation of 99.9% pure nickel over the temperature range of 400°–900°C. The parabolic rate law was found to represent the data, with the rate constant being given as

$$A = 3.09 \times 10^{-5} e^{-38,400/RT} \text{ cm}^2 \text{ sec}^{-1}.$$

Moore's values for A differ from those summarized by Kubaschewsky and Goldbeck (9) by a factor of 20 to 2000.

In a recent work, Campbell and Thomas (11) found that time dependence of the oxidation rate of nickel in the temperature range up to 302°C could be fitted by a logarithmic rate law. Deviations from a parabolic rate law were explained on the basis of a space charge set up in very thin films.

A comparison of the various studies (9, 10) suggests a strong influence of alloying elements, impurities, and contaminants in the gas atmosphere. The fact that other surface reactions of nickel are difficult to reproduce in both liquid (12) and gaseous media is probably related to these same factors.

Evidence exists to show that certain alloying elements affect the rate of oxidation of nickel. Wagner and Zimens (6) have shown that the parabolic rate law constant of nickel is increased by addition of chromium and manganese. According to Horn (13), the oxidation rate constant for a 6% chromium-nickel alloy is increased by a factor of 16. Increase in rate is explained on the basis of an increase in number of nickel ion vacancies. Above 6%, the rate of reaction is found to decrease.

Lithium, on the other hand, is found to decrease the oxidation rate constant. This is reported by Hauffe and Pfeiffer (14) in a study of effect of Li_2O in vapor state on rate of oxidation in air. Other

[1] Manuscript received November 3, 1952. This paper was prepared for delivery before the Montreal Meeting, October 26 to 30, 1952.

elements, as impurities or in the gas atmosphere, will have their characteristic effects depending upon their charge, size of ion, electronegativity, and solubility.

Alloying elements and impurities in the metal or atmosphere may have an additional effect on the course of oxidation. Thus, if impurity or alloying element concentration changes during the reaction, and if vacancies of nickel ions in oxide are sensitive to the particular impurity, the parabolic rate law constant will change during the experiment. Wagner and Zimens (6) found in a study of nickel at 1000°C that the parabolic rate law constant decreased as the oxidation progressed.

The oxide formed on nickel over the temperature range of 300°–700°C was studied by Gulbransen and Hickman (15) and found to be NiO. Wyckoff (16) gives the structure of NiO as a unimolecular rhombohedron with $a_0 = 2.9459$ Å. Rooksby (17) found NiO to be rhombohedral at 18° and face-centered cubic at 275°C, with $a_0 = 4.1946$.

Nickel forms the stable oxide NiO in the temperature range of this work. Thermodynamic calculations show that at 1000°C the decomposition pressure of oxygen over nickel oxide and nickel is 10^{-11} atmospheres. The surface oxide, however, is readily reduced by hydrogen from a thermodynamic point of view at temperatures of 400° to 1000°C.

The purpose of this work is (*a*) to determine the time and temperature dependence of the rate of oxidation and how these values are affected by pretreatment and initial oxide formation, (*b*) to evaluate from this information the heat, entropy, and free energy of activation of the rate-determining process and to compare these values with other metals and alloys, and (*c*) to point out physical and chemical factors in the oxide and metal affecting the mechanism of reaction.

Apparatus and Method

All of the kinetic measurements were made using the vacuum microbalance and associated equipment (18, 19). The sensitivity of the balance was 0.91 micrograms per division (0.001 cm) and weight change could be estimated to 0.25 micrograms. The vacuum system and associated equipment have been described (19, 20, 21). A mullite furnace tube which was sealed directly to the all-glass vacuum system was also used. McLeod gauge pressures of 10^{-6} mm of Hg or lower were achieved over the entire temperature range.

The oxygen purification system has been described (18).

Since specimens were supported by a 2-mil nickel-chromium alloy wire from the balance, a direct measurement of specimen temperature was impractical. Temperature was measured using a platinum and platinum-10% rhodium thermocouple which was fastened to the mullite tube, the head of the couple being at the center of the length of the specimen. Temperature was controlled by an L&N Speedomax controller to within ±2°C.

TABLE I. *Spectrographic analyses of nickel*

Element	Sponge, %	Strip, %
Cu	0.001	<0.0004
Ag	<0.0002	<0.0002
Mg	0.0002	0.0001–0.0005
Si	0.0005	0.0005–0.001
Fe	0.0002	0.0005–0.001
Mn	—	0.0001–0.001
Co	None	0.0002–0.002
Ca	—	0.00005–0.0001
Al	None	0.0002–0.002

Samples.—Samples were prepared from 0.013-cm thick high purity strip purchased from Johnson, Mathey and Company, London. Table I shows the spectrographic analyses of nickel sponge from which the strip was rolled.

The following specimen preparations were used:

Semidegassed abraded specimens.—Specimens were abraded through 4/0 polishing paper. The last two steps were made under purified kerosene. Specimens were then washed successively with soap and water, distilled water, petroleum ether, and absolute alcohol, and heated to the experimental temperature in a vacuum of 10^{-6} mm of Hg. Since they undergo degassing in this treatment, these samples are noted as semidegassed abraded specimens.

Vacuum annealed specimens.—Abraded specimens were annealed in a vacuum of 10^{-6} mm of Hg at 950°C for 24 hr and then lightly abraded under purified kerosene with 2/0 and 4/0 polishing papers. These are noted as degassed or vacuum annealed specimens.

Electropolished and hydrogen annealed.—Unabraded specimens were placed in a glycerol sulfuric acid bath at 62°C for 4 min at a current density of 1 amp/in.^{2} Specimens were then washed in distilled water and heated for 12 hr at 900°C in a hydrogen furnace.

All specimens weighed 0.6830 gram and had surface areas of about 10 cm^2. All samples were stored in a desiccator.

Results

High Vacuum Reaction

Behavior of nickel specimens in high vacuum was studied as a function of temperature to test (*a*) the quantity and composition of gas given off on heating to test temperature, and (*b*) extent of oxidation on heating to test temperature.

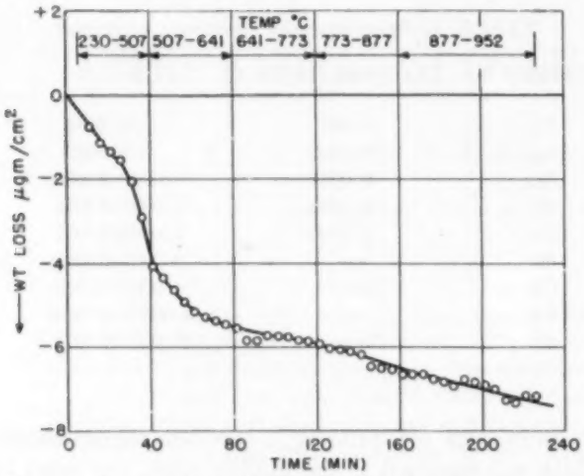

FIG. 1. Vacuum behavior of Ni 230°–952°C, vacuum < 10^{-6} mm of Hg.

Fig. 1 shows the weight loss vs. time curve for the vacuum heating of an abraded specimen from room temperature to 952°C. The gas liberated on heating to 952°C weighed 6.8 micrograms/cm². This corresponds to a weight percentage of 100 ppm. A mass spectrometer analysis of the gas showed a mass peak at 28 which indicated that the gas was either CO or N_2, but the small amount of gas available made it impossible to determine which. This experiment suggested that CO or N_2 was the largest impurity in the metal, and that experiments should be made to test the effect of gas content on rate of reaction.

A visual examination of the specimen showed no evidence of an appreciable oxide film as judged by its temper colors. Electron diffraction analyses showed a pattern of nickel and nickel oxide which suggested that the film was very thin. The oxide formed on heating over a period of 10–20 min to the test temperature would be much less than that formed in this test.

Reaction with Oxygen

The reaction was studied as a function of time, temperature, gas content, surface preparation, and preoxidation. Results are shown in Fig. 2–10. Weight change was calculated in micrograms/cm² with thickness of oxide being related to weight gain by the relation: 1 microgram/cm² = 62.9 Å. This was based on the assumptions that surface roughness ratio = 1 and that the oxide was NiO.

Time and temperature.—Fig. 2 shows the effect of time and temperature on rate of oxidation of semi-degassed specimens at an oxygen pressure of 7.6 cm of Hg over the temperature range of 400°–750°C and over a period of oxidation of 6 hr. In order to test the time variation of the parabolic rate law constant, experiments in the temperature range of 400°–550°C were made over a 30-hr period.

The shapes of the oxidation curves in Fig. 2 are

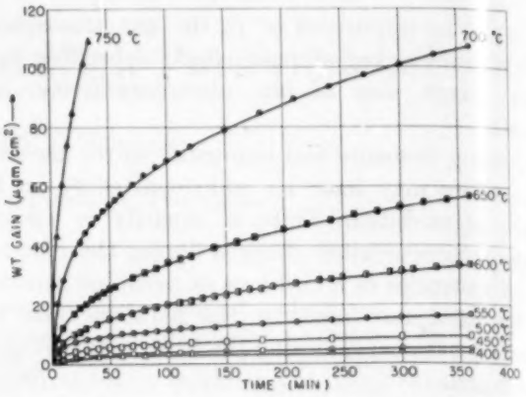

FIG. 2. Effect of temperature 400°–750°C, oxidation of nickel, 0.1 atm O_2.

TABLE II. *Oxide film thickness vs. oxide color*

Temp, °C	Thickness		Color
	μg/cm²	Å(ρ = 1)*	
400	7.15	450	Gray mottled with straw crystallites
425	11.05	695	Light blue
450	8.25	519	Blue
475	16.7	1050	Gray
500	16.7	1050	Gray
550	30.6	1920	Gray
600	33.8	2120	Gray
650	56.9	3580	Gray
700	107.2	6750	Gray
750	109.0	6850	Gray

* Surface roughness ratio = 1.

similar to those found with other metals (1-5). A strong temperature dependence is noted.

The colors of the oxides formed in the oxidation of nickel were not well developed for this thickness range. Table II shows a correlation of oxide color and thickness of the oxide. No evidence was found for cracking of oxide film during the reaction or on cooling.

Parabolic rate law correlation.—Many empirical rate laws have been suggested to explain the time behavior of oxidation. The parabolic rate law based on principles of formation and diffusion of nickel ion lattice defects has been the most successful equation for explaining oxidation. The equation states that $W^2 = At + C$. Here W is the weight gain, t is the time, and A and C are constants.

To test agreement of the experiments with theory, plots were made of the square of weight gain vs. time. Fig. 3 and 4 show two such plots for the 475° and 650°C runs. The 475°C plot shows the slope or parabolic rate law constant A continually decreasing with time, while the 650°C plot shows a smaller decrease with time. Values of A were tabulated in the figure captions to illustrate this effect.

Results in Table II are in agreement with the

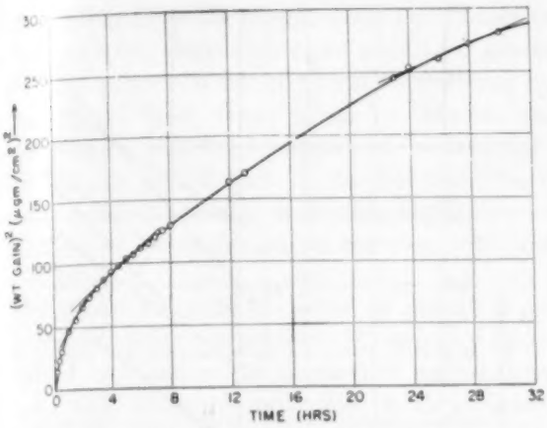

FIG. 3. Oxidation of Ni 475°C—0.1 atm O_2. Parabolic plot, 1–2 hr $A = 5.33 \times 10^{-15}$; 3–6 hr $A = 2.862 \times 10^{-15}$; 24–30 hr $A = 1.385 \times 10^{-15}$.

work of Wagner and Zimens (6) who found a similar behavior at 1000°C. The parabolic rate law can be fitted approximately to the data in the temperature range of 600°–750°C, while below 600°C it is impossible to make a reasonable fit. Experimentally, one must conclude that certain factors are operating between the metal and oxide which improve protective properties of the metal.

Temperature dependence.—The temperature dependence of the rate of oxidation has been interpreted by the Arrhenius law and the transition state theory (21). In previous papers the transition state theory was used for calculating entropy and heat of activation of the rate-controlling process. Since partition functions of the activated complex and normal lattice site were used in developing the theory, the free energy of activation ΔF^* was not defined by a physical process.

Following Zener's (22) restatement of the classical theory of diffusion, it was possible to clarify the processes involved in oxidation. In this theory, free energy of activation of diffusion, ΔF^*, was defined by the work required to produce a given distortion in the lattice. This enables one to apply rigorous thermodynamic operations on ΔF^* and to interpret the entropies and heats of activation. In this sense, the classical theory (22) has an advantage over the transition state theory, although the final equations are similar.

Processes occurring in oxidation are of two types: thermodynamic processes, such as the formation of vacancies which involves the free energy of formation of a vacancy, and rate processes, such as diffusion, which involve a free energy of activation. Thermodynamic functions for the rate processes are designated by an asterisk.

The theory of oxidation developed in an earlier paper (21) is used as a basis for deriving an equation for the parabolic rate law constant, A. The classical

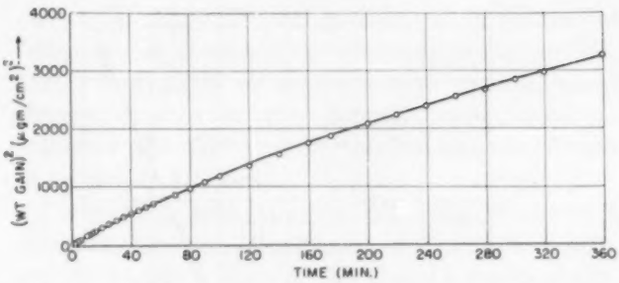

FIG. 4. Oxidation of Ni 650°C—0.1 atm O_2. Parabolic plot, 1–2 hr $A = 1.66 \times 10^{-13}$; 3–6 hr $A = 1.25 \times 10^{-13}$.

expression (22) is used for the diffusion coefficient, D, and the thermodynamic equilibria equations for the concentration of vacancies assuming the vacancies are formed by solution of oxygen in the NiO lattice.

$$A = \frac{2\gamma\nu a^2}{4^{1/3}} \Omega N (p_{O_2}{}^{1/6}) e^{(\Delta S^0/3 + \Delta S^*)/R} e^{-(\Delta H^0/3 + \Delta H^*)/RT} \quad [1]$$

Here $\Delta S^0/3$ is the standard entropy of formation of a vacancy and ΔS^* is the entropy of activation of diffusion; $\Delta H^0/3$ is the standard heat of formation of a vacancy, and ΔH^* is the heat of activation of diffusion; a is the distance between diffusion sites, ν is the frequency of vibration along the direction leading across the saddle configuration; Ω is the volume of oxide formed per ion; N is the number of ions per cm³; R is the gas constant; T the temperature; γ a coefficient determined by the geometry of the atomic jumps; and p is the pressure of oxygen. For vacancy diffusion in a face-centered cubic lattice, $\gamma = 1$.

Although ν has usually been given a value of 10^{13} vibrations per second, a better value can be obtained from the characteristic Debye temperature. Assumptions made and details of the calculations are given in Appendix I. The results show a value of 8.5×10^{12} vibrations/sec for the Ni^{++}—Ni^{++} bond in NiO. Calculations of Appendix II show that presence of a vacancy has only a minor effect on vibration frequencies of oxygen ions in the NiO lattice. A similar small effect would be expected for the Ni^{++}—Ni^{++} bond. The normal lattice distance between Ni^{++}—Ni^{++}, 2.96 Å, is used for a.

Errors in choosing ν and a are less than experimental errors in the calculation of $(\Delta H^0/3 + \Delta H^*)$ from the data.

Substituting the values of the constants, equation [1] becomes

$$A = 7.5 \times 10^{-3} e^{(\Delta S^0/3 + \Delta S^*)/R} e^{-(\Delta H^0/3 + \Delta H^*)/RT} \quad [2]$$

Using this equation, the sums $(\Delta H^0/3 + \Delta H^*)$ and $(\Delta S^0/3 + \Delta S^*)$ are obtained. Unfortunately, there is no way to determine the separate quantities within the sums from oxidation studies alone. However, the entropy of formation of the vacancies can be

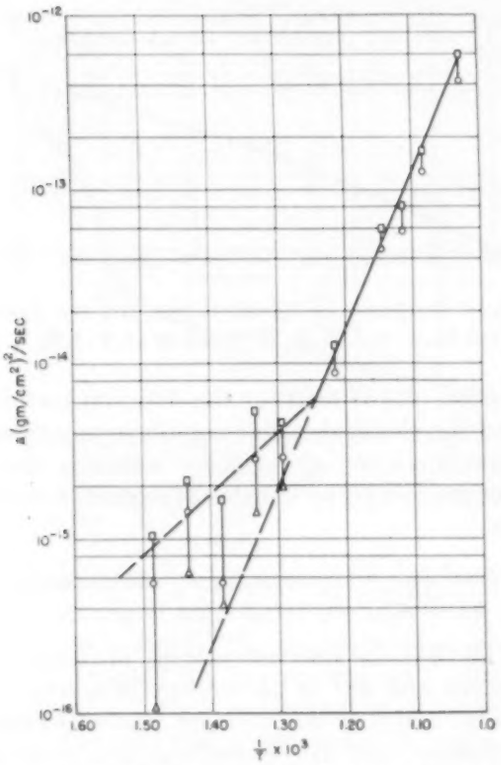

FIG. 5. Oxidation of semidegassed Ni; log plot A vs. $1/T \times 10^3$. □—1–2 hr; ○—3–6 hr; △—24–30 hr. $\Delta H^* = 41{,}200$ cal/mole.

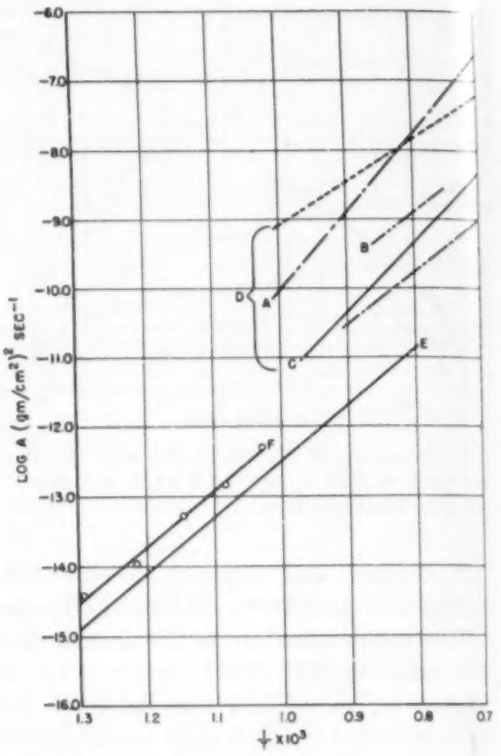

FIG. 6. Oxidation of Ni; log A vs. $1/T \times 10^3$. Curve A—Goldbeck; curve B—Pilling and Bedworth; curve C—Matsunaga; curve D—curves from Kubaschewski and Goldbeck; curve E—Moore [calculated to (gm/cm²)² sec⁻¹]; curve F—present work.

calculated, and it is therefore possible to evaluate ΔS^*. Values calculated from experimental data can be compared with values calculated theoretically from thermodynamic considerations. Such a comparison makes possible the testing of the mechanism of vacancy formation and, in a larger sense, the reaction mechanism.

Fig. 5 shows a plot of the logarithm of A vs. $1/T$. Since the rate constants change with time, these constants were evaluated and tabulated for the time periods of 1–2 hr, 3–6 hr, and in the lower temperature range at 24–30 hr. As was previously noted, a large uncertainty was found for the A values below 550°C. The data can be fitted by a straight line above 550°C. Below 550°C the time variation of A makes it impossible to determine the slope. However, values of A determined in the time range of 24–30 hr approach values given by an extrapolation of the straight line.

A heat of activation of 41,200 cal/mole was calculated from the slope for the temperature range of 500°–700°C. This value is nearly in agreement with the work of Moore (10).

The temperature independent factors, $e^{(\Delta S^0/3+\Delta S^*)/R}$ were evaluated from equation [2]. Table III shows a summary of values of the parabolic rate law constants for 1–2 hr and 3–6 hr oxidation periods, average value of the parabolic rate law constants for the two periods, and heats, entropies, and free energies of the rate-controlling process in oxidation of nickel. Negative entropy values of −5.72 to −6.47 were calculated.

Comparison with the literature.—Fig. 6 shows a comparison of log A vs. $1/T$ with other values in the literature. The curves given by Kubaschewsky and Goldbeck (9) summarizing older work at high temperatures were included. Where possible, the original source of data was given. Results of this study differ by a factor of 10 to 1000 from older results. How-

TABLE III. *Parabolic rate law constants, entropies, heats, and free energies of activation for the oxidation of semidegassed nickel*

Temp, °C	A (1–2 hr) $(g/cm^2)^2/sec$	A (3–6 hr) $(g/cm^2)^2/sec$	A (avg) $(g/cm^2)^2 sec$	$\frac{(\Delta S^0 + \Delta S^*)}{3}$ cal/mole/°C	$\frac{(\Delta H^0 + \Delta H^*)}{3}$ cal/mole	$-T\frac{(\Delta S^0 + \Delta S^*)}{3}$ cal/mole	ΔF^* cal/mole
550	1.28×10^{-14}	8.8×10^{-15}	1.08×10^{-14}	−5.92	+41,200	+4870	+46070
600	5.95×10^{-14}	4.51×10^{-14}	5.23×10^{-14}	−5.72	+41,200	+4990	+46190
625	8.00×10^{-14}	5.65×10^{-14}	6.83×10^{-14}	−6.47	+41,200	+5810	+47010
650	1.66×10^{-13}	1.25×10^{-13}	1.46×10^{-13}	−6.07	+41,200	+5600	+46800
700	5.96×10^{-13}	4.19×10^{-13}	5.08×10^{-13}	−6.02	+41,200	+5860	+47060

ever, agreement with recent work by Moore (10) in temperature dependence is good. In absolute value, the present work gives values differing by a factor of 2.5 from those given by Moore. Since Moore used preoxidized samples in an attempt to eliminate the initial part of the reaction, the difference between results is in the right direction. The effect of preoxidation on reaction rate is discussed later.

The reason for wide deviation in results is probably due to impurities present (13) in many samples of nickel used and in the method of surface preparation. The effect of impurities is to increase or decrease the number of vacancies and thus the rate of oxidation, the particular effect depending upon size, charge, and electronegativity of the added ion. Horn (13) has shown that Th, Zr, Nb, Ce, W, Ti, Ca, Au, Cr, Mn, Ta, Mo, Cu, Al, and Si increase the rate of reaction at 900°C. However, to study the effect of impurities from a fundamental point of view, it is necessary to measure the rate of reaction at a series of compositions of one alloying component at a number of temperatures in order to see the effect of impurities on ($\Delta H^0/3 + \Delta H^*$) and ($\Delta S^0/3 + \Delta S^*$). If the process of formation of vacancies is changed by addition of impurities, $\Delta H^0/3$ and $\Delta S^0/3$ of the formation process would change because of the different mechanism involved, while ΔH^* and ΔS^* of diffusion should not be so greatly affected.

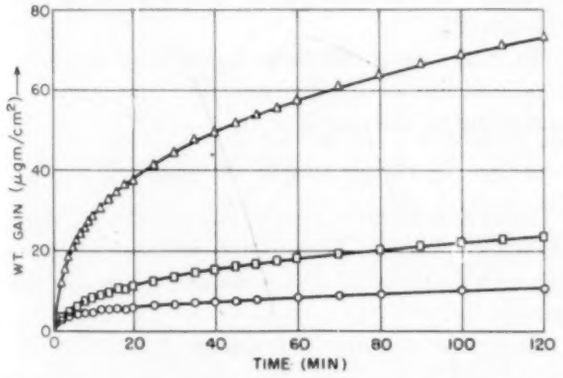

FIG. 7. A comparison of the oxidation of Ni, Cr, and Ni-Cr V at 700°C—7.6 0.1 atm O_2. △—Ni $A = 5.96 \times 10^{-13}$; □—Cr $A = 6.38 \times 10^{-14}$; ○—Ni–Cr V $A = 1.17 \times 10^{-14}$.

Comparison with other metals.—Fig. 7 shows a comparison of rate of oxdiation of nickel, chromium, and 80-Ni, 20-Cr alloy at 700°C and 0.1 atm of oxygen. In order of increasing rate of reaction the metals show the following relation: 80-Ni, 20-Cr alloy < chromium < nickel.

Effect of degassing.—Two sets of samples were tested, semidegassed, and degassed. Procedures for preparing the samples have been described. Fig. 8 shows a comparison of typical results. Degassed specimens show an eight- to tenfold increase in reaction rate for oxidation experiments below 500°C, while at temperatures above 600°C the increase is of the order of two- to threefold. Decrease of the effect with temperature is to be expected from the nature of the degassing curve (Fig. 1).

Experiments suggest that N_2 or CO in the nickel oxide lattice effectively reduces the number of nickel ion vacancies and thus reduces rate of oxidation. This effect will be reported in more detail in a future paper.

Fig. 9 shows the effect of electropolishing and annealing of the metal on rate of reaction. A strong increase in rate of reaction was observed at several temperatures. This increase may be explained in three ways: (*a*) effect of impurities left on the metal from the polishing bath, (*b*) possible addition of gases to the metal during electropolishing, and (*c*) changed nature of the surface resulting from electropolishing. Again, experimental difficulties make it impossible to study this effect thoroughly.

Effect of preoxidation.—A study of the effect of preoxidation is important for two reasons. First, it is

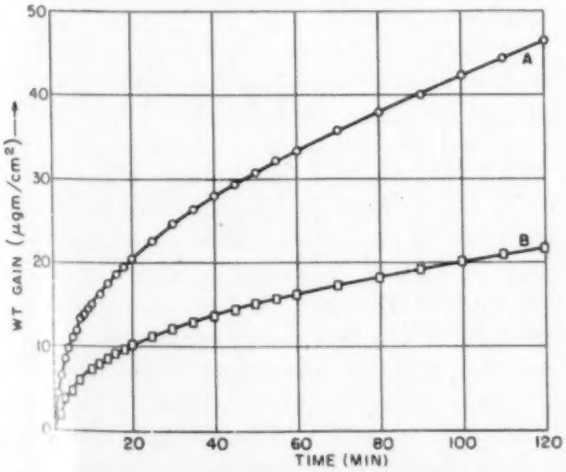

FIG. 8. Oxidation of Ni 600°C—0.1 atm O_2. Curve A—degassed; curve B—semidegassed.

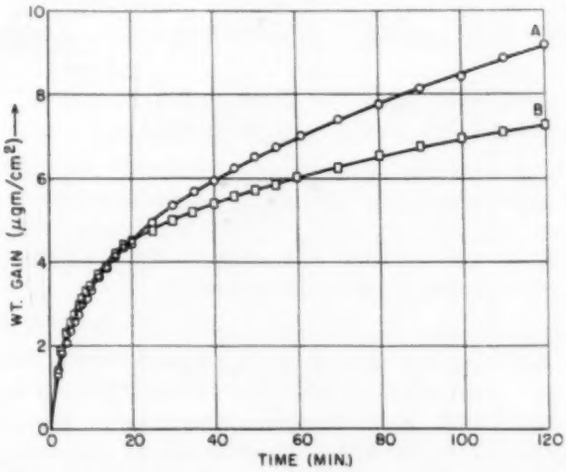

FIG. 9. Effect of pretreatment. Curve A—electropolished and annealed; curve B—abraded through 4/0.

of interest to test whether a set of experiments based on a preliminary preoxidation treatment would give oxidation curves similar to those determined at a single temperature. Second, the use of preoxidized surfaces may make possible the study of the effect of geometrical properties of oxide on rate of reaction. A preliminary set of experiments was made in this work. A series of specimens was oxidized at 600°C and 0.1 atm of O_2 to give an oxide of 15 micrograms/cm². After the oxygen was pumped off, the specimen was heated or cooled to the reaction temperature and a second oxidation made at the new temperature.

To evaluate the effect of preoxidation, the rate of reaction, dW/dt, was calculated at a total thickness W and compared to a similar calculation for a sample oxidized at a single temperature. Results show that preoxidation treatment gives smaller rates of reaction. Fig. 10 shows a parabolic plot of such a comparison at 750°C, while Table IV shows a summary of the effect of preoxidation on the parabolic rate law constant at temperatures of 550°–750°C. The effect was an important one and depends on the temperature difference between preoxidation and subsequent oxidation. These results

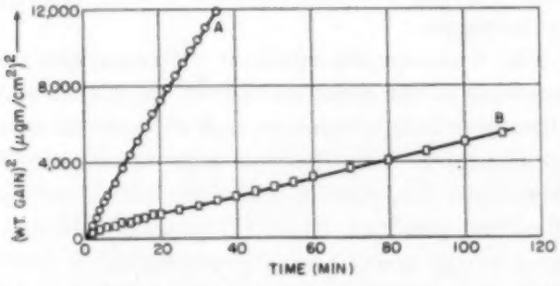

FIG. 10. Effect of preoxidation (600°C—7.6 cm O_2) on oxidation of Ni 750°C—0.1 atm O_2 abraded through 4/0. Curve A—no film; curve B—15 μg/cm².

TABLE IV. *Effect of preoxidation on parabolic rate law constants*

Temp, °C	A (g/cm²)²/sec	Condition	Ratio of $\frac{A \text{ normal}}{A \text{ preoxidized}}$
550	8.7×10^{-15}	Normal	1.39
550	6.25×10^{-15}	Preoxidized*	
600	6.8×10^{-14}	Normal	1.61
600	4.21×10^{-14}	Preoxidized*	
650	1.84×10^{-13}	Normal	1.79
650	1.035×10^{-13}	Preoxidized*	
700	9.32×10^{-13}	Normal	3.9
700	2.40×10^{-12}	Preoxidized*	
750	6.05×10^{-12}	Normal	7.6
750	7.96×10^{-13}	Preoxidized*	

* Preoxidized to 15 μg/cm².

may explain in part the difference in the results of Moore (10) and those of this work.

It should be noted that the effect depends on the difference at a given thickness between the physical structure of oxide film of the preoxidized specimen and that of the film produced at a single temperature. This is discussed in more detail later.

THEORETICAL

Four topics are considered: (*a*) experimental entropy of activation of diffusion, (*b*) theoretical entropy of activation of diffusion, (*c*) time dependence of the parabolic rate law, and (*d*) nature of the preoxidation effect.

Entropy of Activation of Diffusion

Previous studies on oxidation of metals (1–5) have shown that in many cases negative entropies of activation were observed. These values are in contrast to positive values which are predicted and found for self-diffusion processes in metals (22). However, the process of formation of vacancies in a metal occurs by removal of a metal atom from the interior to the surface. From simple considerations of loosening of the binding of metal atoms by the vacancy, this process should give a positive entropy change (22).

In NiO, vacancies were formed by a process of condensation of oxygen gas into the oxide lattice according to the reaction

$$\tfrac{1}{2}\ O_2\ (g) \rightleftharpoons O^{2-} + \square_e + 2\oplus \qquad [3]$$

to form new oxide, a vacant lattice site, $\square_e$, and two positive holes, $\oplus$. Essentially, we are condensing a gas to a solid oxide and a negative entropy change results.

Since the entropy of vacancy formation can be calculated, it was possible to determine the entropy of activation of the diffusion process. From elastic constant considerations, Zener (22) suggested that positive values should be found for the entropy of activation of diffusion.

The entropy of vacancy formation can be evaluated from an analysis of equation [3] if it is assumed that positive holes reside on Ni^{+++} and that vacancies and positive holes are dissociated.

Simple electrostatic calculations show the attractive energy between a positive hole and a cation vacancy to be of the order of 10 times the thermal energy at 1000°K, assuming a dielectric constant of 10 for NiO. However, for low concentrations the $T\Delta S^0$ term in the free energy expression would be larger than ΔH^0 and thus make possible dissociation, since many sites were available for the cation and positive hole to occupy. Assumption of dissociation has been confirmed by experimental studies of the oxygen pressure dependence of conductivity (23)

and rate of oxidation (24) of nickel. At higher vacancy concentrations, association would be expected to occur.

Details of the entropy calculations are given in Appendix II. Results show a negative entropy of -7.5 cal/mole/°C to be associated with formation of one mole of vacancies.

Subtracting this value from the over-all experimental entropy term ($\Delta S^0/3 + \Delta S^*$) gives a value of 1.5 cal/mole/°C for the value of ΔS^*, the entropy of activation of diffusion. This value can now be compared to the theoretical value.

Theoretical Value for Entropy of Activation of Diffusion

Zener (22) has used the sign of the value for entropy of activation to determine whether diffusion is occurring through the lattice or at grain boundaries or other short-circuiting paths. Since a positive value of entropy of activation for diffusion was obtained for nickel oxidation, this would suggest that diffusion was occurring mainly through the lattice. To make such a prediction, it is necessary to ask what is the theoretical value of ΔS^*. This value may be estimated from theoretical considerations from the equation (22).

$$\Delta S^* = \frac{\lambda \beta \Delta H^*}{T_m} \qquad [4]$$

Here λ is a numerical coefficient less than 1 and represents the fraction of free energy of activation or work that goes into straining the lattice. ΔH^* is the heat of activation of diffusion. T_m is the melting temperature of NiO, and β is defined as

$$\beta = -d(\mu/\mu_0)/d(T/T_m) \qquad [5]$$

Here β is a dimensionless quantity involving the temperature coefficient of the appropriate elastic modulus μ, μ_0 is the value of μ extrapolated to absolute zero of temperature.

Zener (22) has determined the value of β from the temperature coefficient of Young's modulus or from the temperature coefficient of the shear modulus. Since data on the temperature coefficient of the elastic modulus were not available for oxides, β has been evaluated from the statistical thermodynamic expression for specific heat and the simple relationship between compressibility of a solid and characteristic frequency of the atoms. The calculations are presented in detail in Appendix III. β was found to have the value 0.345, while λ was assumed to take the value of 0.55.

It is now possible to place upper limits on values that ΔS^* of diffusion may take for NiO. A unique value was not possible to calculate since experimental data gave only the sum of the heat for formation of vacancies and the heat of activation for diffusion, while equation [1] requires ΔH^* of diffusion alone. However, a maximum value can be placed on ΔS^* by assuming that experimental heat of activation is equal to heat of activation of diffusion. Thus, assuming $\Delta H^* = 41{,}200$ cal/mole, ΔS^* is 3.3.

Assuming a more reasonable value for the ΔH^* of diffusion of 20,600 cal/mole, ΔS^* is equal to 1.7. Since the corrected experimental value is of the order of 1.5, agreement is well within experimental errors and assumptions made in calculations. An agreement of 1 in the value of ΔS^* means an agreement of 1.65 in the value of the parabolic rate law constants. Agreement between theory and experiment regarding the sign of ΔS^* suggests that, in high temperature oxidation of nickel, diffusion probably occurs mainly in the lattice and not at grain boundaries or other defects.

During the early part of the reaction in which the parabolic rate law does not apply and for low temperature experiments, the reaction occurs probably by grain boundary diffusion. This interpretation was suggested in a previous paper (26), although a detailed analysis of the entropy of vacancy formation was not included. Conditions for transition from grain boundary growth to growth by diffusion through the lattice depend upon the grain boundary area of oxide particles and upon the particular values of ΔH^* and ΔS^* for the processes.

Time Dependence of Parabolic Rate Law Constant

Two explanations may be given. The first is based on the assumption that concentration of impurities within the oxide is changing as oxidation proceeds, thus changing the number of vacancies for diffusion. Horn (13) has shown that most of the common alloying elements increase the reaction rate. As the reaction proceeds, the tendency is for impurity concentration to decrease because of the limited amount of material available in the metal. This factor could account for the decreasing of the parabolic rate law constant observed by Wagner and Zimens (6) and in this work.

The second explanation is based on assumption of a grain boundary diffusion mechanism for early stages of reaction. As the film thickens, oxide crystallites grow, and at some thickness the influence of grain boundary diffusion becomes small compared to lattice diffusion.

Certain evidence supports this point of view. Previous studies (27) on size of oxide grains in thin oxide films showed that oxide grains changed in size during reaction and that such changes were a function of both temperature and time of oxidation. In the case of Fe oxidized at 250°C for 5 min, the average particle size of oxide crystallites was 350 Å.

This increased to 1200 Å when oxidation was carried out for 30 min. Since the grain boundary area decreases as oxide crystallites grow, the parabolic rate law constant also decreases until at some thickness the reaction is controlled by lattice diffusion.

Nature of the Preoxidation Effect

The preoxidation effect is very difficult to explain if we accept the interpretation that the reaction is essentially controlled by lattice diffusion and that entropy calculations are correct. One may postulate that impurities may concentrate in the oxide during preoxidation treatment, which tends to lower oxidation rate at higher temperatures. Further experimentation, however, is necessary to understand and to explain this phenomenon.

Summary

Reaction of high purity nickel with oxygen was studied using the vacuum microbalance method over the temperature range of 400°–750°C. Colored oxide films were formed even at the lowest temperatures after 30-hr oxidation periods.

A comparison of rate of oxidation showed that nickel oxidizes faster than chromium and 80-Ni, 20-Cr alloy. Data were fitted to the parabolic rate law, and it was shown that the rate law constant decreases with extent of oxidation, the greatest deviations occurring in the temperature range of 400°–550°C. For the temperature range of 550°–700°C, a log A vs. $1/T$ plot gave a straight line and a calculated heat of activation of 41,200 cal/mole.

A comparison with previous work in the literature showed the rate of oxidation of high purity nickel to be 1/10 to 1/1000 of that which other workers found on less pure nickel. The effect of impurities on the oxidation rate was discussed.

Using the classical theory of diffusion, entropies and free energies of activation of the rate-controlling process were calculated and compared to those of other metals. Experimental entropies of activation of −6.0 were corrected for the entropy of formation of nickel ion vacancies to give an entropy of activation of diffusion of +1.5 cal/mole/°C. On the basis of certain assumptions, theoretical considerations suggest that the entropy of activation for diffusion may have a maximum value of 3.3 eu, while a more reasonable assumption leads so a value of 1.7 eu.

This agreement of theory with experiment suggests that in the temperature range of 600°–700°C the reaction is controlled mainly by lattice diffusion.

The effect of a preoxidation treatment on rate of oxidation was studied. It was shown that preoxidation at 500°C greatly affects the rate of reaction at higher temperatures.

Acknowledgments

The authors are indebted to Dr. C. Zener and Dr. R. Heikes for their helpful comments and suggestions on the classical theory of diffusion and the interpretation of negative and positive entropies of activation.

APPENDIX I

Frequency of Vibration of Ni^{++}—Ni^{++} Bond

Assume that the atoms in NiO are vibrating as harmonic oscillators and interacting according to Hooke's law, and that the calculated frequency is characteristic of movement of Ni^{++} ions through the NiO lattice. The assumption of harmonic oscillations is a reasonable one since the atoms spend the great bulk of their time in these energy states.

The value of ν_{max} is calculated from the characteristic Debye temperature:

$$\theta_D = \frac{h\nu_{max}}{k} \qquad [6]$$

Here ν is the maximum frequency, h is Planck's constant, and k is Boltzman's constant. For NiO, θ_D is 404 (25).

From the Debye temperature, $\nu_{max} = 8.5 \times 10^{12}$.

APPENDIX II

Entropy of Vacancy Formation

Change in entropy can be estimated from three considerations: (*a*) change associated with condensation of oxygen gas into the NiO lattice to form a new oxide following equation [3] and assuming no distortion; (*b*) change associated with distortion of the NiO lattice by cation vacancy alone; (*c*) change associated with distortion of the NiO lattice due to formation of two positive holes (Ni^{+++} sites).

Change in Entropy Due to Condensation of Oxygen

At 1000°K the entropy of $\frac{1}{2}$ O_2 (g) (28, 29) is calculated to be 29.10 cal/mole/°C, while the entropy of NiO (28, 29) is calculated to be 18.08 cal/mole/°C.

The entropy, S, of $0^{=}$ in the NiO (s) lattice is assumed to be $\frac{1}{2}$ the entropy of NiO (s) or 9.04 cal/mole/°C.

Entropy Change Due to Distortion of the NiO Lattice

If a Ni^{++} is removed from the NiO lattice and two positive holes are formed (Ni^{+++} sites), the six oxygen ions surrounding each of these sites are disturbed. Assume that removal of a Ni^{++} ion results in a displacement δ_e of oxygen ions toward and in line with adjacent Ni^{++} ions, while formation of a positive hole results in a displacement δ_p of oxygen ions toward and in line with the positive hole. The effect of both displacements to a first approximation is to increase the binding of the oxygen ion to its nearest neighbors. This results in a decrease in entropy of oxygen ions in the lattice of NiO.

Relation between α_M and b.—In the calculations that follow it is necessary to calculate the relationship between the Madelung constant, α_M, and the constant b of the repulsive energy terms.

The equation for the lattice energy W of a mole of NiO crystal, neglecting Van der Waals energy and the zero point energy (31), is

$$W = N\left[\frac{-4e^2\alpha_M}{r_0} + 6w_{+-}(r) + 6w_{--}(r) + 6w_{++}(r)\right] \qquad [7]$$

Here N is Avogadro's number, e is the electronic charge, and r_0 is the cation-anion distance. The first term refers to the electrostatic energy while the terms $w_{++}(r)$, $w_{--}(r)$, and $w_{+-}(r)$ refer to the repulsive or overlap energy terms of the respective bonds.

Each of the $w(r)$ terms is expressed as

$$w(r) = Cb \exp [(r_1 + r_2)/\rho] \exp [(-r/\rho)] \quad [8]$$

Here r is the distance between ions, r_1 and r_2 are ionic radii of the Ni^{++} and $O^{=}$, respectively, b is a fixed constant if C is defined by

$$C = \left(1 + \frac{Z_1}{n_1} + \frac{Z_2}{n_2}\right) \quad [9]$$

Here Z_1 and Z_2 are valences of the ions, and n_1 and n_2 are the number of electrons in the outer shell. Under these conditions, $\rho = 0.345 \times 10^{-8}$ cm. For NiO, $C_{+-} = 1$, $C_{--} = 0.5$, and $C_{++} = 1.5$.

Using 0.74 Å as the ionic radius of Ni^{++} and 1.35 Å for $O^{=}$, we have the following expression for the lattice energy:

$$W = N\left[\frac{-4e^2\alpha_M}{r_0} + 6C_{+-}b \exp[-(r_0 - 2.09)/\rho] + 6C_{--}b \exp[-(\sqrt{2}\, r_0 - 2.70)/\rho] + 6C_{++}b \exp[-(\sqrt{2}\, r_0 - 1.48)/\rho]\right] \quad [10]$$

The relation between α_M and b is found by differentiating and setting $W(r) = 0$. The result shows

$$b = \frac{0.49e^2\alpha_M\rho}{r_0^2} \quad [11]$$

Calculation of the displacement δ_c for a cation vacancy.— Total energy of an ionic lattice, W, containing a cation vacancy can be expressed by the following equation:

$$W = W_0 + \Delta W_1 + \Delta W_2 \quad [12]$$

Here W_0 is the initial energy without a vacancy, ΔW_1 is the change in energy due to a displacement δ_c of oxygen ions surrounding the vacancy, and ΔW_2 is the change in energy due to removing the Ni^{++} ion with the $O^{=}$ ions in the displaced position.

Change in the electrostatic energy part of ΔW_1 associated with displacement alone can be shown to be negligible by a simple example. Consider the energy associated with an oxygen ion in the three ion system—Ni^{++}—$O^{=}$—Ni^{++}—. Let the original cation-anion distance be r_0 and displace the ion a distance δ. If the two Ni^{++} are fixed, then change in the electrostatic energy part of ΔW_1 is

$$\Delta W_1 \text{ (elec)} = \frac{-4e^2}{r_0 - \delta} + \frac{4e^2}{r_0} - \frac{4e^2}{r_0 + \delta} + \frac{4e^2}{r_0} \quad [13]$$

Expanding,

$$\Delta W_1 \text{ (elec)} = \frac{-4e^2}{r_0}\left(\frac{2}{1 - (\delta/r_0)^2}\right) + \frac{8e^2}{r_0} = 0 \text{ for small } \delta/r_0 \quad [14]$$

Initial total energy of an ionic lattice remains in the form W_0 since it does not contain any term involving the displacement δ_c. To evaluate ΔW_1, refer to Fig. 11A which shows a plane through the NiO lattice containing the vacancy together with spacings of nearest neighbor ions. Since it has been shown that the electrostatic part of ΔW_1 is negligible, it is necessary only to consider the following overlap repulsive terms in ΔW_1: (*a*) interaction between $O^{=}$ at A and Ni^{++} at B; (*b*) interaction between $O^{=}$ at A and 4 $O^{=}$ in the plane of Ni^{++} at B and perpendicular to line AB; (*c*) interaction between $O^{=}$ at A and $4Ni^{++}$ in the plane of A and perpendicular to line AB; (*d*) interaction of $O^{=}$ at A and 4 $O^{=}$ in the plane of the vacancy at C and perpendicular to line AB; and (*e*) interaction between $O^{=}$ at A and Ni^{++} at C. Part of the latter term drops out on removing Ni^{++} and forming a vacancy.

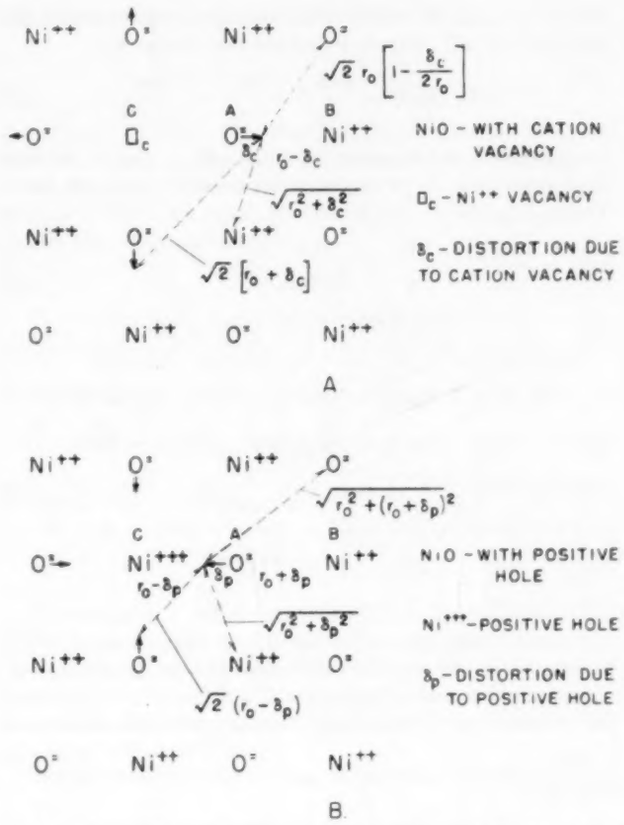

FIG. 11. Effect of vacancy and positive hole on nickel oxide lattice.

$$\begin{aligned}\Delta W_1 = {} & 6C_{+-}b[\exp -(r_0 - \delta_c - r_1 - r_2)/\rho - 1] \\ & + 24\, C_{--}b\left[\exp -\left(\sqrt{2}\, r_0\left(1 - \frac{\delta_c}{2\, r_0}\right) - 2r_2\right)\Big/\rho - 0.47\right] \\ & + 24\, C_{+-}\, b[\exp -(\sqrt{r_0^2 + \delta_c^2} - r_1 - r_2)/\rho - 1] \\ & + 12\, C_{--}\, b[\exp -(\sqrt{2}(r_0 + \delta_c) - 2\, r_2)/\rho - 0.47] \\ & + 6\, C_{+-}\, b[\exp -(r_0 + \delta_c - r_1 - r_2)/\rho - 1]\end{aligned} \quad [15]$$

This equation represents change in energy produced by one vacancy, assuming 6 $O^{=}$ are displaced for each vacancy.

Change in energy ΔW_2 due to removing the Ni^{++} ion can now be evaluated. The electrostatic energy change for one vacancy and six disturbed oxygen ions is evaluated from the potential at Ni^{++}.

$$V = \frac{-2e\alpha_M}{r_0} + \frac{12e}{r_0} \frac{-12e}{r_0 + \delta_c} \quad [16]$$

The first term is the Madelung potential while the latter terms represent the effect of $O^{=}$ on the potential at Ni^{++} at the new distance, $r_0 + \delta_c$. The value of the electrostatic energy to remove the Ni^{++} after the $O^{=}$ ions have been dis-

placed is equal to $-2eV$. Thus, change in electrostatic energy part of ΔW_2 due to removing the charge is

$$\Delta W_2 \text{ (elec)} = \frac{4e^2\alpha_M}{r_0} - \frac{24e^2}{r_0} + \frac{24e^2}{r_0 + \delta_c} \qquad [17]$$

Change in repulsive energy terms in ΔW_2 is due to the fact that removing Ni^{++} removes its repulsive energy term. Thus,

$$\Delta W_2 = \frac{4e^2\alpha_M}{r_0} - \frac{24e^2}{r_0} + \frac{24e^2}{r_0 + \delta_c} - 6C_{+-}\, b\,[\exp -(r_0 + \delta_c - r_1 - r_2)/\rho - 1] \qquad [18]$$

Substitute ΔW_1 and ΔW_2 in equation [12], and

$$\begin{aligned} W = W_0 &+ 6C_{+-}\, b[\exp -(r_0 - \delta_c - r_1 - r_2)/\rho - 1] \\ &+ 24\, C_{--} b[\exp -(\sqrt{2}\, r_0(1 - \delta_c/2r_0) - 2r_2)/\rho - 0.47] \\ &+ 24\, C_{+-} b[\exp -(\sqrt{r_0^2 + \delta_c^2} - r_1 - r_2)/\rho - 1] \\ &+ 12\, C_{--} b[\exp (\sqrt{2}(r_0 + \delta_c) - 2r_2)/\rho - 0.47] - 6C_{+-} b \\ &\frac{4e^2\alpha_M}{r_0} - \frac{24e^2}{r_0} + \frac{24e^2}{r_0 + \delta_c} \end{aligned} \qquad [19]$$

δ_c is determined by taking the derivative of W with respect to δ_c and setting this equal to zero. Carrying out differentiation and substituting $C_{+-} = 1$, $C_{--} = 0.5$, and the value of b in terms of α_M from [11] gives the expression

$$\begin{aligned} \frac{4.65}{(1 + \delta_c/r)^2} &= \exp \delta_c/\rho \\ &+ \sqrt{2} \exp -[2.96(1 - \delta_c/2 \times 2.10) - 2.70]/\rho \\ &- \sqrt{2} \exp -[2.96 + \sqrt{2}\,\delta_c - 2.70]/\rho \end{aligned} \qquad [20]$$

Solving this equation by trial and error, $\delta_c/r_0 = 0.15$.

Calculation of the displacement δ_p for a positive hole.—In this calculation the method just above is followed. Energy of the disturbed lattice is set down in terms of the displacement δ_p. Fig. 11B shows a plane through the NiO lattice containing the positive hole with spacings indicated for nearest neighboring ions.

Since 6 $O^=$ were affected by each positive hole, the following is the equation for total energy of the disturbed lattice with two positive holes present.

$$\begin{aligned} W = &12C_{+-}\, b\,[\exp -(r_0 + \delta_p - r_1 - r_2)/\rho - 1] \\ &+ 12C_{+-} b\,[\exp -(r_0 - \delta_p - r_2 - r_3)/\rho - 1] \\ &+ 48C_{--} b\,[\exp -(\sqrt{r_0^2 + (r_0 + \delta_p)^2} - 2r_2)/\rho - 1] \\ &+ 24C_{--} b\,[\exp -(\sqrt{2}\,(r_0 - \delta_p) - 2r_2)/\rho - 1] \\ &+ 48C_{+-} b\,[\exp -(\sqrt{r_0^2 + \delta_p^2} - r_1 - r_2)/\rho - 1] \\ &- \frac{24e^2}{r_0} + \frac{24e^2}{r_0 - \delta_p} + \frac{4e^2\alpha_M}{r_0} \end{aligned} \qquad [21]$$

The term r_3 represents the radius of the Ni^{+++} ion. δ_p is determined by taking the derivative with respect to δ_p and setting this equal to zero.

Differentiating and substituting $C_{+-} = 1$, $C_{--} = 0.5$, C_{+-} for $Ni^{+++} = 1.125$, and b in terms of A,

$$\begin{aligned} \frac{2.34}{(1 - \delta\rho/r_0)^2} &= -\exp[-\delta_p/\rho] + 1.125 \exp(\delta_p - 0.13)/\rho \\ \frac{-2(2.10 + \delta_p)}{\sqrt{4.40 - (2.10 + \delta_p)^2}} &\exp -(\sqrt{[4.40 + (2.10 + \delta_p)^2} \\ &- 2.70]/\rho + 1.41 \exp(1.41\delta_p - 0.26)/\rho \end{aligned} \qquad [22]$$

Solving by trial and error, there results $\delta_p/r_0 = 0.11$.

Entropy of formation of a cation vacancy.—Entropy of the NiO lattice is related to the frequency of vibration, ν, by

$$S = R \ln Q_v + RT \frac{d \ln Q_v}{dT} \qquad [23]$$

Here Q_v is the vibration partition function, $Q_v = kT/h\nu$, and k is Boltzman's constant.

Substituting and differentiating,

$$S = R \ln \frac{kT}{h\nu} + R \qquad [24]$$

Change of entropy of the NiO lattice due to distortion caused by presence of vacancies and positive holes is given by the relation

$$S = R \ln \frac{\nu_D}{\nu_N} \qquad [25]$$

Here, ν_D refers to the frequency of vibration in the disturbed state and ν_N to the normal state.

Frequencies are calculated from the equation

$$\nu = \frac{1}{2\pi}\sqrt{\frac{\kappa}{m}} \qquad [26]$$

where κ is the force constant and m the mass of the vibrating ions in the lattice. The force constant was calculated from the second derivative of total energy with respect to ΔX.

Lattice situations for force constant calculations are shown in Fig. 12A. ΔX represents the new displacement. Second derivatives of the normal and disturbed lattices $\vec{W}(N)$ and $\vec{W}(D)$ were evaluated at r_0 and $r_0 + \delta$, respectively.

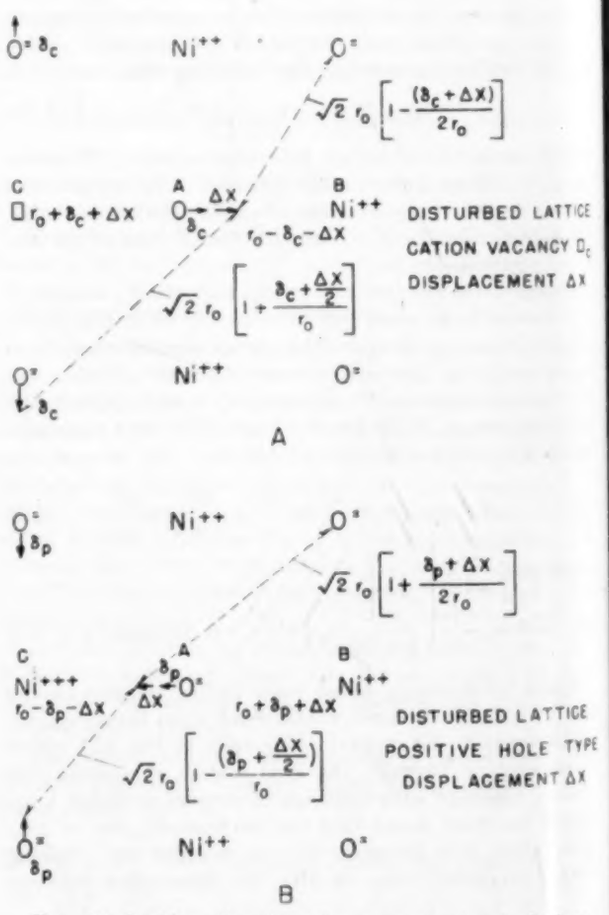

FIG. 12. Lattice situations force constant calculations

Repulsive energy terms in the total energy expression for disturbed and normal lattice cases were set up in a similar manner to that in the second section. Repulsive energy terms between nearest neighbors were used.

The following results were found:

$$\tilde{W}(N) = 2.70\frac{b}{\rho^2} = \kappa_N, \qquad [27]$$

and

$$\tilde{W}(D) = 3.39\frac{b}{\rho^2} = \kappa_D. \qquad [28]$$

Since

$$\frac{\nu_D}{\nu_N} = \left(\frac{\kappa_D}{\kappa_N}\right)^{1/2} = \left(\frac{3.39}{2.70}\right)^{1/2} = 1.12, \qquad [29]$$

and since 6 $O^=$ were involved, $\Delta S_e = -6R \ln \nu_D/\nu_N = -1.34$ cal/mole/°C.

Entropy of positive hole formation.—Following the method of the preceding section, consider the total energy of the lattice with positive holes present. Lattice situations for force constant calculations are shown in Fig. 12B. Again, ΔX represents the new displacement. Setting up the total energy expression in a similar manner to that of the third and fourth sections, and differentiating twice with respect to ΔX,

$$\tilde{W}(D) = 2.92\frac{b}{\rho^2}$$

$$\frac{\tilde{W}(D)}{\tilde{W}(N)} = \frac{2.92}{2.70} = 1.08 \qquad [30]$$

Thus,

$$\frac{\nu_D}{\nu_N} = \left(\frac{\kappa_D}{\kappa_N}\right)^{\frac{1}{4}} = \left(\frac{2.92}{2.70}\right)^{\frac{1}{4}} = 1.04 \qquad [31]$$

$\Delta S_p = -6R \ln 1.04 = -0.47$ cal/mole/°C. Since two moles of positive holes are formed for each mole of vacancies,

$$\Delta S_p = -0.93 \text{ cal/mole/°C.}$$

Calculation of over-all entropy change.—Entropy change of the NiO lattice for condensation of ½ mole of O_2 and for formation of one mole of vacancies and two moles of positive holes at particular lattice sites in a large amount of NiO can now be evaluated. Entropy change on condensation without distortion of ½ mole of O_2 gas is equal to to 29.10 − 9.04, or 20.1 cal/mole/°C. Since order was established in the process, the entropy change is negative or −20.1 eu. Entropy changes associated with the two types of distortion are −1.34 and −0.93 or a total of −2.3 cal/mole/°C. Thus, the total entropy change is −22.5 cal/mole/°C. Since 3 defects were formed, the entropy change per defect is −7.5 cal/mole/°C.

Subtracting this value from the experimental over-all entropy of activation, there is obtained a value of +1.5 cal/mole/°C for the entropy of activation of diffusion, ΔS^*.

APPENDIX III

Estimation of β

β can be estimated from the statistical thermodynamic expression for specific heat, C_P:

$$C_P = \frac{\partial}{\partial T}\left\{RT^2\left(\frac{\partial \ln Q_V}{\partial T}\right)_P\right\} \qquad [32]$$

where

$$Q_V = \frac{kT}{h\nu}$$

Carrying out the necessary differentiation,

$$C_P = R\frac{\partial}{\partial T}\left\{T - T^2\left(\frac{d\ln\nu}{dT}\right)\right\} \qquad [33]$$

According to Einstein (31) there is a simple relation between compressibility, χ, of a solid and characteristic frequencies of the atoms, ν_E. This relationship is $\nu_E \sim 1/\chi^{\frac{1}{2}}$. Since χ is related to the reciprocal of the elastic modulus μ, there results the relationship

$$\nu_E \sim \mu^{\frac{1}{2}} \qquad [34]$$

$$C_P = R\frac{\partial}{\partial T}\left\{T - \frac{T^2}{2}\left(\frac{d\ln\mu}{dT}\right)\right\} \qquad [35]$$

Rearranging and substituting the value of β from [12],

$$C_P = R + \frac{RT}{T_m}\frac{\mu_0}{\mu}\beta \qquad [36]$$

For three degrees of freedom,

$$C_P = 3R + 3\frac{RT}{T_m}\frac{\mu_0}{\mu}\beta$$

To estimate β, substitute 2363°K for the melting point of NiO and a value of 7.4 cal/°C/gram atom (14.8/2) for the specific heat of NiO at 1000°K. Since the ratio of μ/μ_0 is 1 at $T = 0$°K and 0 at the melting point, a linear function of μ/μ_0 with temperature is assumed. This gives a value of μ/μ_0 of 0.6 at 1000°K.

By substituting and solving, it is found that $\beta = 0.345$.

Any discussion of this paper will appear in a Discussion Section, to be published in the December 1954 issue of the Journal.

REFERENCES

1. E. A. Gulbransen and K. F. Andrew, *Trans. Am. Inst. Mining Met. Engrs.*, **185,** 515 (1949).
2. E. A. Gulbransen and K. F. Andrew, *ibid.*, **185,** 741 (1949).
3. E. A. Gulbransen and K. F. Andrew, *ibid.*, **188,** 586 (1950).
4. E. A. Gulbransen and K. F. Andrew, *This Journal*, **97,** 383 (1950).
5. E. A. Gulbransen and K. F. Andrew, *ibid.*, **98,** 241 (1951).
6. C. Wagner and K. Zimens, *Acta Chem. Scand.*, **1,** 574 (1947).
7. N. B. Pilling and R. E. Bedworth, *J. Inst. Metals*, **29,** 529 (1923).
8. Y. Matsunaga, *Japan Nickel Rev.*, **1,** 347 (1933).
9. O. Kubaschewsky and O. Goldbeck, *Z. Metallkunde*, **39,** 158 (1948).
10. W. J. Moore, *J. Chem. Phys.*, **19,** 255 (1951).
11. W. E. Campbell and N. B. Thomas, *Trans. Electrochem. Soc.*, **91,** 623 (1947).
12. R. Piontelli, Private communication.
13. A. L. Horn, *Z. Metallkunde*, **40,** 73 (1949).
14. K. Hauffe and H. Pfeiffer quoted in a paper by K. Hauffe, Wissenschaftliche Zeitschrift der Universitat Greifswald, Jahrgang I, 1951/52, Mathematisch-naturwissenschaftliche Reihe Nr. 1.
15. E. A. Gulbransen and J. W. Hickman, *Trans. Am. Inst. Mining Met. Engrs.*, **171,** 306 (1947).
16. R. W. G. Wycoff, "Crystal Structures," 1, Table III, Interscience Publishers Inc., New York (1948).
17. H. P. Rooksby, *Acta. Cryst.*, **1,** 226 (1948).
18. E. A. Gulbransen, *Trans. Electrochem. Soc.*, **81,** 187 (1942).

19. E. A. Gulbransen, *Rev. Sci. Instruments*, **15**, 201 (1944).
20. E. A. Gulbransen and K. F. Andrew, *Ind. Eng. Chem.*, **41**, 2762 (1949).
21. E. A. Gulbransen, *Trans. Electrochem. Soc.*, **83**, 301 (1943).
22. C. Zener, *J. Appl. Phys.*, **22**, 372 (1951).
23. H. H. von Baumbach and C. Wagner, *Z. physik Chem.*, **B24**, 59 (1934).
24. C. Wagner and Karl Grünewald, *ibid.*, **B40**, 455 (1938).
25. H. Seltz, B. J. DeWitt, and H. J. McDonald, *J. Am. Chem. Soc.*, **62**, 88 (1940).
26. E. A. Gulbransen, International Symposium on "The Reactivity of Solids," Gothenburg, June 1952. To be published.
27. R. T. Phelps, E. A. Gulbransen, and J. W. Hickman, *Ind. Eng. Chem.*, anal. ed., **18**, 391 (1946).
28. Nat. Bur. Standards Circular 500, "Selected Values of Chemical Thermodynamic Properties," Washington, D. C. (1952).
29. K. K. Kelley, Bur. Mines Bulletin 476, Washington, D. C. (1949).
30. M. Born and J. E. Mayer, *Z. Physik*, **75**, 1 (1932).
31. N. F. Mott and H. Jones, "Theory of the Properties of Metals and Alloys," p. 13, Oxford Press, London, England (1936).

The Protective Action of Pigments on Steel[1]

M. J. Pryor

Kaiser Aluminum and Chemical Corporation, Spokane, Washington

ABSTRACT

The action of aqueous extracts from litharge, metallic lead, red lead, basic lead carbonate, zinc, and zinc oxide on the corrosion of steel was investigated. It was found that litharge extracts inhibited the corrosion of steel completely, that extracts from metallic lead and red lead inhibited for a short period, and that extracts from basic lead carbonate, zinc, and zinc oxide lead had no protective action. Protective properties of the decanted extracts were in the same order as their reserve alkalinities. Litharge, metallic lead, and red lead extracts protected only when they contained dissolved air; when deaerated, they attacked steel slowly. The passivity film formed in litharge extracts was found to be composed largely of γ-Fe_2O_3, no lead compounds being detected. It was considered that the lead in the litharge extracts was present partly in the ionic form, possibly as $Pb(OH)^+$ ions, whereas the lead in extracts from metallic lead was present mainly as massive and colloidal lead hydroxide.

Introduction

Attention has previously been directed (1) to the fact that aqueous extracts from certain lead compounds, principally metallic lead, litharge, and red lead, had inhibitive actions on corrosion of steel. It was shown (2, 3) that the inhibitive action of the extract from red lead was of a temporary nature, while similar properties were ascribed to the extracts from metallic lead (4) and basic lead carbonate (5). Inhibitive properties of the extracts have been attributed alternatively to their alkalinity (6, 7), to adsorption of soluble lead compounds (1), and, in the case of red lead, to a combination of alkalinity and oxidizing power (2).

The present examination was carried out to investigate reactions occurring between steel and aqueous extracts from metallic lead powder, litharge, red lead, basic lead carbonate, metallic zinc powder, and zinc oxide. The investigation included determinations of potential-time data and weight losses in solutions freed from and containing dissolved air; the nature of the passivity films and of the aqueous extracts was also examined.

Experimental

Materials

The steel used in the partial immersion tests was annealed autobody steel 0.1 cm thick having the analysis: C—0.12%; Si—0.02%; P—0.014%; Mn—0.32%; S—0.01%; Sn and V—not detected. Steel used in experiments with deaerated solutions was in the form of annealed sheet 0.02 cm thick, the analysis of which was given in a previous paper (8).

Pigments used in this investigation had the following compositions: metallic lead—98.4% Pb; litharge—95.7% PbO; red lead—99.1% Pb_3O_4; basic lead carbonate—80% Pb, 8.25% CO_2; metallic zinc—99.9% Zn; zinc oxide—99.7% ZnO. The balance of the litharge was mainly in the form of Pb_3O_4. All other chemicals were of C.P. quality.

Preparation of pigment extracts.—Extracts were prepared by exposing 50 grams of each pigment to 1 liter of distilled water in a stoppered flask for eight days. The flasks were shaken at frequent intervals to insure dispersion of pigment particles. After eight days the solutions were decanted from the residual pigments and stored in well-stoppered bottles.

Reactions between Steel and Pigment Extracts in Presence of Dissolved Air

Steel specimens measuring 5 x 2.5 cm, which had been degreased in benzene, abraded with 3/0 emery paper, and weighed, were partially immersed in the decanted extracts in such a manner that they did not come into direct contact with any residual particles of pigment. Partial immersion tests of five days' duration were carried out in 30 ml of each solution, an area of 12.5 cm^2 of specimen being immersed in each test solution. Control experiments in distilled water were also carried out. At the end of the experiments the specimens were pickled in inhibited hydrochloric acid, dried in acetone, and reweighed. The weight losses, which are the average of experiments in triplicate, together with the initial and final *p*H values of the solutions, are shown in Table I. The extract from litharge gave complete inhibition, while those extracts from metallic lead and red lead gave inhibition for 24 hours and six hours, respectively, after which time corrosion occurred at a lower rate than in distilled water. Extracts from basic lead

[1] Manuscript received June 17, 1953. This paper was prepared for delivery before the Wrightsville Beach Meeting, September 13 to 16, 1953. Experimental work carried out at the National Research Council of Canada, Ottawa.

TABLE I. *Weight losses in extracts containing dissolved air*

Solution	Initial pH	Wt loss/cm² mg	Average wt loss/cm² mg	Final pH	Reserve alkalinity, ml	Observations
Fresh distilled water	5.5	0.96, 0.80, 0.93	0.90	6.6	—	General corrosion
Distilled water stored in glass bottles for 4 weeks	8.9	0.80, 0.80, 0.85	0.82	6.7	0.1	General corrosion
Decanted Pb extract	9.9	0.52, 0.27, 0.47	0.43	6.9	7.9	Inhibition for one day after which localized corrosion proceeds at a reduced rate
Pb extract filtered through glass wool	9.4	0.72, 0.68, 0.71	0.70	6.8	5.7	General corrosion at reduced rate
Pb extract filtered through Whatman No. 1 filter paper	8.6	0.70, 0.69, 0.69	0.69	6.9	0.6	General corrosion at reduced rate
Decanted PbO extract	9.7	<0.01	<0.01	7.5	15.2	Passivity
PbO extract filtered through glass wool	9.7	<0.01	<0.01	7.5	12.25	Passivity
PbO extract filtered through Whatman No. 1 filter paper	8.0	<0.01	<0.01	7.2	2.1	Passivity
PbO extract filtered through Whatman No. 42 filter paper	7.3	<0.01	<0.01	7.0	1.6	Passivity
Decanted Pb_3O_4 extract	9.7	0.57, 0.58, 0.54	0.56	6.8	4.1	Passivity for a few hours after which time general corrosion proceeds at a reduced rate
Pb_3O_4 extract filtered through glass wool	8.35	0.78, 0.61, 0.73	0.71	6.9	0.8	General corrosion at slightly reduced rate
Pb_3O_4 extract filtered through Whatman No. 1 filter paper	7.3	0.70, 0.71, 0.69	0.70	6.7	0.3	General corrosion at slightly reduced rate
Decanted basic lead carbonate extract	8.95	0.85, 0.86, 0.86	0.86	6.5	0.3	General corrosion
Decanted Zn extract	8.6	0.81, 0.80, 0.81	0.81	6.7	0.15	General corrosion
Decanted ZnO extract	7.7	0.90, 0.93, 0.91	0.91	6.4	0.3	General corrosion

carbonate, zinc, and zinc oxide had no detectable inhibitive properties.

Potential time data were determined in 50 ml of each decanted extract. Control experiments in fresh distilled water and distilled water that had been stored in a stoppered glass bottle for four weeks were also carried out. The area of specimen exposed to each solution was 12.5 cm² and duration of the experiments was five days. Potential difference[2] readings against a standard calomel electrode were recorded continuously by means of a Leeds and Northrup Micromax recording potentiometer. To prevent contamination of the extracts by chloride, the calomel electrode was contained in a beaker of distilled water and bridged to the extracts under examination through a stopcock "greased" with a stiff paste of bentonite, glycerine, and water, and maintained in the closed position (9). The results are shown in Fig. 1. The effect of progressively finer filtration on the form of the potential time curves in extracts from litharge, lead, and red lead is shown in Fig. 2, 3, and 4.

[2] All potentials in this paper are expressed on the Standard Hydrogen Scale.

Reactions between Steel and Deaerated Extracts

Determinations of weight loss and of the relationship between potential and time were carried out in deaerated extracts from metallic lead, litharge, and red lead. The deaeration technique previously described (10), based on the very large decrease in gaseous solubility on freezing solution, was employed.

Weight loss determinations (9) were carried out on degreased specimens measuring 4 x 3 x 0.02 cm; they were abraded with 3/0 emery paper and exposed to 50 ml of deaerated extracts which had been filtered through glass wool to remove massive pigment particles. Duration of experiments, which were carried out in triplicate, was five days; results are shown in Table II, from which it may be seen that the deaerated extracts do not inhibit corrosion of steel.

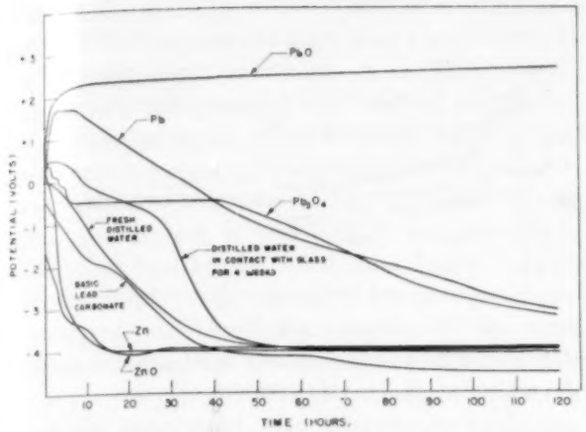

FIG. 1. Potential/time curves in decanted extracts containing dissolved air.

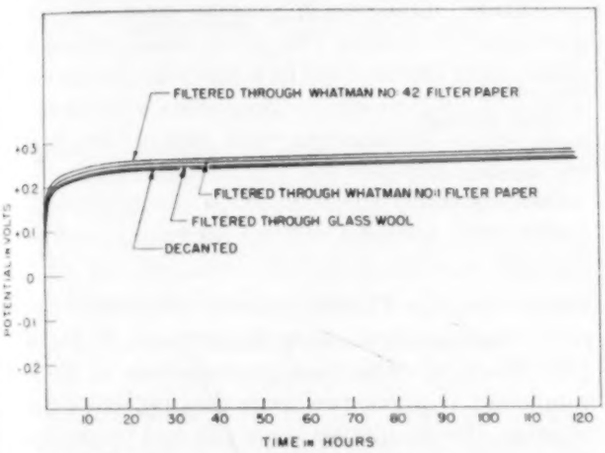
FILTERED THROUGH WHATMAN NO 42 FILTER PAPER
FILTERED THROUGH WHATMAN NO 1 FILTER PAPER
FILTERED THROUGH GLASS WOOL
DECANTED
POTENTIAL IN VOLTS
TIME IN HOURS

FIG. 2. Effect of filtration on potential/time curves in litharge extracts containing dissolved air.

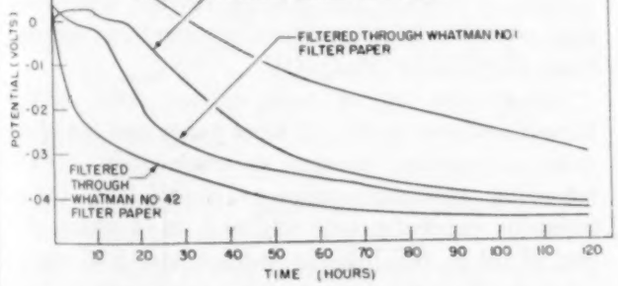

FIG. 3. Effect of filtration on potential/time curves in lead extracts containing dissolved air.

Potential determinations were carried out in apparatus described previously (10) in which a specimen measuring 2.5 x 0.5 cm was exposed to 10 ml of the deaerated decanted extract, to which had been added 10 ppm chloride ion, in order that the chloridized silver wire also contained inside the apparatus could take up a steady potential characteristic of the concentration of chloride in solution. Results,

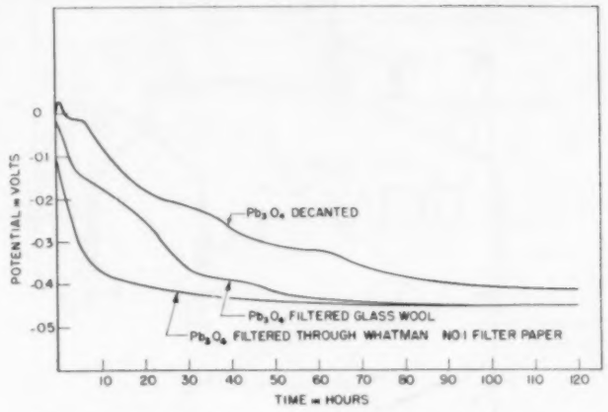
Pb_3O_4 DECANTED
Pb_3O_4 FILTERED GLASS WOOL
Pb_3O_4 FILTERED THROUGH WHATMAN NO 1 FILTER PAPER
POTENTIAL IN VOLTS
TIME IN HOURS

FIG. 4. Effect of filtration on potential/time curves in red lead extracts containing dissolved air.

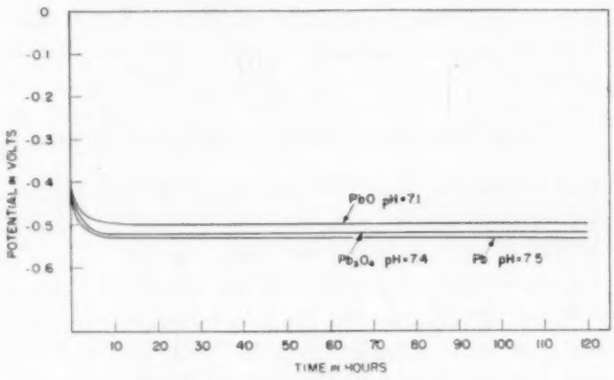

FIG. 5. Potential/time curves in deaerated decanted extracts.

TABLE II. *Weight losses in deaerated extracts*

Solution	Wt loss/cm² mg	Average wt loss/cm² mg
PbO extract filtered through glass wool..	0.024, 0.028, 0.028	0.027
Pb extract filtered through glass wool..	0.024, 0.024, 0.022	0.023
Pb_3O_4 extract filtered through glass wool..	0.028, 0.036, 0.028	0.031

(Fig. 5), show that deaeration results in a large shift in potential in the negative (less noble) direction.

Examination of Extracts

Initial *p*H values of extracts were found to be distinctly alkaline (Table I) which confirms much previous work (6, 7, 11). It was, therefore, decided to determine whether passage of lead or zinc into solution had resulted in any appreciable buffering action. One hundred ml of each deaerated extract was titrated electrometrically with 0.01*N* HCl while being constantly stirred by means of an electromagnetic stirrer. Results (Fig. 6) show that extracts from litharge, lead, and red lead have a pronounced buffering action, whereas those from basic

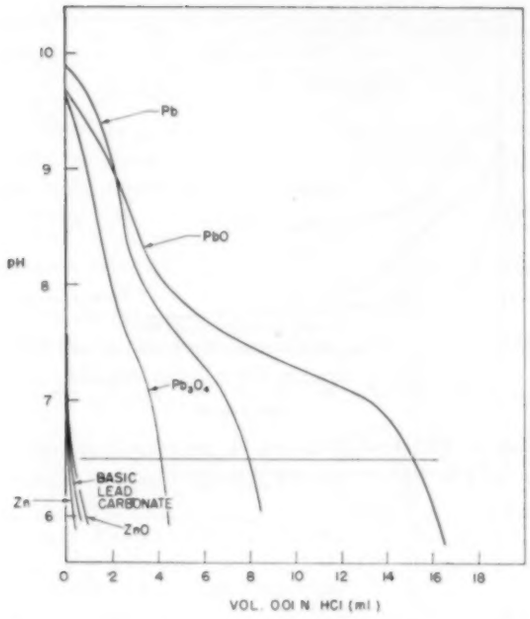

FIG. 6. Neutralization curves of decanted extracts

lead carbonate, zinc, and zinc oxide do not. Reserve alkalinities, which are arbitrarily defined as volumes of 0.01*N* HCl required to bring the *p*H values of 100 ml of the extracts to 6.5, are shown in Table I.

Effect of filtration on the neutralization curves of extracts from litharge, metallic lead, and red lead was next investigated. Methods of filtration used included filtration through glass wool, through Whatman No. 1 filter paper, and through Whatman No. 42 filter paper which should remove progressively greater quantities of insoluble compounds from solution. In every case, progressively finer filtration progressively reduced reserve alkalinities of the extracts (Table I).

Change in *p*H with time due to absorption of atmospheric carbon dioxide was determined by permitting decanted extracts to remain in contact with the atmosphere for five days. Measurements of *p*H were made on the solutions each day (Fig. 7).

An examination of the extracts from lead and from litharge was next undertaken to determine whether the superior inhibitive properties of extracts from litharge were caused by greater concentration of lead in solution or by lead being present in a different form than that in the lead extract.

In order to relate the reserve alkalinities of the extracts to the total quantity of lead in solution, 50 ml of each extract was filtered through glass wool and the reserve alkalinities determined. Total lead concentration of the same solutions was then determined gravimetrically with results as shown in Table III.

The weight of lead required to produce appropriate buffering action was calculated, assuming that it was present in the form of $Pb(OH)_2$. This is probably true for lead extract (12), although it has been

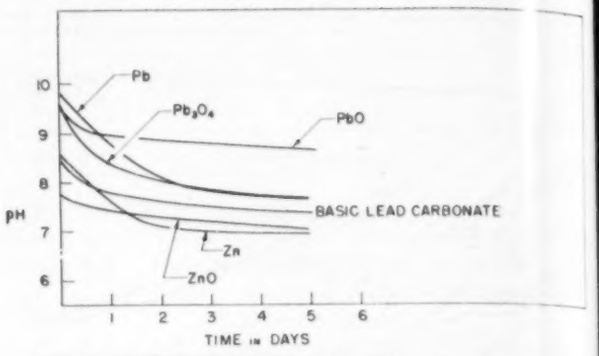

FIG. 7. Effect of atmospheric carbon dioxide uptake in the *p*H values of decanted extracts.

TABLE III

Solution	Reserve alkalinity ml 0.01*N* HCl	Wt of lead in solution, mg	Calculated wt of lead required to produce appropriate buffering action, mg	Wt of lead apparently not contributing to buffering action, mg
Pb extract filtered through glass wool	6.2	3.8	3.2	0.6
Pb extract filtered through glass wool	10.6	7.8	5.5	2.3

stated that the $Pb(OH)_2$ slowly transforms to the more insoluble lead dioxydihydroxide $Pb_3O_2(OH)_2$ (13). Since, in either case, one molecule of the lead compound requires two molecules of HCl for dissolution, the calculation is not affected by the transformation. Lead extract gives quite close agreement between calculated and measured weights of lead in solution, the error of 0.6 mg probably being due to the formation of basic carbonate which has little or no buffering action. There is, however, a marked disagreement between the calculated and observed weights of lead in the litharge extract which may mean that the lead is present in some form different from $Pb(OH)_2$ or $Pb_3O_2(OH)_2$.

Twenty-five ml of each extract were filtered through Whatman No. 42 filter paper and the ultraviolet absorption spectra determined in a Cary recording spectrophotometer (Model 11). Unfortunately concentrations of lead in solution, 0.8 mg/25 ml in the litharge extract and 0.35 mg/25 ml in the Pb extract, were rather low for this type of investigation. Results with lead extract indicated only scattering from particles probably of colloidal dimensions and no absorption bands were present. Results with litharge extract indicated less scatter, although the total lead concentration in solution was higher. There was an absorption band at 2080 Å which is not usually found in molecular litharge (14). Although this band is very near to the lower limit of the instrument it is considered to be significant. It should also be pointed out that a concentration difference of 100% would not cause its disappearance.

Twenty-five ml of the litharge extract were filtered through Whatman No. 42 filter paper and enclosed in a semipermeable membrane of untreated (non-waterproofed) cellophane. The "bag" of cellophane was then placed in 25 ml of distilled water to determine whether an appreciable quantity of the total lead in solution was present in the ionic state. Using the lead sulfide test, it was found that appreciable quantities of lead passed from the extract through the semipermeable membrane and into the surrounding water. A considerable proportion of the total lead was adsorbed by the cellophane so that after dialysis for one day, neither the solutions inside nor outside the membrane were completely inhibitive. Potential-time data subsequently obtained for steel specimens exposed to these solutions indicated that the solution from outside the membrane, containing lead in the ionic form, had temporary inhibitive properties at least equal to the solution from inside the membrane containing a greater total quantity of lead compounds, some presumably in the ionic state and the remainder in the colloidal state.

An attempt was made to repeat this examination using the extract from metallic lead, but it was found that the concentration of lead in solution was not sufficient to give significant results.

Nature of Passivity Films Formed in Litharge Extracts

Specimens passivated for five days in litharge extracts that had been decanted, or filtered through glass wool, through Whatman No. 1 filter paper, or through Whatman No. 42 filter paper, were then washed for 15 min in running distilled water, wiped with filter paper, and dried with methanol. They were then etched with dilute nitric acid to destroy passivity films; the acid was adjusted to a *p*H value of 2.0 with dilute sodium hydroxide and tested for the presence of lead by means of the lead sulfide test. In no case was a positive test for lead obtained and it was concluded that any lead that might be present in the passivity films was so small in quantity (less than 10^{-5} mg/cm^2 of specimen) that it could not be directly responsible for passivity.

The passivity film resulting from two days' exposure of an originally film-free steel specimen to a litharge extract that had been filtered through glass wool was isolated from the metal by a modification of the methanol-iodine method (15). The apparatus, shown in Fig. 8, permits passivity films to be isolated without bringing the specimens into contact with air after passivation. The specimen was suspended in the reaction chamber (R) which was partly filled with 0.1*N* ammonium chloride. The system was flushed with purified nitrogen[3] and the specimen made

[3] Nitrogen was purified by passing it through a column containing finely divided copper, deposited on Fullers earth, at a temperature of 200°C.

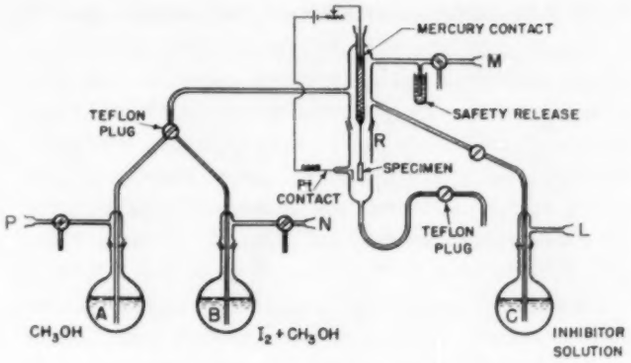

FIG. 8. Film stripping apparatus

cathodic for one minute at a current density of 1 milliamp/cm^2 in order to destroy the air-formed oxide film by cathodic reduction (16). Ammonium chloride was then forced from the reaction chamber by nitrogen admitted through (M) and replaced by the litharge extract, saturated with dissolved air, which was forced from the flask (C) by compressed air. To eliminate contamination by chloride, this solution was drained away and replaced by fresh inhibitor from (C). The apparatus was then opened to the air and the specimen allowed to stand in the inhibitor solution for two days. At the end of this period the apparatus was flushed with nitrogen and flask (A) filled with anhydrous methanol and (B) with 100 ml of anhydrous methanol in which had been dissolved 6 grams of anhydrous iodine. The iodine had previously been dried by standing over phosphorus pentoxide while the methanol was dried by refluxing with, and distilling from, magnesium turnings and a trace of iodine. Both solutions were deaerated by simultaneous boiling and bubbling of nitrogen. The solutions were cooled and the inhibitor solution forced from the reaction chamber. The specimen was washed several times with methanol forced from flask (A) by compressed nitrogen. The film stripping solution in (B) was then forced into the reaction chamber and left in contact with the specimen for approximately 30 min. At the end of this period, the film stripping solution was run from (R) and the specimen again carefully washed with methanol from (A). The specimen was finally removed from the apparatus and placed in a dish of methanol. The passivity film, which should be hanging loosely from the specimen, was detached by gentle agitation of the dish, and suitable samples were collected on copper grids for examination by electron diffraction.

Portions of stripped film were examined by electron diffraction and gave a diffuse ring pattern characteristic of either γ-Fe_2O_3 or Fe_3O_4 (Table IV). Portions of the films were dissolved in 1:1 HCl and tested for the presence of ferrous ions using the

TABLE IV. *Ring pattern obtained from stripped passivity film*

Ring radius	Spacing	Intensity	hkl
cm	*d*(Å)		
1.24	2.50	V.S.[a]	311
1.49	2.07	S[b]	400
1.94	1.60	W[c]	511, 333
2.10	1.49	S	440
2.63	1.20	W	444

[a] V.S.—very strong; [b] S—strong; [c] W—weak.

di-2-piridyl test (17). Failure to detect ferrous ions indicated that the passivity film was largely composed of γ-Fe_2O_3 which compound has been found to be the major constituent of passivity films formed in many anodic inhibitors (8, 18, 19).

Discussion

It is evident that extracts from litharge, metallic lead, and red lead have definite inhibitive properties, whereas those from basic lead carbonate, zinc, and zinc oxide do not. Inhibitive properties of extracts from metallic lead and from red lead appear to be of a temporary nature, which is in accord with previous work (2–4). Similar temporary inhibitive properties have been previously ascribed to basic lead carbonate (5) but this was not confirmed in this examination. However, properties of these extracts may well depend on the method of preparation, which may explain discrepancies in the results of different investigators. The following discussion is, therefore, confined to the behavior of the extracts prepared in the manner described above.

Whereas the protective action of decanted extracts from metallic lead and red lead lasted for only 24 and six hours, respectively, extracts from litharge gave complete inhibition for prolonged periods; this protective action was not destroyed by filtering with a fine quantitative paper such as Whatman No. 42. It is proposed, therefore, to discuss first the protective action of litharge extracts and then to attempt to point out the reasons for the less effective protection afforded by the other extracts.

Protective Action of Litharge Extracts

From the form of potential-time curves in solutions containing dissolved air (Fig. 2) and from the fact that specimens were unchanged in appearance and had no detectable weight loss in five days (Table I), it appears that the litharge extract was behaving as an effective anodic inhibitor, a conclusion previously advanced by Mayne (1). Had the litharge been functioning as a cathodic inhibitor, the potential would have been more negative and some corrosion would have taken place before a protective film was formed.

Anodic inhibition may presumably be brought about either by adsorption of lead compounds from solution onto the anodic areas or by the oxide film mechanism, which has been proposed for such common anodic inhibitors as sodium hydroxide (18), sodium phosphate (10), sodium carbonate, sodium benzoate, and sodium silicate (19).[4] Failure to detect even minute traces of lead compounds in passivity films makes it unlikely that inhibition is caused by adsorption of lead compound from solution. Passivity films isolated from initially film-free steel specimens passivated for two days in filtered litharge extracts were found to be composed largely of γ-Fe_2O_3, no second phase, neither lead compounds nor hydrated oxides of iron, being detected. It should be pointed out that the electron microscope-electron diffraction technique developed by Menter (18, 19) was not employed in this examination and so detection of small amounts of a second phase would not be expected. Chemical examination largely precluded the presence of lead compounds, but some hydrated oxides of iron, such as lepidocrocite (γ-FeO·OH), might well be present in small amounts.

Inhibitive properties of litharge extracts are dependent on the presence of oxygen dissolved in solution since it was shown that, when the extracts were deaerated, the potential became very much more negative (reactive) (Fig. 5) and the iron was slowly attacked (Table II). The form of the potential-time curve indicated that the corrosion was largely under cathodic control and that no film formation was occurring in deaerated solution. This behavior is identical to that of anodic inhibitors having non-oxidizing anions such as sodium hydroxide, carbonate, benzoate, acetate, and silicate previously investigated by the author (9). Inhibition is considered to be primarily due to oxygen dissolved in solution which adsorbs on the surface of the iron and takes part in a heterogeneous reaction with surface iron atoms to form a thin film of γ-Fe_2O_3, probably in a manner similar to that by which oxide films are formed in air. The thickness of similar films of γ-Fe_2O_3 formed in solutions of sodium phosphate and in air was found to be 100–200 Å (20).[5] Since the formation of a protective film of oxide is not instantaneous, it is believed that the initial stages of film formation are accompanied by very slow corrosion which, on account of the very small size of the areas available for anodic reaction, is

[4] It was previously suggested (21) that inhibition might be due to a dilute solution of sodium silicate formed by interaction of water with the glass vessels. Potential/time curves (Fig. 1) and weight loss determinations (Table I) in water that had been stored in glass bottles for four weeks show that this explanation is unlikely.

[5] Calculated on the apparent surface area of the specimens.

mainly under anodic control, and leads to the formation of small inclusions of corrosion product in a matrix of γ-Fe_2O_3. It has been suggested that rate of formation of the oxide film should be independent of the *p*H of the solution (10), but that the rate of the accompanying electrochemical corrosion decreased with a rise in the *p*H value of the solution. Since factors tending to stimulate the rate of electrochemical corrosion should militate against passivity, high *p*H values should be more favorable to passivity and low *p*H values more favorable to corrosion. Formation of the inclusions of corrosion product, usually lepidocrocite (18), from ferrous ions, hydroxyl ions, and dissolved oxygen results in the local production of hydrogen ions which are detrimental to passivity; it has been suggested, therefore, that anodic inhibitors that have a high *p*H value and are also well buffered are likely to be the most effective (19).

Protective Action of Other Extracts

Extracts prepared for this examination were all found to have *p*H values higher than 7.0. In addition, however, their reserve alkalinities were determined (Fig. 6 and Table I). By comparison with the weight-loss results (Table I) it can be seen that the reserve alkalinities of the decanted extracts are related to their efficiencies as anodic inhibitors. The litharge extract with a reserve alkalinity of 15.2 ml protected completely; the metallic lead extract, reserve alkalinity 7.9 ml, protected for 24 hr, while the red lead extract, reserve alkalinity 4.1 ml, protected for 6 hr. The remaining extracts with reserve alkalinities of 0.3–0.15 ml had no detectable inhibitive properties.

In practice, these reserve alkalinities are further decreased by absorption of atmospheric carbon dioxide which leads to the precipitation of basic lead or zinc carbonates. Effect of prolonged exposure to the atmosphere on *p*H values of the extracts is shown in Fig. 7. The *p*H value of all extracts became lower but the proportionately greatest effect was noted with extracts from metallic lead and zinc.

Lack of protective action of the extracts from basic lead carbonate, metallic zinc, and zinc oxide is thus attributed to their lower *p*H, and to their low reserve alkalinities which makes them unable to counteract local drop in *p*H at anodic areas.

Extracts from metallic lead and red lead have higher initial *p*H values and greater reserve alkalinities than those extracts mentioned above. However, lead extract absorbed atmospheric carbon dioxide at an inordinately high rate which must result in a considerable decrease in its reserve alkalinity. Initial stages of passivation in these extracts are considered to be similar to those suggested above for litharge. There is no evidence that the temporary protective action of red lead is in any way connected with its oxidizing properties, as suggested previously (2). The potential-time curve determined in deaerated solution (Fig. 5) showed that these oxidizing powers were insufficient to cause any detectable film formation. Furthermore, it was previously shown by Mayne (11) that lead dioxide, a more powerful oxidizing agent, had no inhibitive action on the corrosion of iron. One of the differences between these extracts and that from litharge is that their lower reserve alkalinities are able to maintain only a temporarily alkaline *p*H value at pores in the oxide film where hydrogen ions are being generated due to the formation of corrosion product. Lead extract, having a higher reserve alkalinity, maintains the temporary protection for a longer time than that from red lead.

Nature of Extracts from Metallic Lead and Litharge

Apart from the fact that extracts from litharge, metallic lead, and red lead have appreciable reserve alkalinities, the composition of these extracts has not yet been discussed. Their reserve alkalinities are undoubtedly associated with the passage of lead into solution. Formation of the extract from metallic lead is, perhaps, most easily understood. It is believed that the lead corrodes in the normal electrochemical manner and that the interaction of the anodically formed lead ions with hydroxyl ions generated at the cathodes leads to the precipitation of sparingly soluble lead hydroxide. It has been stated (13) that this lead hydroxide then transforms into the less soluble lead dioxydihydroxide $Pb_3O_2(OH)_2$ or $3PbO \cdot H_2O$ (13). That lead is present in solution largely as $Pb(OH)_2$ [or $Pb_3O_2(OH)_2$] is supported by the comparison of the calculated weight of lead, as lead hydroxide, required to produce the determined reserve alkalinity, with the observed weight of lead in solution (Table III). The slight discrepancy in results is probably due to action of atmospheric CO_2 which forms some basic lead carbonate which has a very low reserve alkalinity. Filtration with progressively finer filter papers reduces the lead content of the solution and the reserve alkalinity (Fig. 6 and Table I) by removal of greater quantities of insoluble material and probably also by adsorption of lead on the filter paper (1). A portion of the lead in solution appeared to be in colloidal form and was not removed by filtering with Whatman No. 42 filter paper. The ultraviolet absorption spectrum of such a solution was a curve characteristic of scatter from colloidal particles.

Appreciable quantities of litharge are known to be dissolved by distilled water (22) and the resulting solution is alkaline (11). The weight of litharge dissolved is said to be reduced in the presence of

carbon dioxide. Litharge was assumed to be in solution in the form of $Pb(OH)_2$ by Glasstone (23) who quoted a value of 1.7×10^{-15} for its solubility product. According to Pleissner (13), however, the $Pb(OH)_2$ had two stages of ionization, viz.:

$$Pb(OH)_2 = Pb(OH)^+ + OH'$$
$$Pb(OH)^+ = Pb^{++} + OH'$$

for which α, the percentage degree of ionization, was 27% for the first step. This was supported by the observations of Berl and Austerweil (24) who found complete ionization of a solution of $Pb(OH)_2$ containing 0.262 millimole/liter.

Several experiments were performed to determine whether litharge extract differed from lead extract because lead concentration in solution was higher, or because the lead in solution was present in some different form. It was first found (Table III) that, although the reserve alkalinity of the litharge extract was higher than that of lead extract, the proportion of the total lead, calculated as lead hydroxide, apparently contributing to reserve alkalinity, was lower. This appeared unlikely to be due to absorption of atmospheric CO_2 which was less readily absorbed by litharge extracts than by metallic lead extracts (Fig. 7). Furthermore, although the buffering power of decanted extracts accurately reflected their relative inhibitive powers, this was not so with filtered litharge extracts, some of which gave complete inhibition with reserve alkalinities as low as 1.6 ml (Table I). Dialysis experiments indicated that these extracts contained a proportion of lead in the purely ionic form rather than as colloidal $Pb(OH)_2$; this conclusion was supported by the ultraviolet absorption spectrum, which showed that the filtered litharge extract, although containing a greater total weight of lead than the filtered lead extract, gave less random scatter (due to the presence of colloidal particles) but had an absorption band at 2080 Å. This band is not found in the spectrum of molecular PbO and is probably characteristic of some form of ionic lead.

No one section of the above evidence is conclusive in itself, but taken together these points indicate that the lead in litharge extracts is partly present in some different form from that in metallic lead extracts, which appear to contain lead mainly in the form of $Pb(OH)_2$. Since *p*H considerations largely preclude the formation of plumbite ions and lead ions themselves have no inhibitive properties (1), it appears that the lead may be partly present as $Pb(OH)_2$ and also as $Pb(OH)^+$ ions. These ions would be expected to have a greater mobility than colloidal $Pb(OH)_2$ and would react more quickly with hydrogen ions formed at anodic areas and, therefore, produce more effective buffering. This may explain not only the superior buffering action, but also the superior inhibitive properties of the litharge extracts. Since the $Pb(OH)^+$ ions would be expected to have a low transport number their rate of migration away from anodic areas should not be high enough to detract from their local buffering action and hence from their inhibitive properties.

Acknowledgments

The author wishes to thank Mr. J. Harris for supplying the pigments, Dr. D. S. Russell and Mr. P. Tymchuk for carrying out the analyses of the extracts and of the pigments, Dr. C. Sandorfy for determining the ultraviolet absorption spectra, and Dr. F. J. Bowen and Mr. W. E. Stump for their helpful comments.

Any discussion of this paper will appear in a Discussion Section to be published in the December 1954 issue of the JOURNAL.

REFERENCES

1. J. E. O. Mayne, *J. Soc. Chem. Ind. London*, **65**, 197 (1946).
2. R. M. Burns and H. E. Haring, *Trans. Electrochem. Soc.*, **69**, 178 (1936).
3. K. G. Lewis and U. R. Evans, *J. Soc. Chem. Ind.*, **53**, 25T (1934).
4. S. C. Britton and U. R. Evans, *ibid.*, **58**, 90 (1939).
5. J. C. Hudson, 4th Report of Corrosion Committee, Iron and Steel Institute, London 199 (1936).
6. U. R. Evans, "Corrosion, Passivity & Protection," p. 595, Arnold, London (1937).
7. J. E. O. Mayne, *Research, London*, **6**, 278 (1952).
8. J. E. O. Mayne and M. J. Pryor, *J. Chem. Soc.*, **1949**, 1831.
9. M. J. Pryor and M. Cohen, *This Journal*, **100**, 203 (1953).
10. M. J. Pryor and M. Cohen, *ibid.*, **98**, 263 (1951).
11. P. Yorke, *Phil. Mag.*, **28**, 17 (1846).
12. M. Traube-Mengarini and A. Scala, *Kolloid-Z.*, **6**, 240 (1910).
13. M. Pleissner, *Arb. kaiserl. Gesundh.*, **26**, 398 (1907).
14. R. W. B. Pearse and A. G. Gade, "Identification of Molecular Spectra," p. 206, John Wiley & Sons, Inc., New York (1949).
15. W. H. J. Vernon, F. Wormwell, and T. J. Nurse, *J. Chem. Soc.*, **1939**, 621.
16. U. R. Evans and H. A. Miley, *Iron Steel Inst. London, Carnegie Schol. Mem.*, **25**, 197 (1936).
17. F. Feigl, "Qualitative Analysis by Spot Tests," p. 96, Nordemann Publishing Co. Inc., New York (1939).
18. J. E. O. Mayne, J. W. Menter, and M. J. Pryor, *J. Chem. Soc.*, **1950**, 3229.
19. J. W. Menter, *Compt. Rend. du Premier Congrès International de Microscopie Électronique*, Paris 1950; *Éditions de la Revue d'Optique*, Paris 1952.
20. M. J. Pryor, M. Cohen, and F. Brown, *This Journal*, **99**, 542 (1952).
21. R. S. Thornhill, Discussion to J. E. O. Mayne, *J. Soc. Chem. Ind.*, **67**, 199 (1946).
22. H. Remy and A. Kuhlman, *Z. anal. Chem.*, **65**, 161 (1924).
23. S. Glasstone, *J. Chem. Soc.*, **119**, 1689 (1921).
24. F. Berl and G. Austerweil, *Z. Elektrochem.*, **13**, 169 (1907).

Measurement of Particle Size Distribution of Phosphors[1]

MARTHA J. BERGIN AND KEITH H. BUTLER

Sylvania Electric Products Inc., Salem, Massachusetts

ABSTRACT

A quick method of calculating particle size distribution from optical measurements of sedimentation rates is described. It is shown that the apparent mean diameter is greatly influenced by degree of dispersion of the powder and that reproducibility requires careful control of dispersion.

INTRODUCTION

Use of a single mean value to express "particle size" of a nonhomogeneous powder does not adequately define coarseness or fineness of the powder. Depending on the particular method of measurement or calculation employed, there are several different average diameters. For a satisfactory definition of the powder, particle size distribution must be known.

Similarly, there is no universally applicable method for determining particle size distribution of powders because of the tremendous range of sizes encountered. Microscopic counting can be applied over a considerable range by using variable magnification, while extremely small size material may be measured by use of an electron microscope. However, at best, counting is an extremely tedious process.

Within a limited range of particle size, gravity sedimentation in a liquid medium is adequate, but the problem of measuring the amount of material settled in a given time presents some difficulties. Gravimetric methods, such as the Andreasen pipette or the Oden balance are accurate, but again the elapsed time from start to finish is quite long.

Measurement of optical transmission during sedimentation is a very convenient method experimentally, but interpretation of data has required rather slow and complex calculations (1) giving, finally, a histogram of distribution. A somewhat simpler method of calculation is described by Musgrave and Harner (2), but even this requires considerable time, which has limited its use.

The particle size of phosphors used in fluorescent lamps and television tubes lies inside the range for gravity sedimentation. Knowledge of their particle size distribution is valuable both for control of firing procedures and milling methods, as well as for development of new methods of making and processing these phosphors. Limitations of previously described methods have so restricted their general use that important differences between phosphors are frequently not recognized.

This paper presents a simplified method of calculation using optical transmission data, with which a distribution curve can be obtained in minutes rather than hours. It is thus suited for control work. The method is based on two postulates: first, the light scattering coefficient is independent of particle size, and second, the particle size distribution function can be represented adequately by a log-normal probability function.

Using optical transmission data, a simple slide rule calculation gives points for plotting on probability paper, and a simple graphical conversion gives distribution of particle size.

The method is limited by three requirements which are adequately met by most phosphors: (*a*) the distribution must contain few particles smaller than 2 μ, because turbulence invalidates Stokes' law for smaller particles; (*b*) only a small percentage larger than 50 μ should be present to avoid difficulty in obtaining transmission at zero time, as a result of excessively rapid settling; (*c*) there must be an adequate difference in refractive index between the particle and the medium to insure constancy of the light scattering coefficient.

Since the basic purpose of the work was development of a rapid method suitable for comparison measurements on similar materials, rather than that of a precision method for absolute values on a wide range of materials, no attempt was made to estimate absolute errors resulting from approximations used.

MATHEMATICAL DISCUSSION

Basic Principles

Several texts (3, 4, 7) discuss in detail the relationship between transmission and particle size. It should be pointed out that light is scattered by transparent particles suspended in a medium with a different refractive index. Light which enters the

[1] Manuscript received June 26, 1953. This paper was prepared for delivery before the New York Meeting, April 12 to 16, 1953.

slit and thence the photocell has two components: first, all of the unscattered light, and second, part of the scattered light. With the geometry of the Photelometer, the correction for scattered light is small and will be only slightly changed by particle size or concentration.

The amount of light transmitted through the suspension is given by Beer's law which can be expressed in the form

$$L_t/L_\infty = e^{-KB} \qquad (I)$$

where B is the sum of cross-sectional areas of the particles; K is the constant dependent on dimensions of the equipment and on scattering coefficient of the particles, L_t is light transmitted through the suspension at time t, and L_∞ is light transmitted through the system free of particles. The zero subscript (e.g., L_0) denotes the value at a settling time of $t = 0$. Formula (I) can be converted to natural logarithms

$$\ln (L_\infty/L_t) = KB \qquad (II)$$

The assumption that a log-normal probability distribution of particle size is present holds for many industrial products prepared by firing or grinding. Both operations are common in the preparation of phosphors. Separation by centrifuging or elutriation, or in a few cases by screening, may significantly alter the distribution so that the log-normal law does not hold. However, these operations are not customary in phosphor preparation, so they should not affect the validity of the postulate. In any event, an inspection of plotted data shows whether a log-normal distribution does exist.

It is assumed that the constant, K, in Beer's law is independent of particle size. Its variation with particle size, index of refraction, and wave length of light has been thoroughly discussed in recent literature on optical scattering coefficients, with DeVore and Pfund (5) and Gumprecht and Sliepcevich (6) giving excellent summaries.

DeVore and Pfund show a universal scattering curve in which the abscissa is the parameter $d/\lambda\ (m^2 - 1)/(m^2 + 2)$. When this parameter[2] is above 0.6, scattering remains constant at 2.0 over a very large range of parameter values; while, if the parameter falls below 0.6, the scattering coefficient deviates considerably from this constant value. Hence 0.6 may be chosen as a limiting value for the parameter. With zinc sulfide in water, the parameter drops to 0.6 at a particle size of ½ μ. Since most television phosphors are above this size, it can be assumed that the scattering coefficient is constant.

For calcium halophosphates in water, because of the different refractive index, the limiting value 0.6 of the parameter is reached at 2.0 μ diameter. In this case, deviations from Beer's law may be a little more pronounced, but, since these phosphors are usually large in particle size, the assumption that the scattering coefficient is constant seems valid. Even with xylol as the medium, Beer's law holds adequately for most phosphors.

Applying formula (II), it can be seen that the ratio of the total cross-sectional areas of particles in the suspension at time t, to that present at time $t = 0$, is given by:

$$B_t/B_0 = [\ln (L_\infty/L_t)]/[\ln (L_\infty/L_0)]. \qquad (III)$$

This can be converted to common logarithms and simplified by setting $L_\infty = 1$, and expressing L_t and L_0 in terms of this unit, giving

$$B_t/B_0 = (\log 1/L_t)/(\log 1/L_0). \qquad (IV)$$

This ratio can be quickly determined by a slide rule calculation after L_0 and L_t are known. Since B_t is the integral of the cross-sectional area of the particles which have not settled out at time t, while B_0 is the corresponding integral for the complete distribution, then plotting on logarithmetric probability paper 100 B_t/B_0 against time of settling should give a straight line, if the log-normal law for particle size distribution is valid.

Conversion of Data

Having obtained the first graph of the function $(\log 1/L_t)/(\log 1/L_0)$ against time, conversion to a graph of $F(d)$[3] against diameter is quite simple. It is assumed that Stokes' law holds, and this may be written as:

$$d^2 = 18 \times 10^8\ h\eta/(D_1 - D_2)gt \qquad (V)$$

where d is diameter in microns, η is viscosity in poises, h is distance settled in centimeters, D_1 is absolute density of the particles in grams/cc, D_2 is density of the medium, g is 980 (the gravity constant), and t is time in seconds.

Using this formula, the diameter corresponding to a 100-min settling time is calculated. From the graph, the percentage settled at 100 min is determined, and this percentage plotted against calculated diameter. A point corresponding to 1-min settling time is plotted against ten times this diameter, and a straight line drawn through the two points. This plot can be made on the same sheet of log-probability paper used for the original data.

From this graph, it is possible to determine the median diameter, d_{op}, which is the 50% point and also the standard deviation, σ, which is given by σ = diameter at 50.00%/diameter at 15.87%.

[2] d is the particle diameter, λ the wave length of light, while m is the ratio of refractive indices of particle and medium.

[3] $F(d)$ is the cumulative per cent of particles having diameters below diameter d.

The median optical diameter, d_{op}, is also the geometric mean optical diameter based on area. The geometric mean diameter, d_g, as defined by DallaValle (5), is expressed as

$$\log d_g = \Sigma n \log d / \Sigma n \qquad \text{(VI)}$$

This diameter is based on length, as determined by microscopic counting. Similarly, d_g', is the geometric mean diameter based on weight (or volume) in the case of a screen analysis. So there are three separate geometric mean diameters: d_g based on length, d_{op} based on area, and d_g' based on volume.

From the two parameters d_{op} and σ, thus obtained, any desired statistical diameter can be calculated using methods given by DallaValle (3) or Herdan (4). Some of these conversion formulas are listed below[4] for the most commonly used diameters. The parameters d_g and d_g' are defined above; d_{vs} represents the mean volume-surface diameter, and d_w the weight mean diameter in DallaValle's notation.

$$\log d_g = \log d_{op} - 4.606 \log^2\sigma \qquad \text{(VII)}$$

$$\log d_g' = \log d_{op} + 2.303 \log^2\sigma \qquad \text{(VIII)}$$

$$\log d_{vs} = \log d_{op} + 1.151 \log^2\sigma \qquad \text{(IX)}$$

$$\log d_w = \log d_{op} + 3.454 \log^2\sigma \qquad \text{(X)}$$

It is sometimes convenient to have a frequency curve with per cent plotted against diameter or against log of the diameter. This is done by picking off appropriate points and plotting differences against the average of the diameters using uniform intervals. In the case of a plot against log diameter, a geometric progression of diameters is used, e.g., 0.5, 1, 2, 4, 8 μ, with the point being plotted at the geometric mean of the interval.

The probability chart method of representing particle size distribution is not commonly used in the pipette method of measurement. In the present application, the procedure used was very similar to that used for optical measurement. It was tested to confirm by another method the fact that the distribution present in phosphors conformed to the log-normal law. The weight of powder in a unit volume of suspension was determined at a fixed point after various times of settling and expressed as a percentage of initial concentration. These quantities were then plotted against time on log-probability paper, and, by Stokes' law, converted to a plot of diameter. A comparison of the two methods is shown in Fig. 1. It should be noted that in the optical method 100-min settling corresponds to 2.1 μ, while in the pipette method 100 min corresponds to 4.4 μ, because of differences in the distance settled and in viscosity of the media. Both methods show that distribution was of the log-normal type.

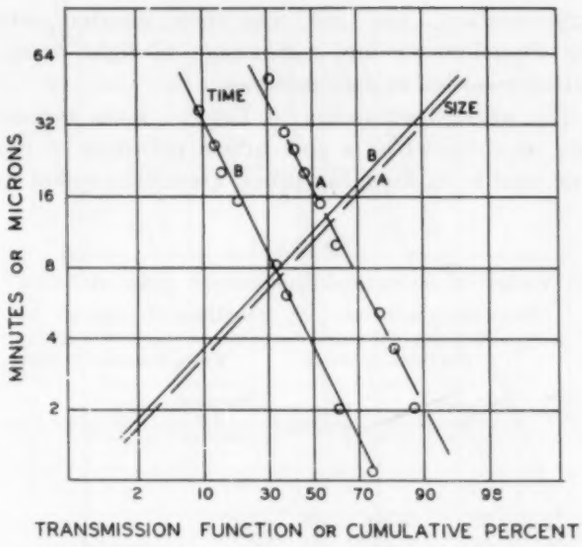

FIG. 1. Comparison of particle size distributions of halophosphates determined; curve A, by pipette method, curve B, by optical method.

EXPERIMENTAL DATA

In the present paper, data are intended to show application of the method to several phosphors, with some examples to show the effect of variables in the testing method on results.

Typical Experimental Run

Experimental data reported in this paper were obtained on the Photelometer.[5] This instrument (1) consists essentially of a tungsten light source, a sedimentation cell, and a photocell whose response is measured on a microammeter. The amount of light which passes through the cell is recorded at predetermined time intervals. A reading of 100% transmission through the clear medium in a duplicate cell is used as reference. Although no provision is made for control of temperature around the cell itself, heat generated from the light source is eliminated by means of a heat absorber placed in the light path. A volume of 13 ml of suspension is normally placed in the cell. These conditions give a settling path of 3.4 cm.

To determine particle size, enough powder to give an initial transmission of between 20–40% (preferably 20–30%) is dispersed in a suitable medium. A more complete discussion of methods of dispersing is included in the next section. For most phosphors, a trisodium phosphate solution (1.0 g/100 ml water) accompanied by hand shaking of the cell for two minutes was found adequate to produce complete

[4] The authors wish to thank Mrs. Mary S. Jaffe, one of the reviewers of this paper, for clarifying the mathematics of this difficult subject and correcting some errors in the formulas.

[5] Central Scientific Company.

deflocculation. The cell was then inserted into the Photelometer and percentage of light transmitted recorded at various times.

The work sheet shown in Table I gives typical data as obtained on a zinc sulfide phosphor of the type used in cathode ray tubes. Data correspond to

TABLE I

Powder type—cathodoluminescent zinc sulfide
Dispersing solution—1% trisodium phosphate

Time (min)	Hand shaking (2 min)			Waring dispersion (5 min)		
	Photelometer reading (L_t)*	Log ($1/L_t$)	100 B_t/B_0	Photelometer reading (L_t)†	Log ($1/L_t$)	100 B_t/B_0
	%					
¼	42	0.376	95			
½	44	0.357	89			
¾	47.2	0.327	82			
1	51	0.282	71	35.5	0.450	86
1¼						
1½	61	0.224	56			
1¾	64	0.194	49			
2	68	0.168	42	41	0.388	74
3	83	0.081	20	45.4	0.342	66
4	92.5	0.034	8.5	49.2	0.308	59
5				53	0.276	53
6				55	0.260	49
7				57	0.244	47
8				60	0.222	43
9				62	0.208	40
10				64	0.194	37
15				70	0.156	30
20				72	0.144	27
25				74	0.131	24

* At zero time (by extrapolation), Photelometer reading 40%.

† At zero time, Photelometer reading 30%.

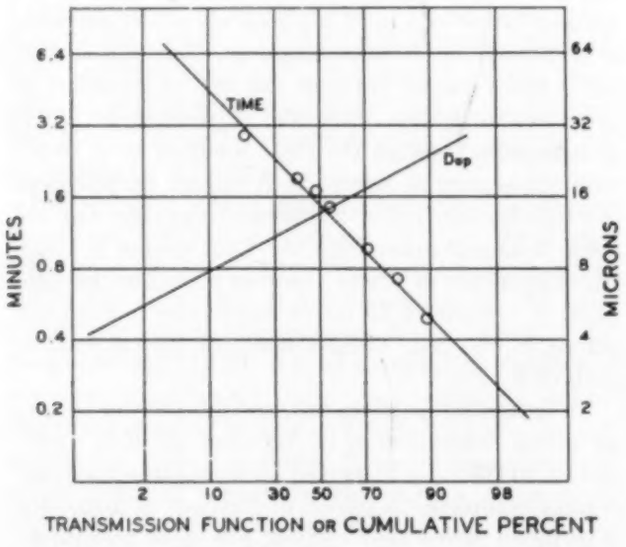

FIG. 2. Transmission function and derived particle size distribution of cathodoluminescent zinc sulfide; dispersed by hand shaking.

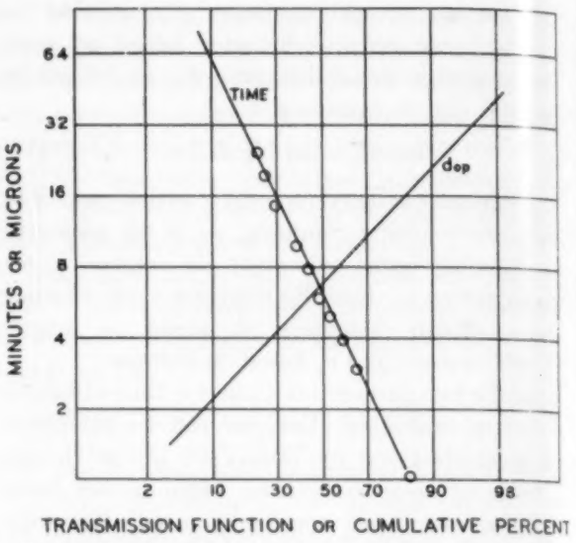

FIG. 3. Transmission function and derived particle size distribution of cathodoluminescent zinc sulfide, dispersed by Waring blendor.

TABLE II. *Data for Stokes' law calculation for* ZnS

Temperature	25°C
Medium	Water
Viscosity	0.009 poises
Settling distance	3.4 cm
Particle density	4.10 g/cc
Medium density	1.00 g/cc
Time in seconds	6000
Calculated particle diameter	1.75 μ

Fig. 2 and 3. Table II gives necessary data for the Stokes' law calculation shown by formula (V).

Method of Testing Dispersion

In dealing with sedimentation, the effect of dispersion is vitally important. Since terminology is very poorly established, "primary particle," "aggregate," and "flocculate" as used in this paper will be defined.

A "primary particle" is one which, when observed in the microscope, has well-defined boundaries and appears to be a single crystal.

An "aggregate" is a group of primary particles held together by some type of cementing agent so that mechanical work is needed to separate them.

A "flocculate" is a group of primary particles or of aggregates present in a suspension, and held together by electrical charges, so that only a minute amount of mechanical work is needed to break them down into smaller particles. Such flocculates are not present if the suspension is properly dispersed.

The major problem in preparing suspensions for any determination of particle size by sedimentation is that of preventing flocculation, since settling rate of a flocculate is approximately that of an equivalent

spherical particle having the same total mass. To obtain accurate results, it is therefore necessary to use a dispersing agent to prevent flocculation.

To determine whether a suspension is deflocculated, a quick test is observation of a drop of the suspension magnified about 250 times. If sufficient dispersing agent is present, smaller particles will be in Brownian motion, and when two of these small particles come in contact, they will promptly separate rather than cohere. Use of an excess of agent may lead to reflocculation.

A more precise test is to determine particle size with varying amounts of dispersing agent present. If dispersion is good, particle size will be reproducible and will be smaller than the size obtained when either insufficient or excess agent is used.

Method of Dispersing Phosphors

Since phosphors as prepared and used are known to contain large numbers of aggregates of various sizes and band strengths, it is obvious that the method of dispersion may have a great effect on particle size distribution.

If severe mechanical work is applied to the suspension, all but the most firmly cemented aggregates will be completely separated and particle size distribution will approach that of primary particles. If this work is performed on a dilute suspension, for example by agitation with a Waring blendor, it is improbable that any primary particles will be broken, but aggregates should be separated. This is discussed in more detail in a later section.

Fig. 4 shows the effect of various periods of agitation in the Waring blendor with 0.2 gram of a fluorescent ZnS and 1.0 gram of phosphate per 100 ml of water. Effects of aggregation on settling rate are quite striking. The shaken suspension is apparently a mixture of coarse and fine material as shown by the break in curve A. The coarse fraction is quite uniform; i.e., on a particle size basis, σ is low. With increasing time of agitation in the blendor this breaks down gradually. At one minute a mixture of coarse and fine exists as seen in curve B; at three minutes there is no evidence of coarse material (curve C); and at ten minutes the settling rate is still slower. Conversion of these data to particle size distributions shows that σ becomes smaller for the fine fraction as time of agitation increases.

Obviously, a great deal of care is needed in setting conditions of dispersion for powders of this type, if reproducible results are to be obtained.

Very gentle agitation, such as shaking by hand or by a wrist-action mechanical shaker, is sufficient to deflocculate the material without breaking down any aggregates except those with very weak bonding.

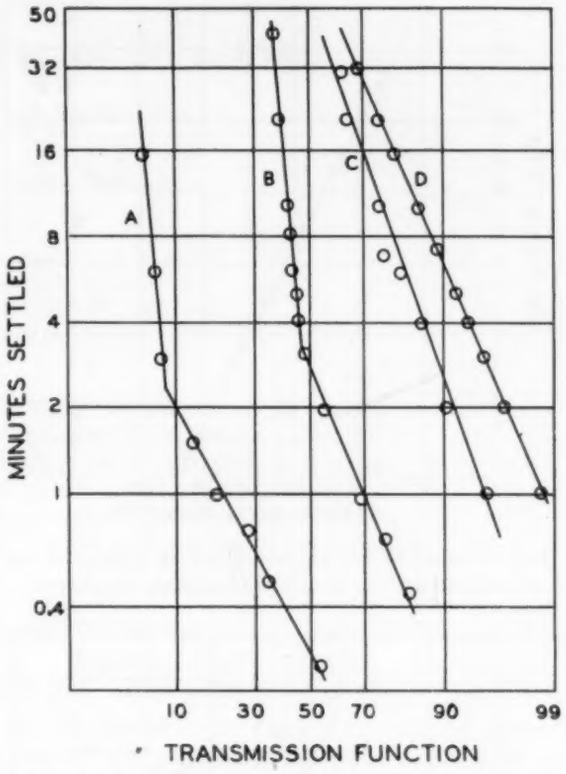

FIG. 4. Effect of dispersion time in Waring blendor on transmission function 100 B_t/B_0; curve A, hand shaken; curve B, 1-min mix; curve C, 3-min mix; curve D, 10-min mix.

Particle sizes obtained have been designated: (*a*) aggregate particle size (D_{op}). This is the result obtained by hand shaking for two minutes; (*b*) ultimate particle size (d_{op}).[6] This result is obtained using the Waring blendor.

As was indicated in the experimental section, phosphors were dispersed with suitable agents in distilled water. Approximately 0.2 gram of phosphor was used per 100 ml of solution in the Waring blendor tests. In hand shaking, sufficient phosphor was added to 13 ml of the solution to give an initial transmission reading of between 20–30%.

Data on Calcium Halophosphates

Several dispersing agents were tried with calcium halophosphates; of these, dilute ammonium hydroxide or dilute trisodium phosphate gave the most reproducible results. The effect of powder concentration during sedimentation was tested by runs with 0.5 gram/100 ml giving an initial transmission of 12% and 0.17 gram with an initial transmission of 39%. The results, shown in Fig. 5, in-

[6] This "ultimate particle size" approximates that of primary particles, but a few aggregates may be present.

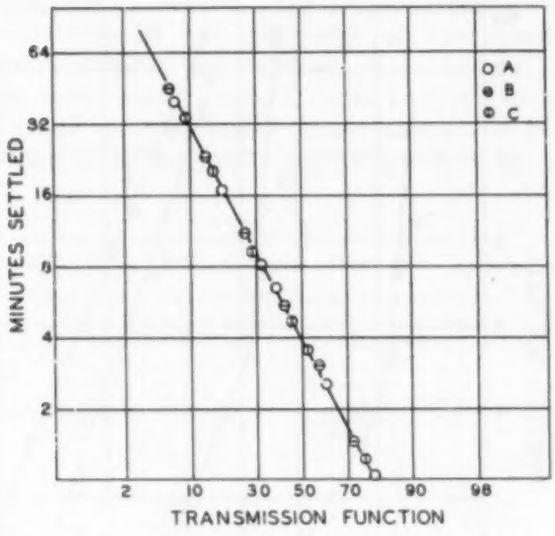

FIG. 5. Effect of concentration during sedimentation on transmission function with halophosphate phosphor.

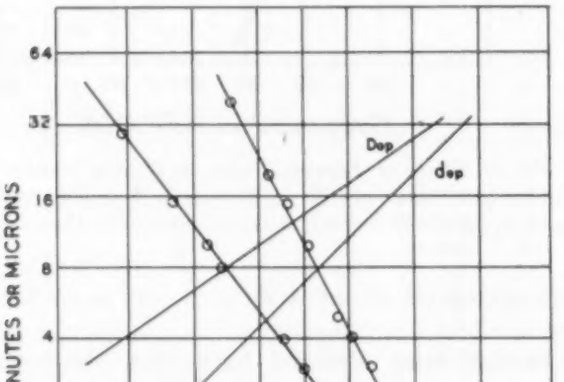

FIG. 6. Transmission function and derived particle size distribution of calcium tungstate; D_{sp}, dispersed by hand shaking; d_{sp}, dispersed by Waring blendor.

dicate that concentration is not an important factor.

It has been found experimentally that the amount of work performed on the halophosphate suspension by the Waring blendor does have some effect on particle size. The effect is, however, much less pronounced than with zinc sulfide. Aggregates are apparently separated in 3 min, and very little change in particle size results from further agitation. Change in amount of sample does have some effect with larger sample sizes leading to apparent smaller particle sizes. This may be due to breaking by impact of one particle against another.

There is a striking difference in behavior of various phosphors when agitated in a Waring blendor. Halophosphate phosphors show evidence of some aggregation, but the breakdown from mechanical work is slight. In contrast, the fluorescent zinc sulfide[7] is composed of large aggregates, which are readily separated by the Waring blendor, indicating that bonding forces are weak. Each particular powder must, therefore, be tested with varying degrees of mechanical work to determine how much dispersion is needed to give the ultimate particle size.

Data on Calcium Tungstate

Fig. 6 shows typical data on a calcium tungstate phosphor dispersed by two methods. The effect of mixing in the Waring blendor was much like that observed with calcium halophosphate.

CONCLUSION

This paper has presented a quick method for determination of particle size distribution of phosphors by measurement of optical transmission during sedimentation. It has been assumed that Beer's law applies, and that distribution conforms to the log-normal law. Accuracy is more than adequate for many control and experimental applications. In addition to phosphors, the method is potentially useful for other powders with particle sizes between 2 and 50 μ.

Any discussion of this paper will appear in a Discussion Section to be published in the December 1954 issue of the JOURNAL.

REFERENCES

1. M. N. STATES, *A.S.T.M. Proc.*, **39**, 795 (1939).
2. J. R. MUSGRAVE AND H. R. HARNER, "Turbimetric Particle Size Analysis," Eagle-Picher Research Laboratories, Joplin, Mo. (1947).
3. J. M. DALLAVALLE, "Micromeritics," Pitman Publishing Co., New York (1943 and 1951).
4. G. HERDAN, "Small Particle Statistics," Elsevier Publishing Co., New York (1953).
5. J. R. DEVORE AND A. H. PFUND, *J. Opt. Soc. Amer.*, **37**, 826 (1947).
6. R. O. GUMPRECHT AND C. M. SLIEPCEVICH, *J. Phys. Chem.*, **57**, 90 (1953).
7. E. K. FISCHER, "Colloidal Dispersions," Chap. II, John Wiley & Sons, Inc., New York (1950).

[7] The fluorescent zinc sulfide was New Jersey zinc #2304, a fine partial size material intended for use in paints.

Electrothermal Heating of Solutions[1]

KENNETH A. KOBE

University of Texas, Austin, Texas

AND

CARL J. CARLSON

Standard Oil Company of California, Avenal, California

ABSTRACT

For heating and evaporation of concentrated solutions of electrolytes, the solution itself can serve as a resistor to give uniform heating throughout. Solutions of salts having a negative temperature coefficient of solubility can be concentrated by electrical heating, provided electrodes are maintained at a temperature below that of the solution. Experimental details are given for solutions of sodium sulfate. The electrical conductivity of saturated solutions of Na_2SO_4, Na_2CO_3, Na_3PO_4, and $MgSO_4$ has been determined from 25°C to 75° or 90°C.

INTRODUCTION

It is difficult to heat solutions of salts which have a negative temperature coefficient of solubility. These salts with an "inverted solubility curve" are well known as ones that form hard deposits of scale on heat transfer surfaces. Sodium sulfate, sodium carbonate, and calcium sulfate are salts of this type. Sodium sulfate is of particular importance because it usually is recovered from natural brines and industrial operations as sodium sulfate decahydrate, $Na_2SO_4 \cdot 10H_2O$, containing 56% water which must be removed before it is economical to ship the salt any distance. This problem of dehydration is one that has been attacked by many methods (1), of which submerged combustion, or internal heating with hot gases, has been the most successful (2). This process requires gaseous fuel which is not available in many localities.

One possible method of heating concentrated solutions has not been investigated. Little use has been made of the fact that the concentrated solution itself can be made the resistor in an electrical circuit and electrical power converted into heat uniformly within the body of the solution. The electric steam boiler is well known, but this has operated on dilute solutions. No work has been done on use of electrical energy for internal heating of saturated solutions, particularly solutions of those salts that are scale-formers.

SALT HYDRATES

Some salts that are dehydrated industrially to produce an anhydrous, or less hydrated, salt are $Na_2SO_4 \cdot 10H_2O$ (which contains 44.2% anhydrous salt), $Na_2CO_3 \cdot 10H_2O$ (37.1%), $Na_3PO_4 \cdot 12H_2O$ (43.2%), $MgSO_4 \cdot 7H_2O$ (48.9%), $FeSO_4 \cdot 7H_2O$ (54.7%). Although the feasibility of using electrical power for the dehydration process depends on economic considerations, the technical merit of the process warrants investigation, as does the action of scale-forming salts on electrodes. Fundamental data should be obtained which can be used for design purposes.

A large amount of data is available on electrical conductivity of dilute salt solutions, but few data are available on saturated solutions. Conductivity of saturated solutions of four salts (Na_2SO_4, Na_2CO_3, Na_3PO_4, and $MgSO_4$) was determined from 25° to 75° or 90°C. Saturated solutions of an analytical grade of these salts were prepared by rotating a bottle containing a salt excess for 1 to 7 days in a thermostat set at the desired temperature. Concentration of the solution was determined to ascertain that it checked known solubility data. The saturated solution was transferred from the bottle to a calibrated conductivity cell immersed in the same thermostat, and conductivity of the solution was determined. Data are given in Table I and shown on Fig. 1. It undoubtedly is safe to extrapolate conductance curves for sodium sulfate and carbonate to their normal boiling points. For sodium phosphate and magnesium sulfate, both the solubility and conductance increase with temperature, so that extrapolation may not give a reliable value.

DEHYDRATION OF SODIUM SULFATE DECAHYDRATE

Because of the industrial importance of sodium sulfate and its well-known tendency to form scale, a small installation was built to study dehydration of sodium sulfate decahydrate to anhydrous salt.

[1] Manuscript received April 17, 1953. The experimental work reported here was conducted in the laboratories of the Department of Chemical Engineering, University of Washington, Seattle, Washington.

TABLE I. *Specific conductance of saturated solutions of four salts*

Temp, °C	Specific conductance, mhos per cm²			
	Na_2SO_4	Na_2CO_3	Na_3PO_4	$MgSO_4$
25.0	0.124	0.103	0.0702	0.0473
27.6	0.137	0.0984	0.0751	0.0494
30.0	0.147	0.0991	0.0821	0.0506
34.8	0.152	0.102	0.0867	0.0524
42.8	0.188	0.134	0.0973	0.0537
50.0	0.218	0.167	0.104	0.0545
64.0	0.278	0.234	0.187	0.0572
75.0	0.334	0.286	0.228	0.0588
90.0	0.394	0.366		

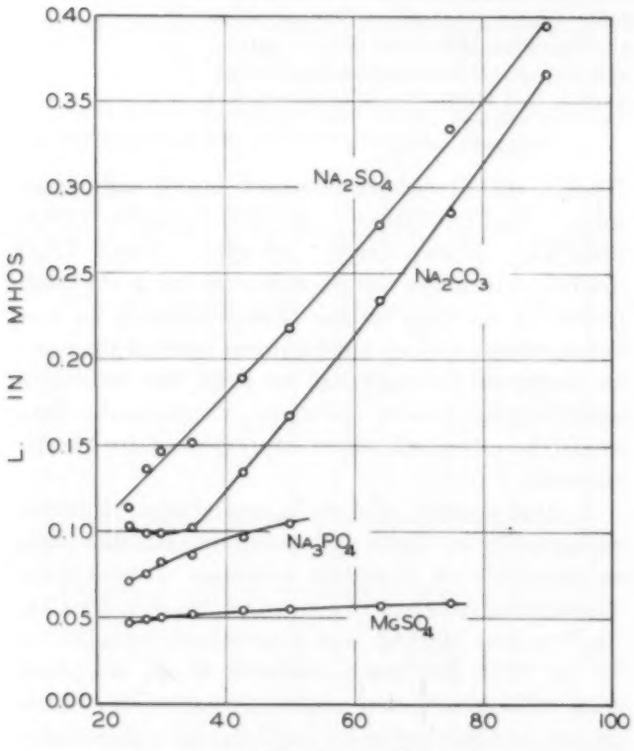

FIG. 1. Electrical conductivity of saturated salt solutions

The transition temperature of decahydrate to anhydrous salt is 32.4°C, above which sodium sulfate has a negative temperature coefficient of solubility. Solid sodium sulfate decahydrate added to a boiling solution will melt incongruently and immediately deposit part (47%) of the anhydrous sodium sulfate. The remainder of the sodium sulfate must be obtained by evaporating the water of hydration. A cycle of operations can be devised which will require a minimum of electrical energy by taking only the anhydrous sodium sulfate deposited on melting and returning the mother liquor to a natural pond for recrystallization of more decahydrate crystals. Such an operation calls for more pumping and handling of solids, so usually it is not practical for operations based on industrial production of decahydrate, or where refrigeration is used to crystallize decahydrate from a solution.

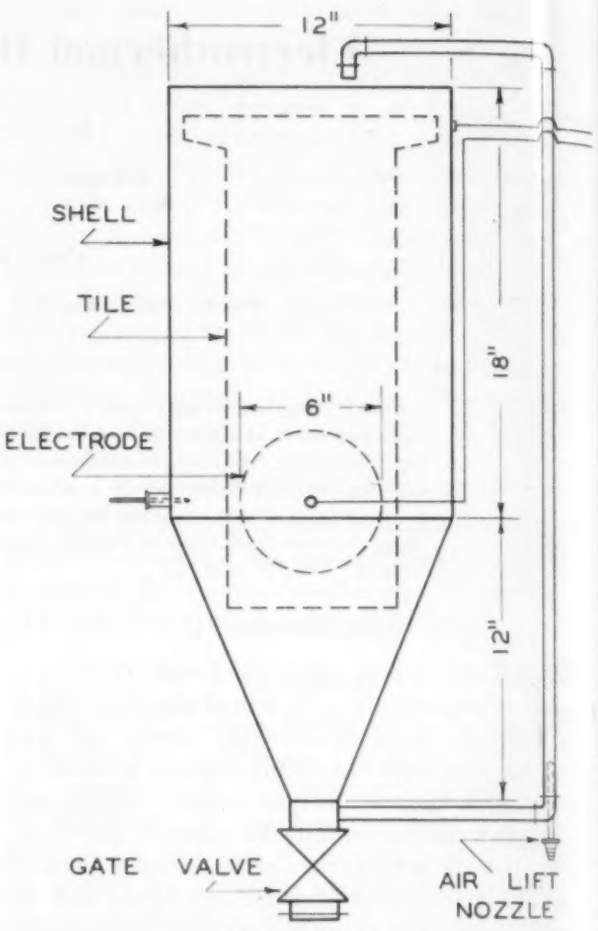

FIG. 2. Evaporator

An evaporator with a conical bottom was adapted for electrothermal heating. Fig. 2 shows the evaporator, 12 in. in diameter, body 18 in. high with a conical bottom 12 in. high terminating in a 2-in. ips coupling to which was attached a rapid opening gate valve. To circulate the solution, a ¾-in. pipe was connected at the bottom with an air inlet to form an air-lift. Because of the relatively small diameter of the evaporator, a glazed sewer tile was hung centrally in the evaporator body and one electrode, a 6-in. diameter disk, was suspended within the tile. The evaporator body served as the other electrode and resistance of the system could be varied by changing the location of the central electrode. The 60-cycle electrical power was passed through a step-down transformer to give 150 amps at 32 volts. A wattmeter in the circuit measured power input to the evaporator. The evaporator body was covered with magnesia insulation to decrease heat losses. A preliminary experiment showed that evaporation was equivalent to 95.0% of power input.

Numerous runs were made varying the central electrode size and position and with various rates of feed of decahydrate to the evaporator and various

rates of circulation of solution within the evaporator. From these experiments it was concluded that the electrothermal method of heating was entirely satisfactory for saturated solutions of sodium sulfate. Boiling took place uniformly throughout the solution. Solid sodium sulfate decahydrate could be fed directly to the solution to take advantage of incongruent melting. Crystal size of anhydrous sodium sulfate deposited from solution depended on crystal size of the decahydrate feed. Large-size feed crystals formed larger crystals of anhydrous salt. In general, most of the anhydrous salt was retained on a 48 mesh screen. Circulation of solution using the air-lift caused a marked increase in size of the crystals formed, as would be expected from the Oslo system of evaporation and crystallization (3).

Scale Formation and Corrosion

In all runs with sodium sulfate, scale formed on the central electrode but none formed on the evaporator body which was the other electrode. Because of small area and high current density on the central electrode, its surface temperature undoubtedly was higher than the solution temperature, so that scale formation on the hotter surface was inevitable. Scale would decrease the amount of current that could pass through the electrode surface. At times the hard scale would crack and fall from the electrode, which would cause a surge of current into the solution, but continued operation would build up another layer of scale.

The problem of scale formation was studied along with electrode corrosion in a different electrolytic cell. This was a rectangular stone cell, 7 x 7 x 18 in., which was covered with thermal insulation. One electrode was a sheet iron box 5.5 x 4.5 x 0.5 in. In two hours this electrode was covered with an impervious coating of scale. A similar electrode was made, differing from the first only by placing copper inlet and outlet tubes so that water could be circulated through the box. On this new electrode, maintained at a temperature below that of the solution, no scale formed after six hours of operation (4). These electrodes after use are shown in Fig. 3.

Corrosion was found with mild steel electrodes, so a study was made of other materials. Electrodes

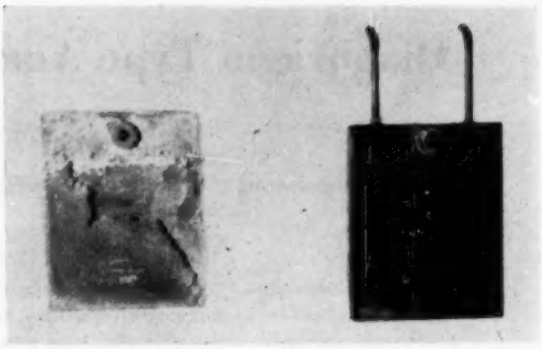

Fig. 3. Uncooled (left) and cooled (right) electrodes operating in boiling sodium sulfate solution.

TABLE II. *Corrosion of electrode materials in ten hours in boiling sodium sulfate solution*

Metal	Loss in wt, %
Galvanized iron	2.3
Copper	9.0
Tin	2.6
Stainless steel, KA2	0.0
Aluminum	13.4 (1 hr only)
Monel metal	2.4
Zinc	3.3
Lead	20.0
Cast iron	Nil

were cut approximately 5 x 6 in. and measured accurately as to area and weight. Current density was maintained at 4.4 amp/dm^2, and time of operation was 10 hr. Results are given in Table II. All metals showed marked corrosion except stainless steel, sheet tin, and cast iron. Monel metal showed deep grooves after ten hours. No quantitative measurements could be made on cast iron because of the weight of the electrode. After 20 hours of operation, no pitting or corrosion could be observed.

Any discussion of this paper will appear in a Discussion Section to be published in the December 1954 issue of the Journal.

References

1. K. A. Kobe and C. W. Hauge, *Can. Chem. Met.*, **18**, 177 (1934).
2. K. A. Kobe, C. J. Carlson, and C. W. Hauge, *Ind. Eng. Chem.*, **28**, 589 (1936).
3. H. Svanoe, *ibid.*, **32**, 636 (1940).
4. K. A. Kobe, U. S. Pat. 2,272,345, Feb. 10, 1942.

Diaphragm Type Amalgam Caustic-Chlorine Cell[1]

CHAS. POTTER[2] AND A. L. BISIO

Department of Chemical Engineering, Columbia University, New York, New York

ABSTRACT

An amalgam-type caustic cell was studied. It consisted of an anode compartment which contained brine and graphite anodes, and a cathode compartment which contained a mercury cathode, denuder water, and graphite chips. The compartments were separated by a horizontal "nylon" cloth diaphragm. Optimum operating characteristics of the cell were: denuder liquor velocity, 8.0 gal/hr/ft² Hg; brine velocity, 1.0 gal/hr/ft² Hg; brine temperature, 50°C; current density, 1.0 amp/in.² Hg, and a voltage drop of 3.70 volts. The cell produced 0.80 lb caustic soda/kwhr at a current efficiency of 90–91%. This indicates slightly improved efficiencies over present commercial operation.

INTRODUCTION

Most commercial amalgam caustic-chlorine cells employ flowing mercury in both the electrolyzer and decomposer sections of the cell. A cell with a stationary mercury pool supported between an electrolyzer section on the bottom and a decomposer section above should be effective. Since sodium amalgam is lighter than mercury, the amalgam should rise from the electrolyzer interface to the decomposer interface.

A similar cell may have been proposed earlier (1, 2). Operation of such a cell was apparently not successful due to failures of construction material. Patents (3–5) have been issued to cover this type of cell construction; however, no extensive studies have been reported.

EXPERIMENTAL

Cell

A diagram of the cell is given in Fig. 1.

Brine solution was kept in a two-liter glass vessel which contained a shelf built around its circumference. On the shelf, supported by rubber blocks, rested a glass cylinder of 350 ml capacity. A taut nylon cloth[3] which acted as the diaphragm was stretched across its lower face. The cloth was fastened around the glass cylinder by a metal band; the edges of the cloth as well as the metal band were covered with de Khotinsky cement. A 0.135 cm thick mercury pool was placed on the diaphragm, and above the mercury pool rested 250 ml of water. Except where otherwise noted, graphite chips completely covered the mercury-water interface to provide a surface of low hydrogen overvoltage. Chip size was $-3.5/+4.0$ Tyler Standard Screens; there was 0.75 gram graphite/cm² mercury surface. The anode was a graphite plate which encircled the inner compartment at mercury level. Thus, electrolyzer and decomposer sections were created.

Electrolyzer or denuder solution could be added independently or removed by means of siphons and dropping funnels. Mechanical agitation was not employed in either compartment of the cell. Brine feed to the electrolyzer was saturated at the brine feed temperature. A standard selenium rectifier was used to provide power needed for experimental work. Auxiliary voltmeters and ammeters were placed in the electrical circuit of the cell as needed, in addition to meters contained in the rectifier assembly.

Ordinary electrode-grade graphite[4] proved suitable for electrolysis of the brine. With proper control of brine composition at 324 ± 30 grams NaCl/liter H_2O, long anode life can be anticipated. Graphite anodes which were kept under 24-hr service for three months showed no change in weight, water displacement, electrical conductivity, or visual appearance. During prolonged electrolysis the cell showed no voltage trend, indicating absence of any significant change in surface characteristics of the electrode.

Contact to the mercury cathode was made by a Monel screen immersed in the mercury. The electrical contact was permanent and effective, and amalgamated after a few moments of operation.

Voltage Studies

Voltage drop across the cell depends upon the average current density at which the cell is operated, temperature, concentration of electrolyte, sodium content of the amalgam, cathode-anode spacing, diaphragm resistance, and means of removing chlorine bubbles. The voltage-current density relationship for the experimental cell is shown in Fig. 2.

[1] Manuscript received May 15, 1953. The work reported in this paper is taken from the thesis of Attilio Bisio presented in partial fulfillment of the requirements for the degree of Bachelor of Science, June 1953.

[2] Present address: Amersil Company, Inc., Hillside, New Jersey.

[3] "Vinyon N" cloth supplied by the Carbide and Carbon Chemical Corporation, New York, N. Y.

[4] Grade A6NX, National Carbon Company.

Exact slope of the curve is influenced by details of cell construction and by the extent to which parasitic resistances have been minimized. Voltage drop across the cell increased relatively slowly with increasing average current density. The fact that no gas is generated at the mercury cathode contributes substantially to this favorable relationship. High conductivity of brine solution is also a contributing factor.

Cell voltage was not influenced by brine flow rate over the range 0.0–10.0 gal/hr/ft² Hg. Flow rate is defined as the turnover in a chamber, in the sense that it is an indication of volumetric contact with the mercury surface. The geometry modifies effects of turnover. At flow rates higher than 10 gal/hr/ft² Hg and constant average current density, the voltage initially decreased with increasing flow rate, then finally levelled off. No quantitative measurements were made in this region. The denuder flow rate had no effect on voltage drop across the cell, which is shown as a function of temperature in Fig. 2.

Since decomposition voltages of brine solutions were not determined, caution should be exercised in extrapolation of these curves. Temperature coefficient of the voltage was 0.035 volt/°C at all current densities. Temperatures given in Fig. 2 are those of the brine; denuder temperatures were generally 5–10°C higher.

The cell was operated with a brine temperature of 50°C in all succeeding work.

Anode potential, cathode potential, and voltage drop across the diaphragm were determined with a calomel half-cell and tubulus (6–8); voltage drop in solution and contact drops were determined by difference. These potentials are plotted in Fig. 3. Probable error in each of the measured potentials is less than 0.01 volt.

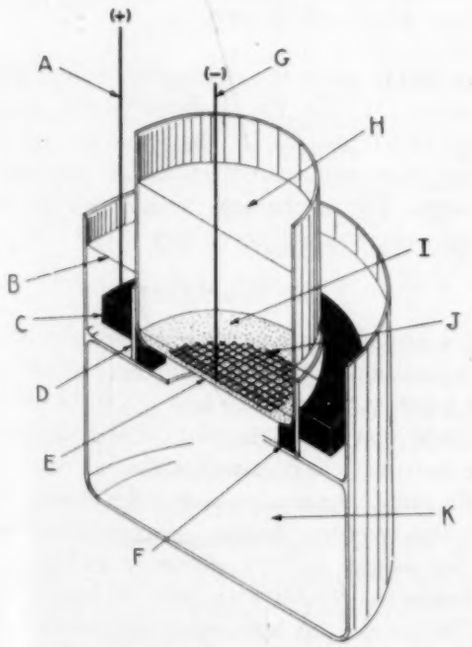

FIG. 1. Cell construction. A—anode lead; B—brine liquid level; C—anode (graphite ring); D—insulation; E—nylon diaphragm; F—rubber block supports; G—cathode lead; H—denuder section (pure sodium hydroxide solution); I—mercury pool; J—Monel screen contact; K—brine.

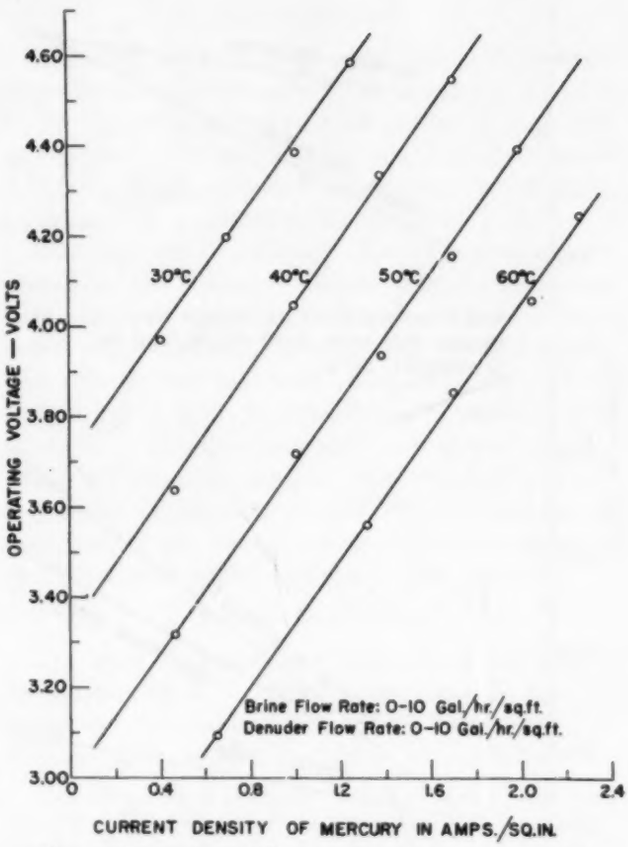

FIG. 2. Operating voltage as a function of current density and temperature.

Voltage drops across the solution, diaphragm, and contact were small in comparison to anode and cathode potentials (Fig. 3). Voltage drops across the diaphragm were of the same order of magnitude as comparable published measurements for the diaphragm of a Vorce cell (9).

Anode potential was an important item in voltage drop across the cell, since its variation with current density was greater than that of the other potentials. Factors governing anode potential in a mercury cell are the same as in a diaphragm cell except that brine concentration and current density are somewhat higher (10, 11). At 1 amp/in.² the anode potential is 1.580 volts. Assuming that chlorine discharge potential on platinum is 1.330 volts (12), a polarization of 0.25 volt results at a current density of 1 amp/in.² This value is a reasonable approximation of published measurements (9, 13).

Anode potential measured during prolonged electrolysis was somewhat lower than that found in short laboratory tests. This occurred repeatedly, the

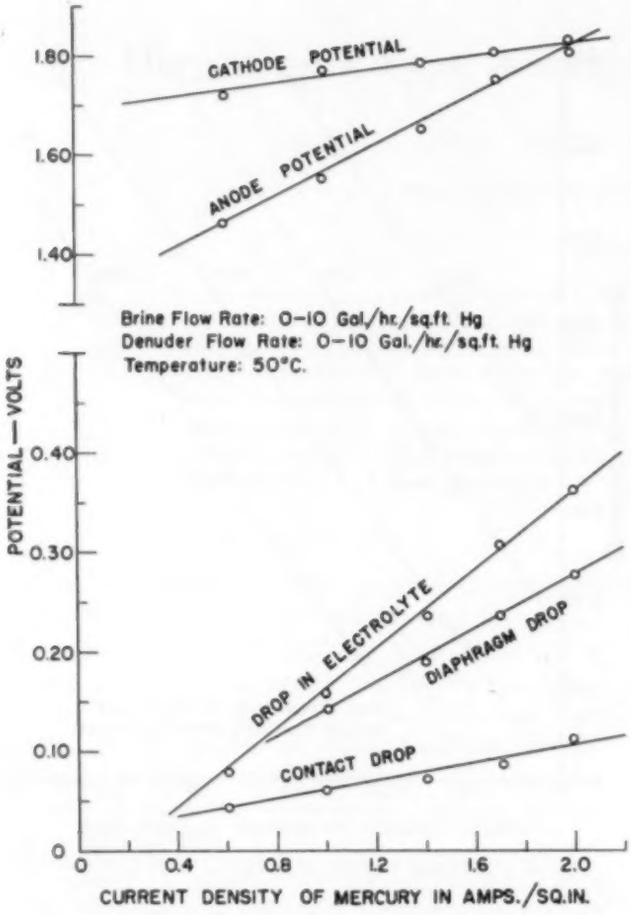

FIG. 3. Individual potentials as a function of current density.

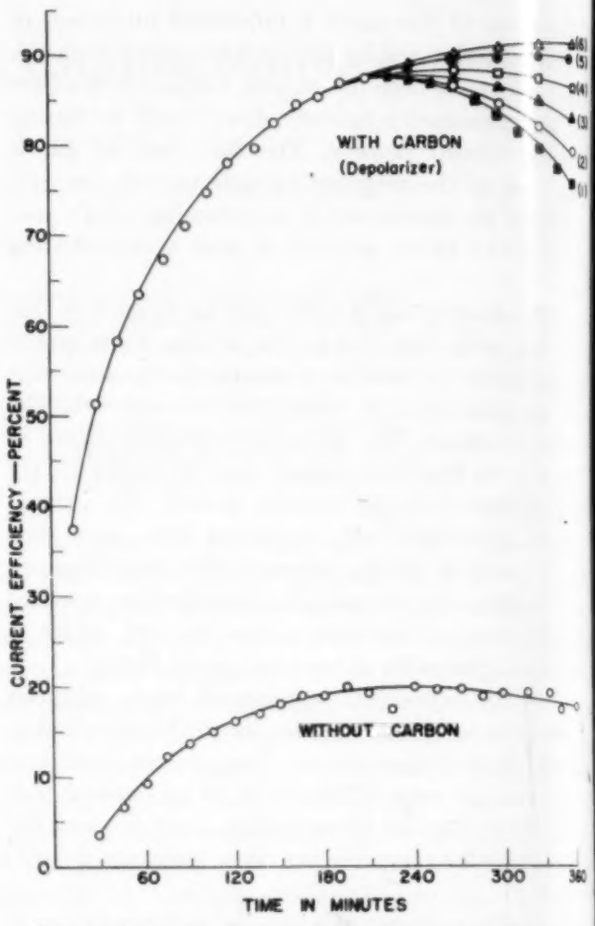

FIG. 4. Instantaneous current efficiency as a function of time of operation and denuder liquor velocity. Current density: 1 amp/in.² Hg; temperature: 50°C. Flow rates in gal/hr/ft² Hg; brine flow: 1.0; denuder flow: (1) 0.0, (2) 2.0, (3) 4.0, (4) 6.0, (5) 8.0, (6) 10.0.

depression being greater than the experimental error; at present no reason is advanced as to why this should occur. The effect, however, may be due to some type of anode conditioning by chlorine evolution.

Cathode potential is influenced only slightly by current density in comparison with anode potential. This is to be expected since polarization is effected by current density only in case of gas evolution (14). Changes in brine concentration influence cathode potential but slightly, whereas a change in amalgam concentration has a more pronounced effect (11).

Operating Current Density

Current efficiency of the cell over a wide range of brine and denuder velocities depended upon the average current density at which the cell was operated. Visible gas evolution at the cathode occurred above a current density of 1.2 amp/in.² It is also probable that incipient gas generation occurred at lower current densities. All succeeding work was carried out at a current density of 1 amp/in.² Operating voltage at 50°C was 3.70 volts.

Amalgam Denuder Studies

Graphite chips were floated on the mercury pool surface in an effort to provide low hydrogen overvoltage and promote the reaction of sodium amalgam with water (11, 13). Fig. 4 shows that at a denuder velocity of 0.0 gal/(hr/ft² Hg), presence of the depolarizer increased current efficiency approximately four times. The mechanism of amalgam decomposition has been studied previously (13).

Flow Rate Studies

Fig. 4 also shows instantaneous current efficiency to be a function of time of operation and of denuder liquor velocity. During the first 3½ hr of cell operation, there was a slow buildup of sodium amalgam in the mercury which caused a slow increase in current efficiency, irrespective of denuder liquor velocity. When the average caustic concentration reached 8.3% by weight, current efficiency at low denuder flows began to decrease with time. At higher denuder flows, however, the apparatus approached steady state as indicated by curves 5 and 6 of Fig. 4. Raising denuder liquor velocity above 10.0 gal/hr/ft² Hg when the average caustic concentration is less than 32% had no effect on current efficiency.

Decrease of current efficiency at low denuder liquor flows was due to concentration polarization at

the mercury-caustic interface which slowly increased with time. There were indications that caustic concentration at the mercury-caustic interface was over 35% by weight. Higher denuder liquor flow rates reduced this concentration polarization.

Although brine velocities were varied over the range 0.0 to 10.0 gal/hr/ft² Hg, this variation did not have any effect on the relationship between current efficiency and time as presented in Fig. 4. This was anticipated since the amount of brine consumed during a run amounted to less than 10% of total brine present. If electrolysis were continued for a longer period, however, cathodic polarization would be expected.

Inasmuch as turnover had no effect on early stages of amalgam buildup, one may speculate that rate of buildup was due to transfer of sodium controlled by a chemical step. After 3½ hr of operation, turnover did have an effect on rate of buildup, and here one may speculate that transfer of sodium was controlled by a convectional or diffusional process.

Steady-state cell operation after 3½ hr of buildup at a denuder velocity of 8.0 gal/hr/ft² Hg and a brine velocity of 1.0 gal/hr/ft² Hg permitted operation at a current efficiency of 90–91% and attainment of a caustic concentration of 32.0% by weight. Concentration polarization then increased to such a point that current efficiency was less than 90.0%. If at this time denuder liquor velocity was increased above 30 gal/hr/ft² Hg, caustic concentration could be built up to 40% by weight before concentration polarization increased to such a point that current efficiency was less than 90%. At this point, however, heavy gas generation occurred at the mercury-brine interface. Gas generation was probably due to sodium concentration in the amalgam being greater than 0.2%, thus raising the sodium ion discharge potential above the potential for hydrogen discharge. This was confirmed in other experimental work (8). Titration of the sodium amalgam indicated that concentration of sodium was above 0.25% under these conditions.

The necessary increase in denuder liquor velocity after onset of concentration polarization was eliminated by operating two cells in series at a denuder liquor velocity of 8 gal/hr/ft² Hg. Transfer between the two denuder compartments caused mixing to occur, thus decreasing the tendency for concentration polarization. A caustic concentration of 40% by weight was obtained at this velocity, whereas 30 gal/hr/ft² Hg was previously necessary.

Conclusions

Operation of the experimental cell with a two-stage denuder and denuder liquor velocity of 8.0 gal/hr/ft² Hg, brine velocity of 1.0 gal/hr/ft² Hg, current density of 1 amp/in.² Hg, and voltage drop of 3.70 volts, produced 0.80 lb caustic soda/kwhr (1600 kwhr/ton) at a current efficiency of 90–91%.

It is difficult to compare this cell to others reported in the literature, since complete operating data are rarely given. However, the following statements can be made: (*a*) brine and denuder velocities noted above were well below those reported in the literature (10); (*b*) circulation of mercury was eliminated; (*c*) current density and over-all voltage drop were about the same as those reported for commercial operating units (15); and (*d*) the cell had the same output per kilowatt hour as commercial units of both the amalgam and diaphragm types.

Acknowledgments

The work presented here was greatly encouraged by the interest of Dr. Henry Linford and Dr. Edward Saubestre. The aid of Mr. David Feder and Mr. Edward Foley is also gratefully acknowledged.

Any discussion of this paper will appear in a Discussion Section to be published in the December 1954 issue of the Journal.

References

1. E. A. LeSueur, *Trans. Electrochem. Soc.*, **63**, 315 (1933).
2. E. A. LeSueur, *Trans. Am. Inst. Chem. Eng.*, **6**, 168 (1915).
3. V. Engelhardt and N. Schonfeldt, German Pat. 549,724, April 14, 1932.
4. B. Cataldi, U. S. Pat. 1,336,281, April 6, 1920.
5. T. Matayushima, U. S. Pat. 1,368,955, February 15, 1921.
6. U. R. Evans, "Metallic Corrosion, Passivity and Protection," Chap. 1, Arnold, London (1948).
7. J. N. Agar, as quoted by U. R. Evans, *J. Iron Steel Inst.*, **141**, 220 (1940).
8. U. R. Evans and T. P. Haas, *Proc. Roy. Soc.*, **A125**, 370 (1932).
9. W. W. Stender, M. M. Stronganov, and P. B. Zivotinsky, *Trans. Electrochem. Soc.*, **65**, 189 (1934).
10. G. L. Mantell, "Industrial Electrochemistry," 3rd ed., Chap. 17, McGraw-Hill Book Co., New York (1950).
11. R. B. MacMullin, *Chem. Eng. Progr.*, **46**, 440 (1950).
12. H. J. Creighton and W. A. Kohler, "Electrochemistry," 4th ed., Vol. II, p. 194, John Wiley & Sons, Inc., New York (1943).
13. W. C. Gardiner, *Chem. Met. Eng.*, **52**, No. 7, 110 (1945).
14. S. Glasstone, "An Introduction to Electro-Chemistry," p. 438, D. Van Nostrand Co., New York (1942).
15. J. H. Perry, (Editor), "Chemical Engineers Handbook," 3rd ed., p. 1810, McGraw-Hill Book Co., New York (1950).

Technical Note

Anhydrous Ethylenediamine[1]

R. M. Creamer and D. H. Chambers

Bureau of Mines Eastern Experiment Station, College Park, Maryland

Ethylenediamine has been used frequently in electrochemical investigations as a nonaqueous ionizing solvent, as a chelating agent, and as a starting material for organic synthesis. One difficulty encountered in its use has been the preparation of a dry sample. Several methods have been advanced for drying ethylenediamine (1–3). These methods, however, are time consuming, present handling difficulties, and usually give a poor yield; therefore, an attempt was made to develop a more satisfactory method. Water removal by addition of a third material that forms a low-boiling azeotrope has been used extensively in other systems for dehydration. An effort was made to employ this procedure in dehydrating ethylenediamine.

The first agent used, isopropyl ether, was found to be capable of accomplishing the desired dehydration. The main objection to this dehydrating agent was the rate of reaction; it required about 25 hr to dehydrate 350 ml of 70% diamine. Benzene proved to be a much faster dehydrating agent than isopropyl ether, probably as a result of the larger percentage of water in the benzene-water azeotrope. It was also found that a total condensing, phase-separating stillhead permitted drying to be completed with only a small quantity of dehydrating agent. This stillhead retained a portion of the condensed vapors. The light benzene fraction of the distillate was returned to the column as reflux, and only the heavier immiscible water layer was removed from the system.

Ethylenediamine was dehydrated with benzene in the following manner: 100 ml of dry benzene was added to 500 ml of 70% ethylenediamine. This two-phase mixture was placed in a 1-liter flask at the bottom of a fractionating column 90 cm long and 30 mm in diameter that was filled with 3 mm glass helices. To permit rapid dehydration, the boil-up rate from the flask was adjusted close to the column's maximum capacity. A manometer that measured the pressure in the flask was useful in preventing column flooding. The water and the small quantity of ethylenediamine that distills with it were separated from the benzene, the other component of the azeotrope, by means of the stillhead previously mentioned. The system was protected from the outside atmosphere by soda-lime tubes. During distillation, the stillhead temperature slowly increased from about 75°C to the boiling point of pure benzene, 80°C. Removal of water by the azeotrope was rapid until only the monohydrate remained, at which point the rate of water removal became slower. When the ethylenediamine was dry, a point indicated by collection of a distillate of only one phase, benzene was discharged from the stillhead and the dry diamine distilled from the column. The time required to dry 500 ml of ethylenediamine in the apparatus described was about 15 hr, a time that could probably be decreased by the use of a column of greater capacity. The concentration of ethylenediamine in the product was at least 99.5% and had a specific conductivity of 1×10^{-5} ohm^{-1} cm^{-1} or less. The yield was 88%. Most losses could be attributed to hold up in the fractionating column and still base.

This method gives a product that compares favorably in physical and chemical characteristics with the product obtained by the use of chemical methods of dehydration. The yield from the dehydration is high, the amount of dehydrating agent required is small and is easily recovered, and the dehydration and purification are completed in only a single piece of apparatus.

[1] Manuscript received May 25, 1953.

Any discussion of this paper will appear in a Discussion Section to be published in the December 1954 issue of the Journal.

REFERENCES

1. G. L. Putnam and K. A. Kobe, *Trans. Electrochem. Soc.*, **74**, 609 (1938).
2. W. H. Bramley and W. F. Luder, *J. Am. Chem. Soc.*, **66**, 107 (1944)
3. J. T. Clarke and E. R. Blout, *J. Polymer Sci.*, **1**, 419 (1946)